Papel de la helicasa UAP56/DDX39B y otros factores asociados al metabolismo del ARN en la integridad del genoma

Carmen Pérez Calero

Tesis doctoral

Universidad de Sevilla

2019

Papel de la helicasa UAP56/DDX39B y otros factores asociados al metabolismo del ARN en la integridad del genoma

Trabajo realizado en el Departamento de Genética, Facultad de Biología, y en el departamento de Biología del Genoma, CABIMER, de la Universidad de Sevilla, para optar al grado de doctora en la Universidad de Sevilla por la licenciada Carmen Pérez Calero.

Sevilla, 2019

La doctoranda,

Carmen Pérez Calero

El director de tesis,

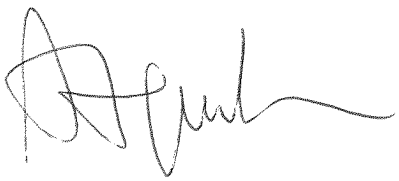

Andrés Aguilera López

TABLE OF CONTENTS

INDEX OF FIGURES

INTRODUCTION

RESULTS

INDEX OF TABLES

ABBREVIATIONS

A	Alanine
AID	Activation-Induced cytidine Deaminase
AREX	Alternative mRNA Export complex
AS	Alternative splicing
ATM	Ataxia Telangiectasia Mutated
ATP	Adenosine triphosphate
ATRIP	ATR Interacting Protein
A.U.	Arbitrary Units
bp	base pairs
BRCA	BReast CAncer
BrdU	Bromodeoxyuridine
CBC	Cap-Binding Complex
CBP	Cap-Binding Protein
CDC25	Cell Division Cycle 25
cDNA	complementary DNA
ChIP	Chromatin Immunoprecipitation
ChIP-seq	Chromatin Immunoprecipitation-sequencing
CIN	Chromosome Instability
CldU	Cloro-deoxyuridine
CNVs	Copy Number Variants
Co-IP	Co-immunoprecipitation
CTD	Carboxyl-Terminal Domain
DDR	DNA Damage Response
DDX	DEAD box
DNA	Deoxyribonucleic Acid
DNase	Deoxyribonuclease
dNTP	Deoxyribonucleotide triphosphate
DRIP	RNA-DNA immunoprecipitation
DRIP-seq	RNA-DNA immunoprecipitation-sequencing
DRIPc-seq	RNA-DNA immunoprecipitation followed by cDNA conversion-sequencing

dsRNA	Double-stranded RNA
E	Glutamic acid
EGFP	Enhanced Green Fluorescent Protein
EJC	Exon Junction Complex
EMT	Epithelial-mesenchymal transition
GCR	Gross chromosomal rearrangements
FA	Fanconi Anemia
FACS	Fluorescence-Activated Cell Sorting
FACT	Facilitates Chromatin Transcription
G+C	Guanine and Cytosine
GFP	Green Fluorescence Protein
H3S10-P	Histone H3 Phosphorylation at serine 10
HBD	Hybrid-binding domain
HDAC	Histone Deacetylase
hnRNP	heterogeneous nuclear Ribonucleoprotein
HR	Homologous recombination
HU	Hydroxyurea
IdU	Iodo-deoxyuridine
IF	Immunofluorescence
Ig	Immunoglobulin
K	Lysine
Kb	Kilobases
KDa	Kilodalton
lncRNA	long non-coding RNA
LOH	Loss Of Heterozygosity
MCM	Mini chromosome maintenance
mESC	mouse embryonic stem cells
MRN	Mre11-Rad50-Nbs1
mRNA	messenger RNA
mRNP	messenger Ribonucleoprotein particle
NES	Nuclear export signal
NHEJ	Non-homologous end joining

NMD	Nonsense mediated decay
NPC	Nuclear Pore Complex
nt	Nucleotides
NTS	Non-transcribed strand
NXF1	RNA export factor 1
OHT	Hydroxytamoxifen
ORF	Open reading frame
PCR	Polymerase Chain Reaction
PIKK	Phosphatidylinositol 3 like kinase
Pol	Polymerase
PRO-seq	Precision nuclear run-on-sequencing
qPCR	quantitative Polymerase Chain Reaction
RBP	RNA-binding protein
rDNA	Ribosomal DNA
RF	Replication fork
RFB	Replication fork barrier
RNAi	RNA interference
RNAP	RNA polymerase
RNase	Ribonuclease
RPA	Replication protein A
RT-PCR	Reverse Transcription Polymerase Chain Reaction
SEM	Standard Error of the Mean
siRNA	small interfering RNA
snRNP	small nucleolar ribonucleoprotein
SR	Serine/arginine-rich protein
SSB	Single-Strand Break
ssDNA	single-stranded DNA
TAM	Transcription-associated mutation
TAR	Transcription-associated recombination
TC-NER	Transcription couple nucleotide excision repair
TCR	Transcription couple Repair
Top	Topoisomerase

TREX	Transcription-Export complex
TS	Transcribed Strand
TSA	Trichostatin A
UV	Ultraviolet
U2AF	U2 Small Nuclear RNA Auxiliary Factor
WT	Wild Type
XPF	Xeroderma Pigmentosum Complementation Group F
XPG	Xeroderma Pigmentosum Complementation Group F

RESUMEN

Para la transmisión fidedigna de la información genética es indispensable preservar la integridad del genoma. Las células han desarrollado procesos complejos altamente regulados que velan por la estabilidad del mismo, evitando o resolviendo problemas que puedan comprometerla. La causa de dicha inestabilidad genética no sólo radica en la acción de agentes genotóxicos externos, sino también en aquellos derivados del propio metabolismo celular, resultado de fallos en los propios procesos endógenos de la célula como la transcripción, replicación y recombinación. La manifestación de la inestabilidad genética se presenta generalmente en forma de mutaciones y reordenaciones cromosómicas, características asociadas a la predisposición a envejecimiento y procesos tumorales.

Paradójicamente, uno de los procesos más esenciales para la supervivencia de la célula, la transcripción, puede constituir a su vez una de las fuentes más importantes de inestabilidad genética. Esto se debe principalmente a la aparición de ADN de cadena sencilla durante su desarrollo, que es más susceptible a sufrir daños que el ADN de doble cadena. Asimismo, la propia maquinaria de transcripción puede suponer un obstáculo para otro proceso esencial en la célula como es la replicación, pudiendo derivar todo ello en un aumento de roturas y recombinación en el ADN. Durante la transcripción, el ARN naciente puede hibridar con la hebra molde de ADN, de manera que la hebra no transcrita se mantiene en forma de cadena sencilla. Estas estructuras generadas se conocen como bucles R (*R loops*) y están compuestos por un híbrido de ADN-ARN y la cadena sencilla de ADN desplazada. Si bien se ha demostrado que los *R loops* pueden desempeñar funciones fisiológicas importantes, cuando se forman o acumulan de manera incontrolada pueden suponer una amenaza para la integridad del genoma.

El ARNm naciente ha de ser correctamente empaquetado en forma de ribonucleoproteínas mensajeras (mRNPs) para la elongación de la transcripción,

la integridad y el procesamiento del ARNm, previo a su transporte al citoplasma. Dicho ARNm, como sustrato potencial en la formación de *R loops*, ha de ser pertinentemente procesado, empaquetado y protegido para evitar que hibride con el ADN molde. Es por ello que, durante su procesamiento, existen numerosos factores que se unen al ARNm y contribuyen a proteger el genoma de la formación de *R loops*. En esta tesis nos hemos centrado en factores que tienen un papel en la biogénesis de las mRNPs y en particular en la helicasa UAP56/DDX39B perteneciente a la familia de helicasas DEAD/H box. Esta proteína, además de desempeñar un papel en el acoplamiento del madurosoma (*spliceosome*), interviene en la interfaz de la transcripción con la biogénesis y transporte de mRNPs. En concreto, UAP56 interacciona con el complejo THO, involucrado en la formación de la mRNP, y promedia el transporte de la mayoría de los mRNAs a través del reclutamiento del factor ALY/REF. El silenciamiento de UAP56 genera una alta inestabilidad genética en las células. Esto se atribuye a defectos en la formación de la mRNP, pero se desconoce si este fenotipo está mediado por *R loops.*

En la presente tesis hemos querido profundizar en los mecanismos por los cuales UAP56 contribuye al mantenimiento de la integridad del genoma. Hemos corroborado que el silenciamiento de UAP56 causa inestabilidad genética, determinada por un incremento de roturas en el ADN y descubierto nuevos fenotipos asociados, como defectos en la replicación. Además, hemos desvelado que tanto la inestabilidad como los defectos en replicación están mediados por *R loops*. En colaboración con el laboratorio del Dr. Patrick Sung en la Universidad de Yale, hemos descubierto que UAP56 es una helicasa de ADN-ARN capaz de resolver *R loops in vitro*. *In vivo*, la sobreexpresión de UAP56 suprime los fenotipos de inestabilidad mediados por *R loops* característicos de diversos mutantes, confirmando su actividad helicasa. Por último, hemos determinado en todo el genoma las regiones más propicias a acumular *R loops* y a donde se une preferentemente UAP56, así como el transcriptoma resultante tras el silenciamiento de UAP56.

Debido al creciente número de estudios que relacionan el silenciamiento de diferentes helicasas de la familia DEAD/H box con la acumulación de *R loops*, hemos comparado a nivel de todo el genoma los sitios de acumulación de *R loops* tras el silenciamiento de UAP56 y otra helicasa de la misma familia, DDX5, para investigar si ambas proteínas presentan una actividad redundante.

Finalmente, hemos estudiado la contribución del factor de transcripción Snail1 a la integridad del genoma. Tradicionalmente, el estudio de esta proteína se ha enmarcado en el contexto de la transición epitelio-mesenquima (EMT), gracias a la cual las células epiteliales adquieren las características propias de las células mesenquimales como la pérdida de los contactos intracelulares e interacción con la membrana basal. Aunque, este proceso es esencial para el desarrollo, se ha demostrado que se activa de manera anormal en los procesos cancerosos. Su activación permite a las células adquirir una mayor capacidad de invasión y metástasis. Un factor crucial encargado de desencadenar el inicio de esta transición es Snail1. En este trabajo hemos demostrado que el silenciamiento de Snail1 causa inestabilidad genética y defectos en la replicación mediados por *R loops*. Estos datos son particularmente relevantes al sugerir que pueda existir una posible conexión entre los *R loops* y la inestabilidad asociada a cáncer, dado el papel de Snail1 en determinados procesos cancerígenos.

INTRODUCTION

1. GENOME INSTABILITY

Cells are able to maintain order in a disordered world due to a large extent to the genetic information encompassed in the genome and stored in form of DNA molecule. Since the prime objective for cells is to faithfully transmit this genetic material in each cell division to its offspring, cells have developed a wide variety of highly regulated coordinated processes to guarantee genome stability. However, DNA is constantly assaulted by endogenous and environmental agents that might propitiate genome changes. This paradoxical situation drives to genetic variability, which although can have detrimental consequences, is also the basis for evolution (Aguilera and Gomez-Gonzalez, 2008). Thereby, genome instability can be a source of genetic diversity as is the case of immunoglobulin diversification. Nonetheless, under certain circumstances such as the ones that affect a proper DNA repair and/or replication, genome alterations can compromise genome integrity leading to an increased genome instability, which is a hallmark of aging, hereditary genetic diseases and cancer-related disorders (Gaillard and Aguilera, 2016; Negrini et al., 2010).

Such changes in the genome can be the consequence of lesions in the DNA generated by different sources of DNA damage, including endogenous metabolites from cellular processes like transcription or replication, and exogenous sources, such as external genotoxic agents. Indeed, DNA can undergo distinct type of lesions that cover abasic sites, bases mismatch, DNA adducts, inter- and intra-strand crosslinks, single-stranded DNA (ssDNA) gaps and double-strand breaks (DSBs). Therefore, genome instability comprises different form of mutations from point mutations to microsatellite contractions and expansions and chromosomal changes, such as chromosome instability (CIN), gross chromosomal rearrangements (GCRs), copy number variants (CNVs), loss of heterozygosity (LOH) and hyper-recombination (Aguilera and Garcia-Muse, 2013).

To counteract this threat to genome integrity, cells have evolved several systems based on the sensing and repair of DNA damages and coupling to the

cell cycle to warrant proper cell proliferation or, alternatively apoptosis, which are collectively termed DNA Damage Response (DDR) (Gaillard and Aguilera, 2016).

1.1. DNA damage response

The DNA damage response (DDR) is based on a complex signally network that detects DNA damage and replication stress and orchestrates DNA repair and cell cycle progression in order to counteract DNA damage. This system comprises a wide variety of DNA repair mechanisms, given the diversity of DNA-lesion types. The DDR signaling cascades are triggered by the recognition of specific DNA lesions by sensor proteins such as the MRN (Mre11 Rad50 Nb1) sensor complex that detects DSBs and RPA (replication protein A). These proteins signal the accumulation of ssDNA generated during replication stress, which are sensed by the ataxia telangiectasia mutated (Tel1/ATM) and ataxia telangiectasia and Rad3 related (Mec1/ATR) via its partner protein ATRIP (ATR-interacting partner) (as named in yeast/humans), respectively. Afterwards, ATM/ATR phosphorylates various proteins that trigger cell cycle progression arrest in coordination with DNA repair pathways to preserve genome integrity (Sulli et al., 2012). Among them, there are important mediators such as the histone variant H2AX, p53-binding protein (53BP1) or BRCA1. The DDR signaling can be spread from the damage locus thanks to the phosphorylation of the histone variant H2AX on Ser139 (known as γH2AX) by ATM/ATR or the activation of the downstream kinases including the checkpoint kinases 1 and 2 (Chk1/CHK1 and Rad53/CHK2) phosphorylated by ATR and ATM, respectively. Finally, all these complex signaling pathways converge on downstream effectors such as p53 and the cell division cycle 25 (CDC25) phosphatases. At the end, cells have different alternatives: cell cycle can be arrested to permit DNA repair before proliferation and cell cycle resumption or, if the DNA damage is persistent or irreparable, cell apoptosis and senescence pathways can be activated (Sulli et al., 2012).

1.2. Replication

DNA replication is essential for genome duplication, and then, for transmission of genetic information to the offspring. Each time a cell divides, only once during S

phase, billions of nucleotides must be accurately copied in coordination with cell cycle. For this purpose, replisomes are required to maintain an accurate rate through the chromatinized DNA template and overcome different impediments such as DNA lesions, torsional stress, non-B DNA structures or the transcription machinery itself that can hamper replication fork (RF) progression (Gaillard et al., 2015; Gomez-Gonzalez and Aguilera, 2019). However, these obstacles can alter the proper function of the replisome leading to replication stress, which in turn could drive to persistent RF stalling and then to, the collapse of the replication machinery causing replisome disassembly, ssDNA gaps and DNA breaks threatening genetic integrity (Aguilera and Garcia-Muse, 2013; Aguilera and Gomez-Gonzalez, 2008; Kim and Jinks-Robertson, 2012). To counteract this situation, cells have evolved refined mitotic and S phase checkpoint pathways that ensure DNA integrity and chromosome transmission (Gaillard et al., 2015).

1.3. Transcription-associated genome instability

Gene expression encompasses different processes from transcription to the proper processing of the messenger RNA (mRNA), export and translation of that RNA into a protein in the cytoplasm (Gaillard et al., 2013). During transcription the two DNA strands separate locally within the RNA polymerase (RNAP) to form the transcription bubble in which the RNAP uses one of the DNA strands as template (transcribed strand) to generate a complementary RNA chain, forming an RNA-DNA hybrid. Meanwhile, the non-transcribed strand remains unpaired as ssDNA. Furthermore, transcription generates DNA topological changes and even chromatin remodeling changes required to permit the movement of the transcription machinery through the DNA (Selth et al., 2010). Numerous studies from the last decades have revealed that transcription represent also a source of DNA variability. Since any DNA lesions or secondary structure with the potential to stall a DNA polymerase, could also block an RNA polymerase, transcription has been found to be responsible for high levels of mutation (Transcription-associated mutation, TAM) and recombination (Transcription-associated recombination, TAR) (Gaillard and Aguilera, 2016).

Genome instability associated with transcription can be adduced to several factors. For instance, the transient exposure of a ssDNA after the RNAPII passage increase its vulnerability toward mutagenic agents (Figure I1A). This is consistent with previous reports showing a synergistic effect between the transcriptional stated of a DNA regions and its susceptibility to DNA damaging agents (Garcia-Rubio et al., 2003). Moreover, during this process the DNA is also subjected to topological changes that nucleic acids must accomplish to allow the movement of the transcription machinery, which leads to positive and negative supercoiling ahead and behind the RNAPII, respectively. Such changes can facilitate the transient formation of the ssDNA. This stretched ssDNA could be damaged (Bermejo et al., 2009), but it can also facilitate the appearance of non-B structures such as RNA-DNA hybrids (known as R loops when formed outside the transcription bubble), hairpins, triplex DNA or G-quadruplexes (Figure I1B), among others. All such structures that could lead to genome instability due to its potential to block the replisome (Aguilera and Garcia-Muse, 2013; Gaillard and Aguilera, 2016; Kim and Jinks-Robertson, 2012).

In other cases, the RNA itself can facilitate aberrant structures such as RNA-DNA hybrids or R loops. For instance, if the nascent mRNA is not properly packaged into a messenger ribonucleoprotein particle (mRNP), as in the case of mRNA biogenesis mutants, it can invade the DNA duplex (Huertas and Aguilera, 2003)(Figure I1B). However, the mechanisms of TAR are not completely understood. Since homologous recombination (HR) is the main pathway responsible for repair of DNA breaks occurring preferentially during replication, mounting evidence suggest that TAR is the consequence of transcription-replication collisions which can cause RF collapse (Aguilera, 2002; Gaillard and Aguilera, 2013; Garcia-Muse and Aguilera, 2016).

1.4. Transcription-replication conflicts

Since transcription and replication are crucial for cell survival and proliferation and they use the same DNA as a template, collisions between both machineries are unavoidable when both encounter each other at the same DNA region in

certain occasions in prokaryotes and eukaryotes (Gomez-Gonzalez and Aguilera, 2019). These two processes are significantly different: whereas the RNA polymerase embraces both DNA strands during transcription, the replicative machinery uses two DNA polymerases embracing each one each ssDNA. Furthermore, while several RNA polymerases can simultaneously transcribe the same gene, replisomes always move alone once per cell cycle. Additionally, in prokaryotes the fact that DNA replication and transcription exhibit different rates (Helmrich et al., 2013) make these conflicts to occur often (Merrikh et al., 2012). Therefore, how the replisome advance along the double-stranded DNA despite the presence of the transcription machinery becomes an abiding question. Moreover, as mentioned above, RNA polymerases are considered one of the main impediments to the progression of the RFs (Bermejo et al., 2012; Deshpande and Newlon, 1996; Liu and Alberts, 1995). And of utmost importance, these encounters are prone to occur at transcribed sites driven by different RNAPs (Gaillard et al., 2013; Gottipati et al., 2008; Prado and Aguilera, 2005) representing a common issue for both prokaryotes and eukaryotes (Helmrich et al., 2011; Prado and Aguilera, 2005). Attending to the direction of these conflicts, transcription-replication collisions can be co-directional or head-on. When transcription and replication machineries are located in the leading strand using the same DNA as template, both move in the same direction (co-directional). Conversely, if the transcribed strand coincides with the lagging strand, direction of transcription and replication converges (head-on). In any case, these collisions that compromise genome integrity not always require a physical contact between both machineries. Given that both processes modify topology, chromatin organization and structure of the DNA, different mechanism have arose by which transcription compromise genome integrity in a replication-mediated manner (Gomez-Gonzalez and Aguilera, 2019). Regardless the directionality of the conflict, replisomes are impeded to progress through an RNA polymerase. However, experimental evidence suggests that head-on collisions are more deleterious (Figure I1C) (Prado and Aguilera, 2005).

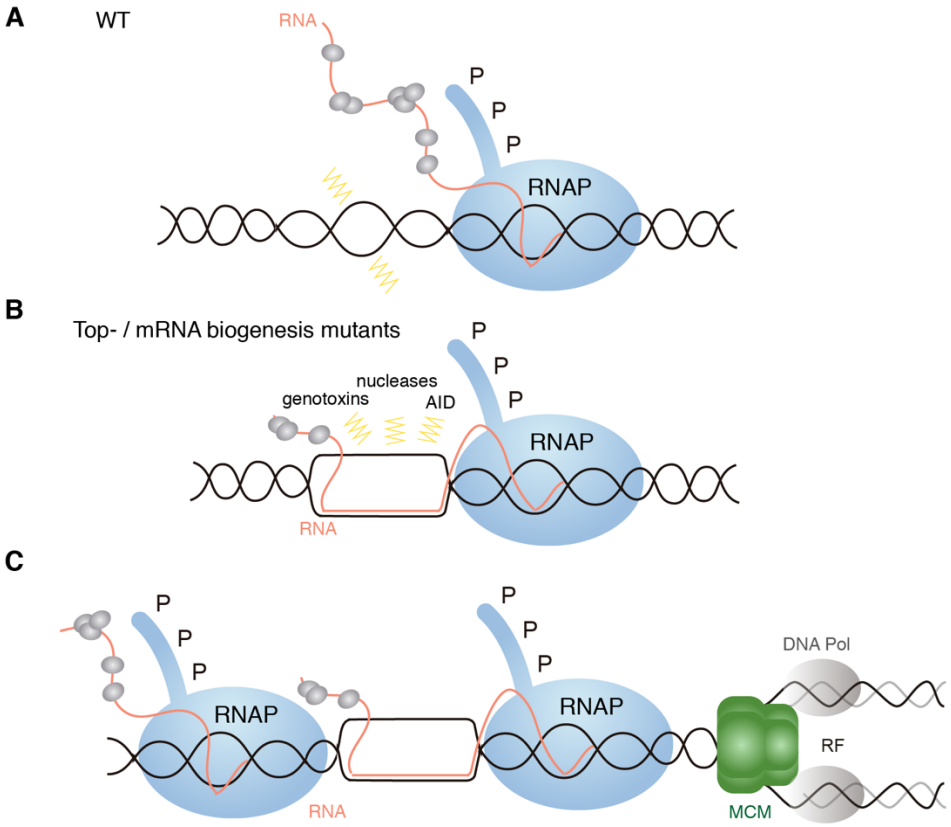

Figure I1. Transcription-associated genome instability.
Transcription could compromise genome integrity by itself. **(A)** Local positive supercoiling ahead the RNAPII and negative supercoiling behind it make the DNA more vulnerable to damage. **(B)** Non B-structures such as R loops can emerge when the nascent RNA hybridizes with the template DNA. Under circumstances with high level of R loops, as is the case of mRNP biogenesis mutants such as THO, the displaced ssDNA is more vulnerable to damage by genotoxins or nucleases. **(C)** Transcription-replication collisions as a result of the encounters between replication and transcription machineries. If these encounters are head-on (if both machineries progress in the opposite direction), they are more deleterious than when they are co-directional (both machineries advance in the same direction). MCM, minichromosome maintenance complex; DNA pol, DNA polymerase; RF, Replication Fork; RNAP, RNA polymerase. Figure adapted from (Gaillard et al., 2013).

Cells have evolved different strategies to minimize the harmful impact of such collisions. In bacteria, highly transcribed and essential genes are orientated co-directionally with replication to avoid head-on collisions (Brewer, 1988). In the human genome, this co-orientation bias is also present (Petryk et al., 2016). However, the considerable complexity of eukaryotic genomes demand further solutions. For instance, in budding yeast, RF barriers downstream of rDNA loci prevents head-on collisions with the RNA polymerase I by physically blocking RF (Linskens and Huberman, 1988). In general, transcription and replication in eukaryotic cells have some spatial and temporal separation but some highly

expressed genes are transcribed during the S-phase (Wei et al., 1998). Interestingly, those mechanisms and factors that contribute to eliminate the RNAPII stalling also help to suppress the consequences of these encounters.

2. RNA METABOLISM AND GENOME STABILITY

2.1. Transcription and RNA processing

In eukaryotic gene expression, the nascent pre-mRNA undergoes maturation by processing factors and protein-packaging leading to an export-competent mRNP particle apt to its translation in the cytoplasm. These mRNA processing steps comprise 5′-capping, splicing and 3′-end processing. During these events, numerous RNA-binding proteins (RBPs) are loaded co-transcriptionally to the nascent RNA. The processing steps and mRNP export are interlinked and they influence one another's specificity and efficiency but at the same time, they are also tightly linked to transcription. This fact allows the regulation of the process at different steps during transcription and makes the composition of the mRNP a dynamic process (Bentley, 2014; Proudfoot et al., 2002).

The first processing step that occurs when the RNA emerge from the RNAPII is the addition of a cap structure to the 5' end of all the mRNAs by capping enzymes that binds to the phosphorylated Carboxy-Terminal Domain (CTD) of the RNPII largest subunit. This initial structure is then recognized by the Cap Binding Complex (CBC) (Figure I2). This first step initiates during the assembly of the mRNP and it is believed to play a major role in the stabilization of the mRNA and required for further processes that occur on the mRNA molecule (splicing, transcription termination export, nuclear mRNA decay, translation, non-sense-mediated decay and decapping) (Aguilera, 2005a; Gonatopoulos-Pournatzis and Cowling, 2014; Proudfoot et al., 2002)

Splicing is also an important step to which pre-mRNAs are subjected in order to obtain a mature mRNP. The pre-mRNA is spliced by different splicing factors that eliminate introns and join the remaining exons to obtain the mature mRNA. Splicing factors associate rapidly with the nascent RNA and introns are

removed co-transcriptionally, but some of them can be eliminated after transcription (Kornblihtt et al., 2004). Splicing occurs in eukaryotes from yeast to human. However, whereas introns in the budding yeast are scarce and the larger part are found in ribosomal protein genes; in humans, almost all RNAPII transcribed genes contain introns (Izquierdo and Valcarcel, 2006; Shkreta and Chabot, 2015). The splicing process is catalyzed by a dynamic ribonucleoprotein structure called spliceosome, whose formation involves the stepwise assembly of five uridine (U)-rich small nuclear ribonucleoproteins (snRNPs) (U1, U2, U4, U5 and U6), along with many associated protein cofactors (Will and Luhrmann, 2011). The spliceosome recognizes short consensus sequences at the nuclear pre-mRNA introns: the 5' splice site, the branch site and the 3' splice site (Gersappe et al., 1999). Nuclear pre-mRNA introns are removed by two consecutive transesterification reactions that are necessary to excise introns and join together the remained exons. In general, splice sites that are more adjusted to the consensus sequence ("strong" splicing site) lead to constitutive splicing and full usage of the site. However, those splice sites that diverge from the consensus sequence ("weak" splice sites) are less efficiently recognized and used leading to alternative splicing (Kornblihtt et al., 2013). Alternative splicing is predominant in higher eukaryotes and permits the production of multiple mRNA variants from a single pre-mRNA contributing to transcriptomic and proteomic diversity. The selection of the final splice site is regulated by diverse factors including members of the SR and hnRNP protein families which bind to enhancers and silencers sequences, respectively. Moreover, alternative splicing when occurred co-transcriptionally is also regulated by a more complex process that involves the transcription machinery (Kornblihtt et al., 2013). Indeed, RNAPII pausing at the 3' end on yeast genes have been shown to favor the co-transcriptional excision of introns, and *vice versa*, splicing could also promote pausing in transcription (Alexander et al., 2010).

Other relevant step in gene expression is the 3' end cleavage of transcripts generated by RNAPII. This is an universal step that consists on the cleavage of the nascent transcript and the acquisition of the poly(A) tail in the majority of

genes. This poly(A) tail is essential for stability, translocation to the cytoplasm and translation of the transcripts. Thus, the 3' end processing reaction requires multiple protein factors that recognizes poly(A) signals on the nascent transcripts and produce the endonucleolytic 3' end cleavage and the addition of a polyadenylated tail. This step serves as a bridge in the network connecting different transcription and other steps in the mRNP biogenesis. Indeed, 3' end polyadenylation factors and sequence elements of the poly(A) signal modulate transcription termination and, in turn, transcription factors/activators affect processing at the poly(A) signal. Indeed, there is a connection between 3' end processing and mRNP export. Accordingly, mRNPs that are not processed at the 3' end will be degraded or not transported efficiently to the cytoplasm (Millevoi and Vagner, 2010).

Finally, others RBPs binds co-transcriptionally to the nascent mRNA and help in the formation of the mRNP, preventing its degradation and promoting its export. The export competent mRNP are drive to the cytoplasm by the export receptor factor NXF1/TAP-p15 (yeast Mex67-Mtr2) that interacts with nucleoporins that form the nuclear pore complex (NPC). This complex operates together with different adaptor proteins including proteins from the THO/TREX and THSC/TREX2 complexes (Figure I2) (Kohler and Hurt, 2007)

2.2. THO/TREX as a paradigm of the connection between RNA metabolism and genome integrity

After the diverse mRNA processing steps, the mRNP is mature and ready for nuclear export. Initial studies in *S. cerevisiae* about the mRNA export pathway allowed the identification of the key components of this machinery (Aguilera, 2005a; Reed and Cheng, 2005; Reed and Hurt, 2002; Vinciguerra and Stutz, 2004). These include THO/TREX, a conserved eukaryotic complex involved in transcription elongation and RNA export that contributes to the mRNP biogenesis and the maintenance of genome integrity (Chavez et al., 2000; Luna et al., 2012). In yeast, THO is formed by five subunits: Tho2, Hpr1, Mft1, Thp2, constituting a robust complex and Tex1, which is less tightly associated (Chavez et al., 2000;

Pena et al., 2012). In agreement, removal of any of this four subunits results in THO destabilization and strong transcription and genome instability in yeast (Garcia-Rubio et al., 2008; Huertas et al., 2006). Whereas, this is not the case for *TEX1* (Luna et al., 2005; Pena et al., 2012). The THO complex associates with a number of RBPs including the DEAD-box RNA helicase UAP56/DDX39B (yeast Sub2) or the mRNA export adaptor protein ALY/REF (yeast Yra1) in a supramolecular structure termed TREX (Transcription-Export) coupling transcription and export (Strasser et al., 2002). However, these interactions seem to be transient and do not contribute to the integrity of the THO complex (Huertas et al., 2006; Pena et al., 2012).

The recruitment of THO to chromatin involved redundant mechanism from the transcription machinery, the nascent mRNA and other mRNP components (Gomez-Gonzalez et al., 2011; Jimeno et al., 2002; Meinel et al., 2013). Genome-wide studies in yeast pointed that THO/TREX complex is recruited to the active transcribed chromatin and it is found in active ORFs with a tendency to accumulate towards the 3' end (Gomez-Gonzalez et al., 2011). In chromatin, THO is found in association with RNA processing and splicing factors (Chanarat et al., 2011; Cheng et al., 2006; Masuda et al., 2005; Saguez et al., 2008). And, as other factors needed for RNA maturation, It has been shown that THO interacts with the phosphorylated CTD of RNAPII probably to be loaded into the mRNP (Meinel et al., 2013).

In concordance with all the exposed, yeast THO/TREX mutants present mRNA export defects, transcription-elongation impairment and transcription-dependent-hyper-recombination phenotypes (Aguilera and Klein, 1990; Chavez et al., 2000; Jimeno et al., 2002; Piruat and Aguilera, 1998). Indeed, the link between RNA export and genome stability was proposed by the observation that THO/TREX were required for mRNA export (Jimeno et al., 2002; Strasser et al., 2002) and the fact that yeast THO mutants accumulate RNA-DNA hybrids (Huertas and Aguilera, 2003).

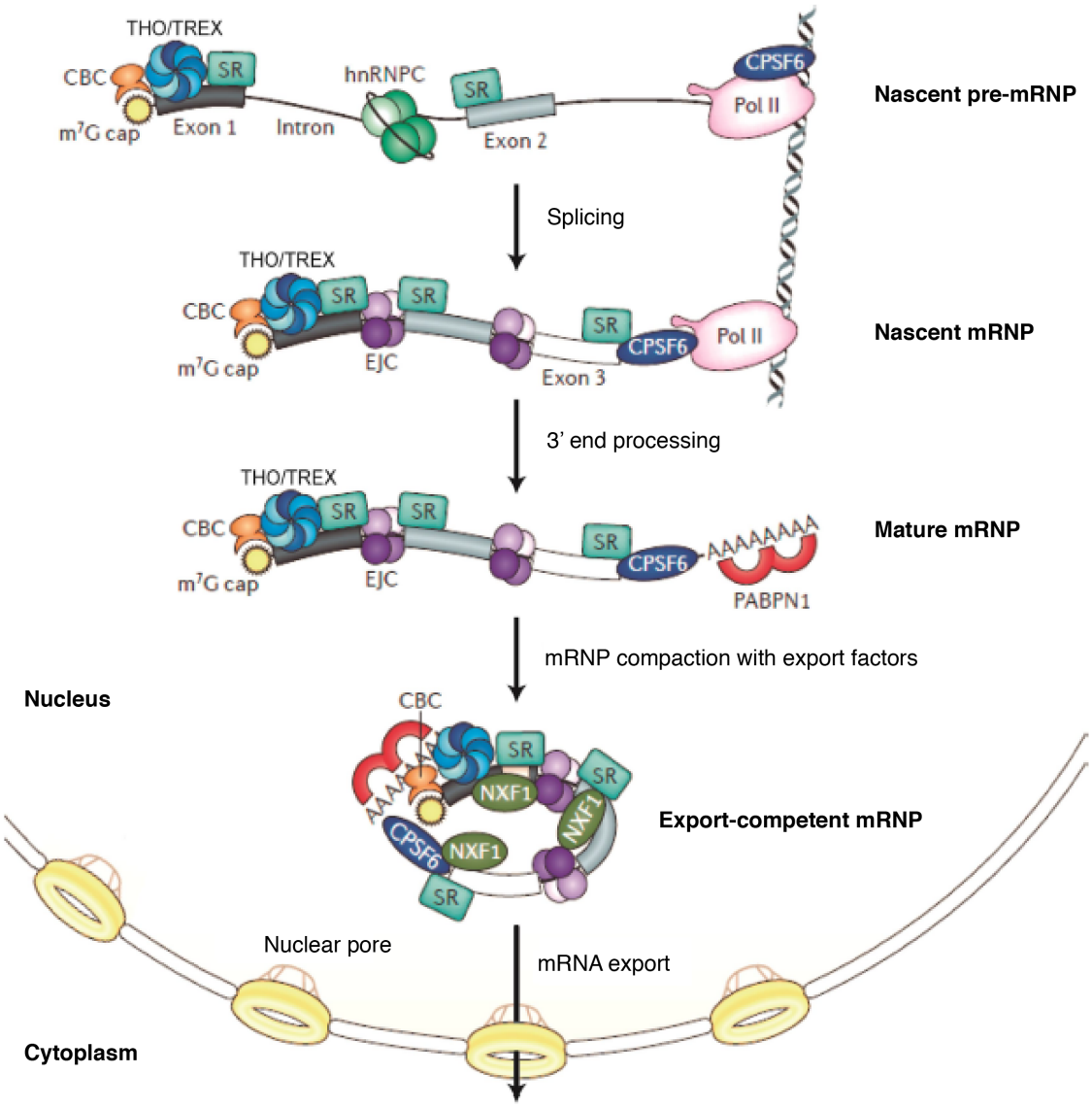

Figure I2. Co-transcriptional assembly of the mRNPs.
Illustration representing the co-transcriptional assembly of messenger ribonucleoprotein particles (mRNPs) in mammalian cells. During transcription, the cap-binding complex (CBC) binds to the 7-methylguanosine (m'G) and facilitates splicing. The splicing and the binding of numerous RNA-binding proteins occur co-transcriptionally. The recruitment of the THO/TREX complex is mediated by the interaction with proteins of the CBC. The exon junction complex (ECJ) and serine/arginine rich (SR) proteins contribute to mRNP biogenesis and export. After cleavage and polyadenylation, THO/TREX and other export adaptor factors recruit the RNA export receptor NXF1 to permit efficient nuclear export through the nuclear pore. hnRNPC, heterogeneous nuclear ribonucleoprotein C; PABPN1, nuclear poly(A)-binding protein 1; Pol II, RNA polymerase II; pre-mRNP, mRNP precursor ; CPSF6, cleavage factor and polyadenylation factor 6; NXF1, RNA export factor 1. Figure adapted from (Muller-McNicoll and Neugebauer, 2013).

This connection between RNA metabolism and genome integrity has been extended to other factors. These involved different RNA nuclear processes which are also associated to genome instability. Among them, there have been found proteins with a role in splicing as is the case of SRSF1 (Li and Manley, 2005),

mRNA 3' end processing and degradation factors such as Trf4, Rrp6 and FIP1L1 (Gavalda et al., 2013; Luna et al., 2005; Stirling et al., 2012) or helicases such as SETX/Sen1, DDX19 and DDX23 (Hodroj et al., 2017b; Skourti-Stathaki et al., 2011; Sridhara et al., 2017).

2.3. DEAD-box RNA helicases and genome integrity

In the last years, there has been an emerging interest in the role of different helicases in the maintenance of genome integrity. Helicases are nucleic acid–dependent ATPases capable of unwinding DNA or RNA duplex substrates. They play roles in almost every process involving nucleic acids, including DNA replication and repair or transcription (Singleton et al., 2007). Among them, the DEAD/H box family is the largest family of superfamily 2 helicases, which in turn comprehends two groups: the DEAD-box group with 44 members and the DEAH-box family with 15 proteins. The majority of these helicases use ATP to bind or remodel RNA and RNA-protein complexes and for this reason, they are involved in nearly all aspects of RNA metabolism, from transcription and translation to mRNA decay. These proteins are characterized by the presence of an Motif/Motif II, D-E-A-D (asp-glu-ala-asp) or D-E-A-H (asp-glu-ala-his), which inspired the name of the family (Linder and Jankowsky, 2011). Hence, DEAD-box proteins can act as RNA chaperones unwinding and refolding of RNA (Jarmoskaite and Russell, 2014; Putnam and Jankowsky, 2013). Importantly, emerging evidence suggest that these helicases are involved in genome instability and cancer onset since mutations in many of them lead to the appearance of such phenotypes (Cai et al., 2017; Fuller-Pace, 2013; Sarkar and Ghosh, 2016). Interestingly, these features are linked to R loop imbalance in the cases of DHX9 (Cristini et al., 2018), DDX1 (Li et al., 2016) DDX23 (Sridhara et al., 2017), DDX21 (Song et al., 2017) or DDX19 helicases (Hodroj et al., 2017a), among others.

2.3.1. The helicase DDX5/DBP2

Human DDX5/p68 (yeast Dbp2) is one of the prototypic members of the DEAD box family of RNA helicases (Ford et al., 1988). It was initially identified due to its

cross-reactivity with an antibody generated against the simian virus (SV40) large T antigen (Lane and Hoeffler, 1980). DDX5 and another highly related protein, DDX17/p72 (Lamm et al., 1996), are RNA-dependent ATPases and ATP-dependent RNA helicases. Both proteins share 90% identical central core but with different N- and C-termini. DDX5 presents the characteristic “helicase core” divided into two flexibly linked RecA-like domains, which are critical for RNA binding, ATP binding and hydrolysis, and intermolecular interactions. (Dai et al., 2014). DDX5 and DDX17 have been shown to function in multiple cellular processes, in most cases as RNP chaperones (Figure I3). However, despite these proteins being predominantly nuclear, different reports have shown that DDX5 is a nucleocytoplasmic shuttling protein (Iggo et al., 1991; Wang et al., 2009).

DDX5/Dbp2 act in multiple steps of RNA metabolism. It is involved in the regulation of transcription through lncRNAs (Wongtrakoongate et al., 2015; Zhang et al., 2016); mRNP processing, being required for the spliceosome assembly and alternative splicing (Dardenne et al., 2014; Wang et al., 2016), and mRNP export. Curiously, DDX5 co-immunoprecipitates with the export factors ALY and TAP (Zonta et al., 2013) and likewise Dbp2 in *S. cerevisiae* genetically interacts with Yra1 and Mex67 (Ma et al., 2016). In addition to these roles, DDX5 has also been proposed to be involved in the regulation of the mRNA levels in the nonsense-mediated decay (NMD), an RNA surveillance pathway that targets a selection of mRNAs for degradation (Geissler et al., 2013; Lykke-Andersen and Jensen, 2015), and of microRNA processing, which are non-coding RNAs that target mRNAs for silencing (Gregory et al., 2004; Ha and Kim, 2014), and even DDX5 is also involved in ribosome biogenesis (Saporita et al., 2011). DDX5 also acts as a transcriptional co-factor to activate transcription, as is the case of MyoD (Caretti et al., 2006), Snail1 (Carter et al., 2010) or p53 (Bates et al., 2005). (Figure I3). Finally, recent reports have also uncovered broader effects of DDX5 in glucose metabolism and carcinogenesis (Mazurek et al., 2014; Xing et al., 2017). The importance of DDX5 in tumor development is also provided by the fact that its overexpression is well established in breast cancer (Wortham et al.,

2009). Therefore, it has been proposed that the multiple roles in which DDX5/Dbp2 is found to intervene are dictated by the wide range of RNA targets acted on by DDX5/Dbp2 (Xing et al., 2019).

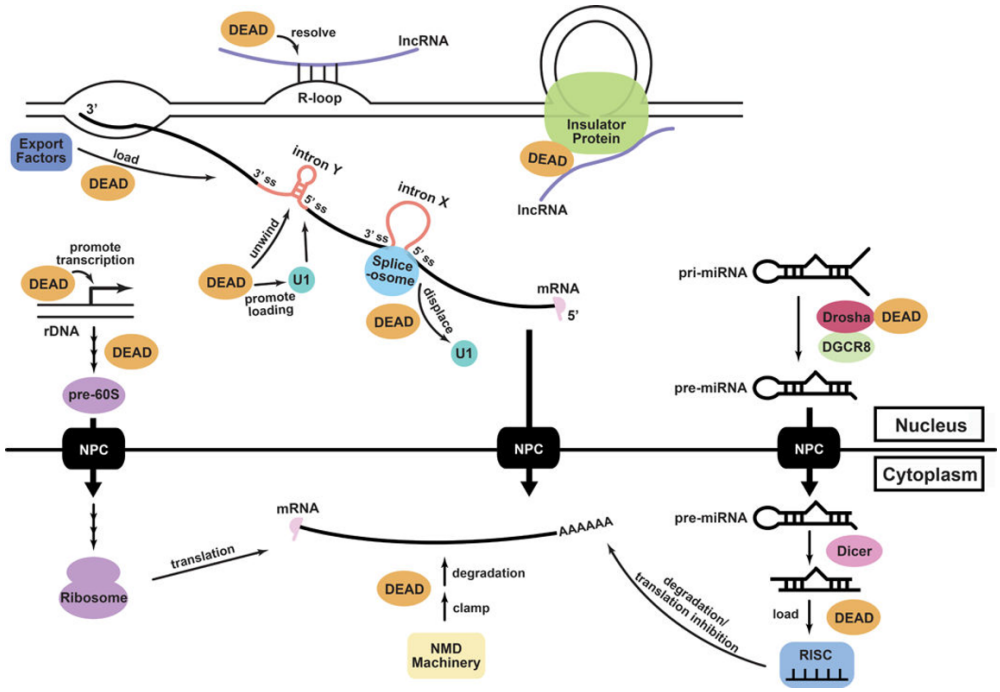

Figure I3. DDX5/Dbp2 functions as a RNP chaperone.
DDX5/Dbp2 (orange circle, "DEAD") participates as a RNP chaperone in multiple processes such as alternative splicing, the regulation of lncRNA activities, mRNA export, miRNA processing, nonsense mediated decay (NMD) and ribosome biogenesis. Adapted from (Xing et al., 2019).

2.3.2. The helicase UAP56/DDX39B: a key player in mRNP biogenesis

The DEAD-box helicase UAP56/Sub2 is a conserved RNA-dependent ATPase and ATP-dependent RNA helicase discovered through its interaction with the human splicing factor U2AF65 (Fleckner et al., 1997). Human UAP56 comprises the minimal helicase core with two canonical RecA-like helicase domains connected with a flexible liner (Figure I4). The N-terminal domain contains the conserved helicase motifs motifQ, I, Ia, GG, Ib, II, and III, whereas the C-terminal domain contains helicase motifs IV, QXXR, V, and VI. (Shi et al., 2004; Zhao et al., 2004). Structures of several DEAD/H-box proteins and other helicases have shown that Lys in motif I (GKT) interacts with the phosphate group of ATP and is important for ATP binding (Sengoku et al., 2006; Shi et al., 2004). The Glu in motif II (DEAD) has been postulated to be the key catalytic residue that activates a water molecule to hydrolyze ATP in DEXD/H-box proteins and other helicases (Cordin et al., 2006; Sengoku et al., 2006).

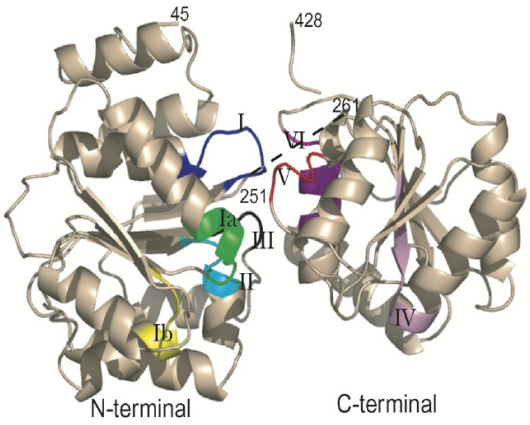

Figure I4. Human UAP56 structure.
Picture represents both N-terminal and C-terminal domain joined by the flexible linker (black line). Conserved helicase motifs are mapped on the structure in different colors. Adapted from (Zhao et al., 2004)

Regarding its activities, UAP56 plays a role in splicing by facilitating the unwinding of U4/U6 snRNA duplex and it is also required for the first ATP-dependent spliceosome assembly step (Fleckner et al., 1997; Shen et al., 2008). UAP56 is also essential for the export of the majority of mRNAs from the nucleus to cytoplasm in *S. cerevisiae, D. melanogaster*, *C. elegans* and human (Herold et al., 2003; Kapadia et al., 2006; Luo et al., 2001; MacMorris et al., 2003). It recruits the mRNA export factor ALY to the intron-containing and intron-less pre-mRNAs. The THO complex together with UAP56 and ALY participate in the export of bulk mRNAs through the interaction of the adaptor factor ALY with the mRNA export factor NXF1 linking the nascent mRNA to its export factors, which allow translocation to the NPC (Strasser et al., 2002). Although UAP56 associates with THO, it is not an integral part of this complex (Chavez et al., 2000; Pena et al., 2012) (Figure I5). However, it displays an important role in the assembly of the TREX complex by mediating the ATP-dependent interaction of CIP29, Aly, PDIP3 and ZC11A with THO (Dufu et al., 2010; Folco et al., 2012; Sugiura et al., 2007). Likewise, the TREX components Aly and Chtop stimulate the UAP56 helicase activity and are recruited to mRNAs by UAP56 (Chang et al., 2013). UAP56/Sub2 is the most abundant protein of the THO/TREX complex (Heath et al., 2016). Interestingly, an additional UAP56-related helicase called URH49/DDX39A is also present in humans (Pryor et al., 2004). This protein shares 90% amino acid sequence homology with UAP56. Both proteins, UAP56

and URH49, are able to complement Sub2 deletion and interact with the Yra1 adaptor in yeast. However, URH49 has been found to bind preferentially to CIP29 (yeast Tho1) in what it is believed to be a novel complex called AREX (alternative mRNA export complex) (Yamazaki et al., 2010).

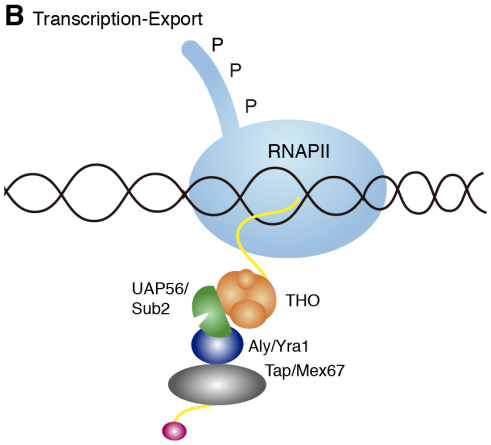

Figure I5. Role of UAP56 in transcription and nuclear export.
During transcription, the THO complex associates with the RNAPII travelling along the entire transcribed region. UAP56 and Aly associate with the 3'-end of the gene forming the active TREX complex. Thanks to UAP56, different proteins could be transferred to the mRNAs. Afterwards, the Tap-p15 heterodimer recognizes the mRNAs through Aly facilitating the formation of an export competent mRNP. Finally during or after release from genes locus, mRNPs can be subject to more rearrangements prior its translocation through the nucleopores and its following translation in the cytoplasm.

In yeast, Sub2 is involved in multiple stages of mRNA maturation and its inactivation leads to non productive spliceosome assembly (Kistler and Guthrie, 2001; Libri et al., 2001), decreased polyadenylation efficiency and mRNA instability (Rougemaille et al., 2008; Saguez et al., 2008). Therefore, this RNA helicase seems to be a kind of RNA chaperone that participates in the process of assembly of the mRNP (Saguez et al., 2013). In addition, Sub2 also plays a role in the maintenance of genome instability since mutations of *SUB2* lead to hyper-recombination phenotype, whereas Sub2 overexpression partially suppresses the growth-defect and hyper-recombination phenotypes associated to the *hpr1Δ* mutants of the THO complex (Jimeno et al., 2002). In human cells, UAP56 depletion leads to mRNA export defects and a strong genomic instability phenotype (Dominguez-Sanchez et al., 2011). Altogether, these findings suggest a double role of UAP56/DDX39B in mRNP biogenesis/export and the maintenance of genome, as it seems to be also the case of THO.

3. R LOOPS AS A SOURCE OF GENOME INSTABILITY

Co-transcriptional R loops represent one of the elements that contributes to exacerbate the negative impact of transcription and transcription-replication conflicts on genome integrity. These three-stranded-structures are the result of the hybridization of the nascent RNA with the transcribed DNA strand, thus displacing the non-template DNA strand (Figure I6).

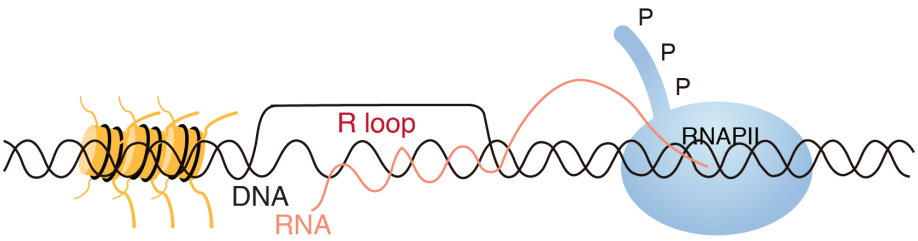

Figure I6. R loop structure.
R loops are the resulting structures formed by a RNA-DNA hybrid and the displaced ssDNA.

3.1. R loops as a cellular regulators

RNA-DNA hybrids occur naturally during transcription and replication. These structures are normally found at the active site of the RNA polymerase at the transcription bubble or during lagging-strand synthesis (Aguilera and Garcia-Muse, 2012). RNA-DNA hybrids are also found at certain regions of the genome where they perform a physiological role. Reports have widely described transient programmed R-loops with a role in different physiological processes such as *E. coli* plasmid replication (Kogoma, 1997), mitochondrial DNA replication (Xu and Clayton, 1996), immunoglobulin (Ig) class-switch recombination in the B-cells (Yu et al., 2003) or CRISPR-Cas9 gene editing (Jiang et al., 2016). Strikingly, recent reports have also shown the implications of R loops in suppression of chromosome instability through R loop-driven ATR pathway that acts at centromeres and promotes faithful chromosome segregation (Kabeche et al., 2018).

R loops are formed in multiple regions of the eukaryotic genomes, such as the ones transcribed by RNA polymerases I, II and III (El Hage et al., 2010; Tran et al., 2017). At RNAPII-transcribed genes, genome-wide approaches have

provided evidence showing that the R loops are preferentially found at promoters of genes enriched in CpG island showing a strong GC skew (Chen et al., 2017; Dumelie and Jaffrey, 2017; Ginno et al., 2012; Nadel et al., 2015; Sanz et al., 2016). Indeed, it has been shown that R loops may regulate gene expression. On one hand, R loops may assist transcription by suppressing DNA methylation (Ginno et al., 2012; Grunseich et al., 2018) and by influencing the binding of chromatin remodelers at promoters. Reports in mouse embryonic stem cells (mESCs) suggest that R loops inhibit the binding of repressive chromatin-modifying enzymes and recruit activating chromatin-remodeling complexes such as Tip60-p400 to favor differentiation genes expression (Chen et al., 2015). On the other hand, R-loops can impede the binding of other transcription-factor as occurred in the case of the human vimentin gene (Boque-Sastre et al., 2015). This dual situation may reflect the capacity of R loops in regulating gene expression through multiple context-dependent mechanism (Crossley et al., 2019).

Importantly, R loops have also been found to be enriched at the 3' end of some mammalian genes where they are supposed to mediate efficient transcription termination (Skourti-Stathaki et al., 2011). R loops can hamper transcription and it could be used as an initial pause signal to slow-down RNAPII that would facilitate the co-transcriptional splicing process or the correct termination and polyadenylation of the nascent mRNA (Proudfoot, 2016; Wahba et al., 2016). Thus, these findings suggest that R loops might play regulatory roles such as the control of the gene expression through epigenetic mechanisms or by transcriptional interference (Chan et al., 2014; Ginno et al., 2012; Wahba et al., 2016). Importantly, despite their important regulatory roles, they can also interfere with DNA replication, repair and transcription.

3.2. R loops as genomic threats

3.2.1. R loop-mediated genome instability

Given their structure and effects, R loops constitute a putative threat to genome stability. As said above, the formation of an RNA-DNA hybrid and the concomitant

displacement of the ssDNA drive to a major exposure of the DNA strand, which is more mutagenic than dsDNA. This could lead to SSBs, that if remaining unrepaired might block RF progression and could lead to DSB formation (Figure I7A). The ssDNA can be object of the action of different mutagenic agents or DNA-modifying enzymes, as it is the case of the human activation-induced cytidine deaminase (AID) (Figure I7A), which participates in immunoglobulin class switching recombination and somatic hypermutation in mammalian activated B cells (Chaudhuri and Alt, 2004). However, the action of AID is not restricted to such genes and it could act over other transcribed genes, particularly when R loops accumulate at high levels, as it occurs in THO yeast mutants (Gomez-Gonzalez and Aguilera, 2007). In addition, R loops can also promote hypermutation by non-canonical replication that arises when the R loop is used as a primer, as described in *E. coli* (Kogoma, 1997) or in the rDNA region of yeast deprived of Top1 and ribonuclease H (RNase H) enzymes (Stuckey et al., 2015).

R loops can also alter transcription. Excessive pausing, arrest or backtracking of RNP can lead to transcription stress (Saponaro et al., 2014). Hybridization between the nascent RNA and the DNA template strand within an R loop could destabilize the transcription complex, that could render the RNAP prone to blockage at randomly-occurring weak pausing/termination mode. Indeed, R loops have been shown to become obstacles for RNA polymerase progression *in vitro* (Tous and Aguilera, 2007) and *in vivo* (Bonnet et al., 2017; Lang et al., 2017) Although it is not clear whether problems with transcription derive from a RNAP stalled with the R loop or whether the R loop by itself act as a barrier to upstream polymerases.

3.2.2. R loops and replication stress

Since the most prevalent source of R loop-dependent DNA damage seems to take place during S phase (Gan et al., 2011; Wellinger et al., 2006), R loops are supposed to exacerbate transcription-replication conflicts. Although the mechanisms by which R loops lead to the formation of ssDNA gap or DSBs need to be clarified, there is a large body of work that has provided a mechanistic

connection between recombination and replication-stress induced by R loops. Evidence from yeast to human cells corroborate this idea. RF progression defects have been detected in several R loop-accumulating cells by different techniques as 2D-gel electrophoresis, DNA combing or the recruitment of the Rrm3 DNA helicase (Gomez-Gonzalez et al., 2011; Herrera-Moyano et al., 2014; Salas-Armenteros et al., 2017; Tuduri et al., 2009; Wellinger et al., 2006). Additionally, in these cases, the overexpression of ribonuclease H1 (RNase H1), which specifically degrades the RNA moiety of RNA-DNA hybrids, reduces or even suppresses replication defects, DNA breaks and recombination. Definitely, part of the harmful potential of R loops relies on its ability to hamper RF progression (Aguilera and Garcia-Muse, 2012).

Different explanations can be proposed in order to justify how DNA breaks can arise as a consequence of R loops. As said above, the fact that the ssDNA, which is present in an R loop to DNA lesions, is more susceptible to be damaged can lead to SSBs. Thus, if these DNA lesions remain unrepaired can block RF progression and in turn, can lead to DSBs formation (Figure I7A). Indeed, the ssDNA can also propitiate the formation of non-B DNA structures such as G-quadruplexes and hairpins, that could be also an obstacle for replication. In addition, the own structure of the RNA-DNA hybrid acts itself directly as major barrier for replication. Indirectly, R loops can block replication by the appearance of transcription-replication conflicts. This appears when the RNAP remains attached at the transcription site due to the presence of a stable R loop (Aguilera and Garcia-Muse, 2012). Recent studies show that R loop levels are also affected by the orientation of the conflict (Hamperl et al., 2017; Lang et al., 2017). This suggests that head-on formed R loops blocked replication and can result in DNA breaks and in the end, genome instability and chromosome fragility (Figure I7B) (Aguilera and Garcia-Muse, 2012; Zeman and Cimprich, 2014). However, the mechanism by which R loops block RF still need to be fully understood. It could be even possible that the impediment would not be the RNA-DNA hybrid by itself but the compacted chromatin structure induced by it (Castellano-Pozo et al., 2013; Garcia-Pichardo et al., 2017; Rondon and Aguilera, 2019) .

3.2.3. R loops and chromatin modifications

Recent finding suggests that epigenetic mechanisms can act to regulate R loop homeostasis. Chromatin acetylation has been proposed to influence the R loop formation. A hyper-acetylated state of the chromatin could lead to a more opened and relaxed structure that would theoretically facilitate the probability of R loop generation. In human cells, it has been shown that depletion of the histone deacetylase mSin3a complex or the acetyltransferase MOF leads to an accumulation of R loops and genome instability (Salas-Armenteros et al., 2017; Singh et al., 2018). In addition, the treatment with histone deacetylase inhibitors such as trichostatin A (TSA) boosted a major acetylated state of the chromatin and R loop accumulation (Salas-Armenteros et al., 2017).

However, the accumulation of aberrant R loops have been linked to heterochromatin and chromatin condensation marks in yeast, *C. elegans* and human cells. Specifically, depletion of the THO complex or the helicase SETX/Sen1 triggers an accumulation of histone H3 serine 10 phosphorylation (H3S10-P) in yeast and human cells, a mark of chromatin condensation (Castellano-Pozo et al., 2013). Given that replisomes have difficulties to advance through a condensed chromatin (Castellano-Pozo et al., 2012b; Castellano-Pozo et al., 2013; El Achkar et al., 2005), it is logical to speculate about the role of chromatin condensation as a cause of RF stalling and genome instability mediated by R loops (Figure I7C) (Castellano-Pozo et al., 2013). Another piece of evidence linking chromatin with R loops is the FACT complex, necessary for the proper DNA replication and whose deprivation leads to an increase in R loops and genomic instability in yeast and human cells (Herrera-Moyano et al., 2014). Interestingly, recent studies in yeast have identified specific histone mutants that accumulate R loops without compromising genome integrity. This fact suggests that R loops may not generate DNA damage by themselves. Instead, it would require a subsequent chromatin-remodeling step connected to chromatin compaction that includes H3S10-P to cause genome instability (Garcia-Pichardo et al., 2017). Indeed, other studies have also shown the H3S10-P accumulation

at centromeres together with R loops and ATR, supporting the link between R loops and H3S10-P in these regions (Kabeche et al., 2018).

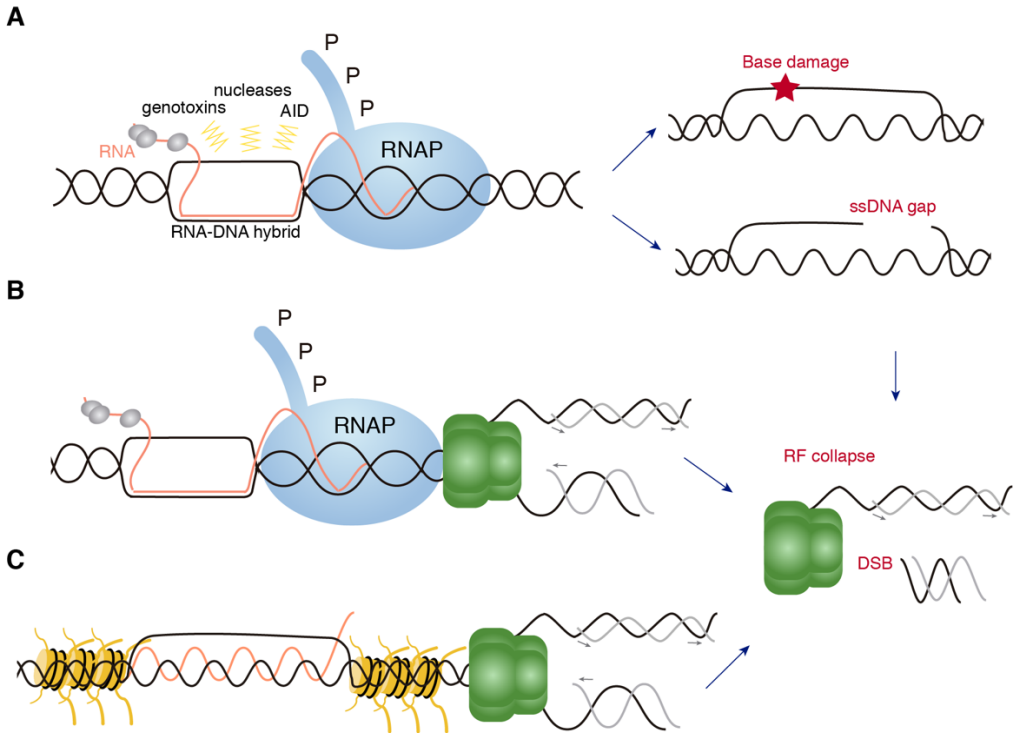

Figure I7. R loop-mediated genome instability.
R loops by themselves constitute a major source of genome instability. **(A)** R loop formation implies an increase in the exposition of the ssDNA, which is more sensible to suffer assaults from genotoxins or enzymatic activities such as AID. This could lead to DNA lesions such as base damage (red star) or ssDNA gaps, which can hamper RF progression leading to genome instability. **(B)** R loops by themselves could constitute an impediment for replication facilitating transcription-replication collisions. **(C)** Chromatin compaction after R loop formation could also hamper replication. Definitely, R loops could constitute a major barrier for RF progression and lead to fork stalling, subsequently fork collapse and breakage, leading to genome instability. Adapted from (Gaillard and Aguilera, 2016).

3.3. Mechanisms and elements involved in R loop prevention

As we previously indicated, R loops can occur naturally in cells. They are regularly generated over a large part of the genome (Chedin, 2016). Consequently, R loop homeostasis need to be controlled. For this purpose, cells have evolved different protection mechanisms and factors to overcome the R-loop formation and mitigate their harmful effect if deregulated (Santos-Pereira and Aguilera, 2015; Skourti-Stathaki and Proudfoot, 2014). In general, these factors are classified in two categories: those that prevent R loop formation

(topoisomerases and mRNP biogenesis) and those which remove R loops once formed (ribonucleases, helicases and others).

3.3.1. Topoisomerases

During transcription, local topological changes need to be controlled since the accumulation of negative supercoils behind the RNAP is thought to facilitate R loop formation. Topoisomerases can relax negative supercoiling and prevent R loop accumulation. This has been observed in bacteria where the growth defect of *topA* mutants, defective in Top1, are rescued by RNase H1 overexpression (Drolet et al., 1995), in yeast, in which *top1* and *top2* mutants present R loop accumulation at the rDNA locus (El Hage et al., 2010), and human cells, where TOP1-deficient cells show DNA breaks at active genes, replication defects and R loop accumulation that are suppressed by RNase H1 overexpression (Manzo et al., 2018; Tuduri et al., 2009).

3.3.2. mRNP biogenesis

The nascent mRNA is considered other important element that is target of the R loop prevention mechanisms, since deficiencies in the assembly of the messenger ribonucleoparticle (mRNP) can prompt to R loop formation. Eukaryotic gene expression is a tightly coupled process where transcription and mRNA processing need to be coordinated for the export of a functional mRNP. During this process, RNA-binding proteins (RBPs) associate with the nascent mRNA, contributing to the conformation of a correctly packaged and coated RNA molecule and thus, preventing its hybridization with the DNA template and R loop formation (Rondon et al., 2010). Evidence considering co-transcriptional R-loops as a source of genome instability were first shown in yeast cells where the absence of the yeast THO/TREX complex lead to hyperrecombination and instability phenotypes (Huertas and Aguilera, 2003). Since THO contributes to the co-transcriptional formation of export-competent mRNP, THO mutants increase the possibility of the nascent mRNA of hybridizing back to the DNA template during transcription forming an R loop (Aguilera, 2005b). Accordingly, THO-mutant phenotypes in yeast can be suppressed by the overexpression of

specific RNA-binding proteins such as Sub2 (human UAP56) or Tho1. Remarkably, the role of this complex seems to be conserved since deficient cells of yeast, *C. elegans* and human exhibit analogous transcription and mRNA export effects, as well as R loop-mediated genome instability that are accompanied by altered RF progression (Castellano-Pozo et al., 2012a; Chavez and Aguilera, 1997; Dominguez-Sanchez et al., 2011; Gomez-Gonzalez et al., 2011; Huertas and Aguilera, 2003; Wellinger et al., 2006).

Later on, many other transcription factors involved in R loop prevention have come to light. For instance, the human serine/arginine-rich splicing factor 1 (SRSF1) gene involved in splicing and mRNA export also prevents R loop formation (Li and Manley, 2005). In addition, the mRNAs half-life is another target to prevent R loop formation, as is the case of the Trf4 (polyadenilation polymerase) component of the TRAMP complex (Gavalda et al., 2013) or the human exosome components EXOSC3 and EXOSC10 (Pefanis et al., 2015) (Figure I8A). In fact, many global and specific studies have uncovered more elements related with RNA metabolism that have a role in R loop prevention (Chan et al., 2014; Paulsen et al., 2009; Stirling et al., 2012; Wahba et al., 2011). Consequently, these findings have evidenced that almost every defective RNA processing function can lead to R-loop accumulation, strengthening the importance of the RNA protection to guarantee genome integrity.

3.3.3. Ribonucleases, helicases and others

Since R loops are dynamic and reversible structures, when formed, they can be removed by different mechanisms that prevent their long-live and accumulation. R loops can be directly resolved by RNase H enzymes: RNase H1 (monomeric) and RNase H2 (three subunits in eukaryotes). Despite their different composition and specialized roles, both proteins are able to degrade the RNA moiety of an RNA-DNA hybrid (Cerritelli and Crouch, 2009; Skourti-Stathaki and Proudfoot, 2014). However, RNase H1 is considered to be the key player in eliminating co-transcriptional R loops (Chon et al., 2013) and its overexpression is continuously used to suppress R loop-dependent genome instability phenotypes.

Additionally, R loops can be removed by RNA-DNA helicases which unwind the RNA-DNA hybrids. One well-studied example is the helicase senataxin SETX (Sen1 in yeast). This protein and others such as DHX9 are proposed to unwind R loops, specially at transcription termination pause sites (Cristini et al., 2018; Mischo et al., 2011; Skourti-Stathaki et al., 2011). Thus, after the unwinding of the RNA-DNA hybrid, the nascent RNA is exposed for its degradation by exonucleases such as Xrn2, leading to termination. Subsequently, absence of either of these factors results in R loop accumulation and altered termination (Cristini et al., 2018; Skourti-Stathaki et al., 2011). In this context, the human RNA helicase aquiarius (AQR) protein, which belongs to the same family as SETX, has been also suggested to have a role in R loop resolution since its depletion lead to an R loop accumulation phenotype (Sollier et al., 2014) (Figure I8B).

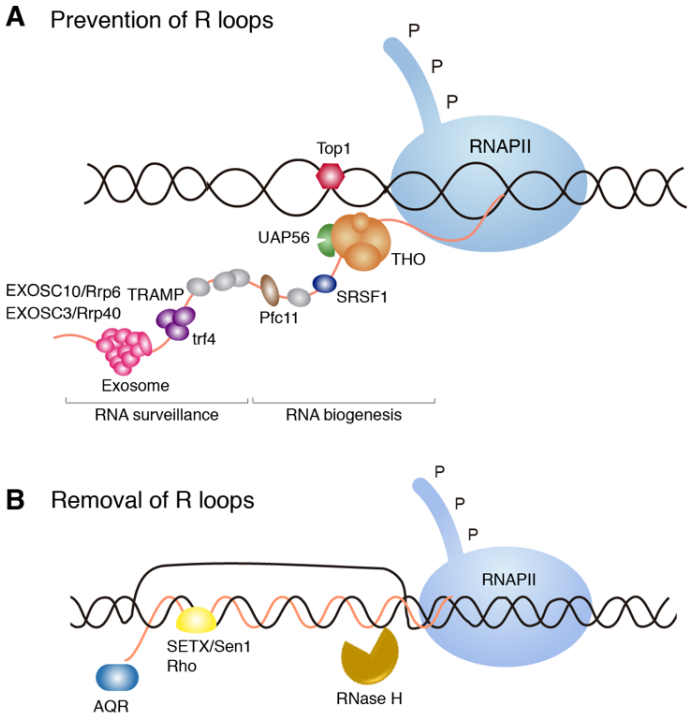

Figure I8. Action to prevent or resolve R loop accumulation.
(A) R loop control can occur at different steps during transcription. On one hand, topoisomerases (TOP1) avoid supercoiling accumulation that could facilitate R loop formation. On the other hand, specific RNA-binding proteins acting at different steps of RNA metabolism from RNA biogenesis (THO complex, UAP56, SRSF1 and Pcf11) to RNA surveillance (including the exoribonucleases exosome component 3 (EXOSC3) and EXOSC10 (Rrp40 and Rrp6 in yeast, respectively) and the TRAMP complex prevent the RNA to hybridize back with DNA. **(B)** R loop removal could be achieved by different mechanisms. RNase H recognizes RNA-DNA hybrids and degrade the RNA moiety. Moreover, helicases such as SETX/Sen1 in human and yeast, Rho in bacteria and

putative ones such human aquarius (AQR) could unwind R loops. Adapted from (Santos-Pereira and Aguilera, 2015).

There are other factors that normally resolve other forms of stresses that might indirectly help resolve R loops. For instance, the transcription-coupled nucleotide excision repair (TC-NER) factors can help process R loops (Shivji et al., 2018; Sollier et al., 2014; Yasuhara et al., 2018). Although the mechanism involved is not completely understood, it is proposed that TC-NER nucleases XPG and XPF could excise R loops, leaving a ssDNA gap that could progress to a DSB (Sollier et al., 2014). Importantly, the breast cancer susceptibility factors BRCA1 and BRCA2 have also been found to help resolve R loops (Bhatia et al., 2014; Hatchi et al., 2015; Shivji et al., 2018). Generally, as both factors associates with RNAPII, they are able to suppress R loop-mediated transcriptional stress by promoting elongation and resolving R loops (Shivji et al., 2018; Zhang et al., 2017). It is proposed that BRCA1 recruits the helicase SETX to remove R loops at termination sites. Fanconi Anemia factors or the FACT chromatin reorganizing complex involved in RF progression also help prevent R-loop accumulation and R loop-mediated genome instability at transcription-replication conflicts (Figure I9) (Garcia-Rubio et al., 2015; Herrera-Moyano et al., 2014).

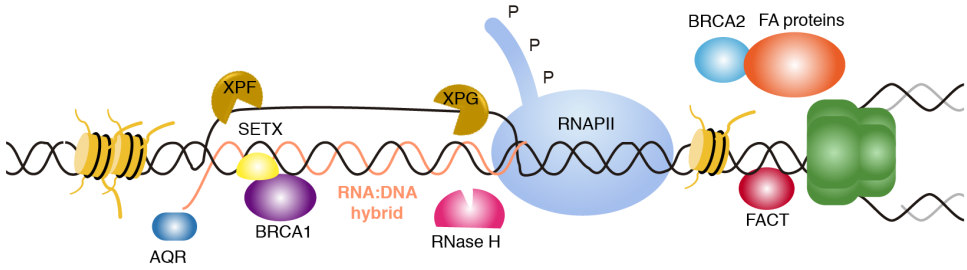

Figure I9. Multiple factors involved in R loop-mediated T-R conflicts.
R loops and R loop-mediated chromatin compaction can hamper RF progression. In addition to the already mentioned RNase H and SETX, which could be recruited by BRCA1 to R loop sites, there are other factors implied in R loop resolution under these circumstances. For instance, BRAC2, TC-NER factors and potentially other Fanconi anemia (FA) proteins or the FACT chromatin-reorganizing complex can help to counteract this situation.

3.4. Techniques to detect R loop accumulation

Direct detection of R loops has relied on the use of the S9.6 monoclonal antibody, which recognizes RNA-DNA hybrids. However, the suspicion of the lack of

specificity of this antibody has always been a concern. Indeed, recent reports have demonstrated its ability to bind also to dsRNA (Hartono et al., 2018; Silva et al., 2018). As a consequence, other indirect strategies have been performed to demonstrate the existence of R loop accumulation, including the suppression of R loop-dependent phenotypes by RNase H overexpression. In particular, RNase H1 presents a hybrid-binding domain (HBD) in the N-terminus (Nowotny et al., 2008), whereas the RNase H2 main activity is to cleave a single ribonucleotide embedded in the DNA duplex (Eder et al., 1993). The combination of both strategies using the S9.6 and the subsequent overexpression of RNase H to suppress the R loop-dependent phenotype has served to overcome the S9.6 limitations. In addition to S9.6 immunofluorescence (IF) or DRIP (DNA-RNA hybrid immunoprecipitation), numerous techniques have been applied for genome-wide detection of R loops using the S9.6 antibody such as DRIP followed by sequencing (DRIP-seq) (Ginno et al., 2012) or the most accurate DRIP followed by cDNA conversion coupled to high-throughput sequencing (DRIPc-seq) (Sanz et al., 2016). In addition, bis-DRIP-seq (Dumelie and Jaffrey, 2017) combines *in situ* ssDNA bisulfite footprinting with S9.6 hybrid pull-down to theoretically improve the specificity by targeting both, the hybrids and the ssDNA. However, there have been increasing efforts in the field to abandon the use of the S9.6 antibody. Due to these facts, new alternatives beyond the use of the S9.6 have been proposed such as R-ChIP, where the expression of the exogenous catalytically inactive form of the RNase H1 is followed by chromatin immunoprecipitation (ChIP) of the tagged RNase H1 (Chen et al., 2017) or the use of the fusion protein HB-GFP formed by the 52-residue DNA-RNA hybrid-binding (HB) domain of the RNase H1 and the enhanced green fluorescent protein (eGFP), which is able to detect RNA-DNA hybrids *in vivo* (Bhatia et al., 2014).

4. EPITHELIAL-MESENCHYMAL TRANSITION AND THE TRANSCRIPTION FACTOR SNAIL1

4.1. Epithelial-Mesenchymal transition

The epithelial-mesenchymal transition (EMT) is a crucial and reversible cell plasticity program occurring during embryonic development and in adult tissue homeostasis. When completed, it promotes the transition from an immotile epithelial to a motile mesenchymal cell type. When aberrantly activated, it could lead to pathogenic effects, particularly cancer. Phenotypically, cells undergoing EMT lose their apical-basal polarity, tight intercellular contacts and interaction with the basal membrane. They acquire a spindle-like appearance, gain motility and invasiveness. These profound cellular attribute changes require an extensive transcriptional reprogramming, that relies on down- and upregulation of epithelial and mesenchymal gene expression programs, respectively. Under a wide range of pleiotropic signaling factors, the EMT is triggered in association with the activation of the expression of specific transcription factors such as Snail1 (SNAI1), Slug (SNAI2), Twist-related protein 1 (TWIST1) and zinc-finger E-box-binding homeobox 1 (ZEB1) and ZEB2; and miRNAs and epigenetic and post-translational regulators. These transcription factors are responsible of the control of the expression of two broad functional groups of genes: epithelial genes, whose expression is repressed and, mesenchymal genes, whose expression is induced. From a molecular point of view, the hallmark of EMT is the down-regulation of E-cadherin. Other epithelial markers such as claudins and occludins are also down-regulated. While Fibronectin 1 (FN1) or Vimentin, typical mesenchymal markers are up-regulated during EMT (Figure I10) (Nieto et al., 2016; Stemmler et al., 2019).

As mentioned before, EMT is also important under pathological circumstances, where a reactivation of developmental programs take place, such as cancer progression. EMT is thought to enhance stemness of cancer cell during the process of tumor metastasis, facilitating the execution of most of the steps of the invasion-metastasis cascade. Invasion permits the translocation of tumor cells from the initial neoplastic focus into neighbouring host tissues, allowing them

to penetrate vessel endothelium and enter the circulation to form distant metastasis. (Guarino et al., 2007; Mani et al., 2008; Thiery, 2003; Thiery et al., 2009).

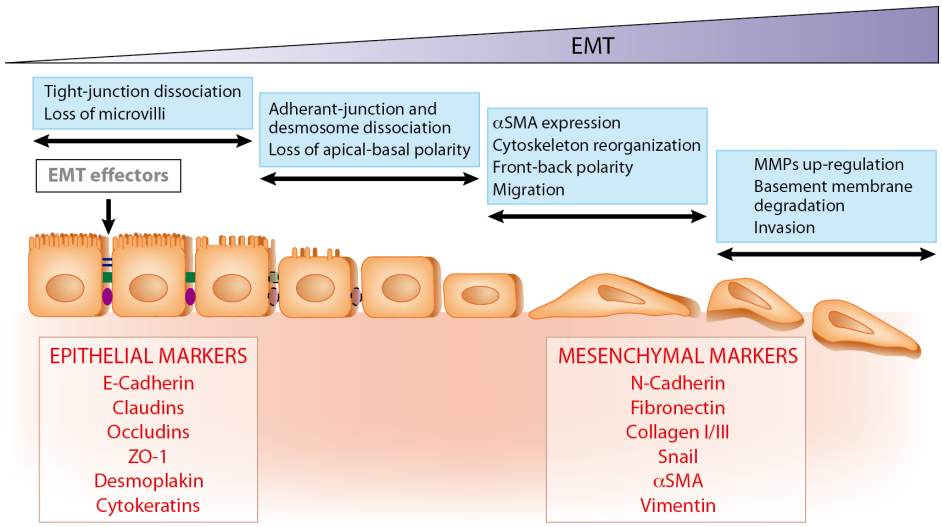

Figure I10. Principal traits during epithelial-mesenchymal transition.
During this process cells undertake different events to accomplish the entire EMT course. Image also shows the main epithelial and mesenchymal markers. Adapted from (Aroeira et al., 2007).

4.2. Snail1

Snail1 is a conserved zinc-finger transcription factor. Its C-terminal domain contains four zinc fingers of the C_2H_2 type that bind to the E-box motif 5′-CANNTG-3′ or 5'-CAGGTG-3' in target gene promoters. The divergent N-terminal region is involved in the repressive activity and is essential for the interaction with several co-repressor complexes such as mSin3A, Ajuba LIM proteins or the Polycomb repressive complex 2 (Wang et al., 2013). Lastly, the central part of the protein comprises a nuclear export signal (NES), a destruction box domain and a serine-proline rich region, involved in the stability and subcellular location of the protein (Figure I11).

Importantly, Snail1 has been purposed as a prototype inductor of EMT. It is fast induced by citokynes or stress conditions activating EMT and it is able to bind and repress the expression of E-cadherin and other epithelial genes and activate the expression of other mesenchymal genes. Given its relevance in this process, Snail1 expression and function are regulated at multiple levels from

gene transcription to protein modifications, affecting its interaction with specific cofactors including TGFβ, NOTCH, WT or NF-κB (Thiery and Sleeman, 2006).

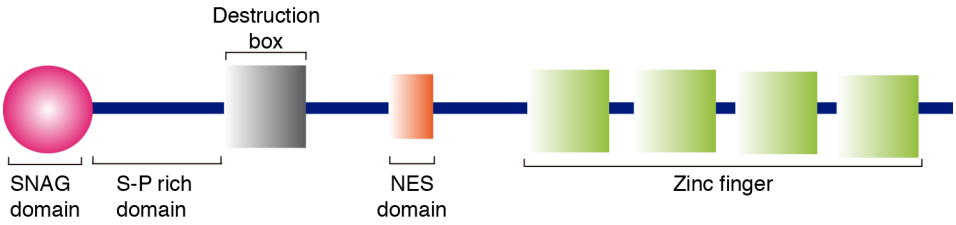

Figure I11. Structure of Snail1.
Snail1 contains an N-terminal SNAG domain, which interacts with different co-repressors and epigenetic remodeling complexes and the C-terminal zinc finger domain for DNA binding. The serine-rich domain, the destruction box and the nuclear export sequence (NES) are involved in the stability and subcellular location of the protein. Adapted from (Peinado et al., 2007)

Research in the last decade has revealed a connection between Snail1 and the co-repressor interactor LOXL2 in regulating major satellite transcription and heterochromatin reorganization during EMT. Upon the binding of Snail1 and LOXL2 to pericentromeric regions, HP1α is released from heterochromatin with a down-regulation of major satellite transcription, enabling chromatin reorganization and acquisition of mesenchymal traits. Notably, the histone-modifying enzyme LOXL2 replaces the active mark from histone H3 (H3K4me3) by a deaminated lysine generating the variant H3K4ox. Given that a particular chromatin state can influence the DDR response (Burgess and Misteli, 2015; Goodarzi et al., 2008), recent findings have suggested a connection between LOXL2 and the activation of the DDR pathway in the absence of any detectable DNA lesions in specific breast cancer cell lines. It has been proposed that the lack of LOXL2 and the reduction of H2K4ox levels modify the regulation of chromatin condensation (leading to decondensation) and trigger DDR (Cebria-Costa et al., 2019).

OBJECTIVES

The main goal of this thesis is to determine the implication of UAP56 and Snail1 in genome integrity and their mechanisms of action. For this purpose, we addressed the following specific objectives:

1. To define the role of UAP56 in the maintenance of genome integrity, with the aim of obtaining new insights into the molecular mechanism of this factor to prevent genome instability.
2. To assay the contribution of UAP56 to genome stability all over the genome and evaluate its significance in comparison with the helicase DDX5.
3. To explore the possible implication of Snail1 as a novel factor involved in R loop-mediated genome instability.

RESULTS

1. ROLE OF UAP56 IN THE MAINTENANCE OF GENOME INTEGRITY

Given the reported interaction between THOC1 and UAP56 (Strasser et al., 2002), we speculated about the possible role of UAP56 in the maintenance of genome integrity, as it occurs with THO (Dominguez-Sanchez et al., 2011). For this purpose, we performed a functional analysis of UAP56 using RNA interference (RNAi) in human cells.

1.1. Depletion of UAP56 via siRNA

In order to analyze the role of UAP56 as a genome stability protector, UAP56 was depleted via small interfering RNA (siRNA) from HeLa cells. As can been seen by RT-PCR and Western blot experiments, UAP56-depleted cells exhibit almost undetectable levels of mRNA and UAP56 protein after 72 hours of transfection corroborating the efficiency of this siRNA pool (Figure R1).

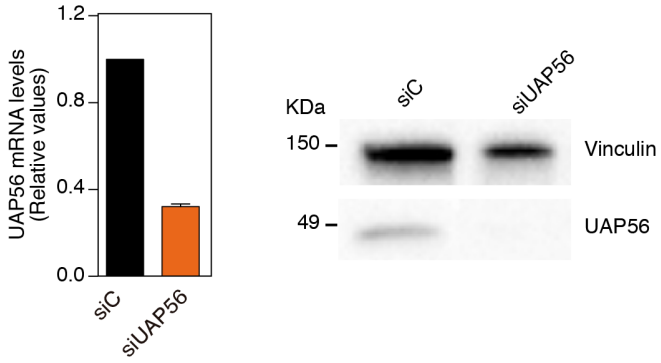

Figure R1. siRNA silencing of UAP56 in human cells.
(Left) RT-qPCR in siRNA transfected HeLa cells to measure the relative levels of *UAP56* mRNA, using the HPRT housekeeping gene to normalize those values. (Right) UAP56 expression in siC control and UAP56-depleted HeLa cells determined by Western blot. Vinculin protein used as a loading control.

1.2. Association between UAP56 and Sin3A complex

Since, as previously reported, UAP56 is known to interact with the THO complex subunit THOC1 (Strasser et al., 2002) and THOC1 physically interacts with the mSin3A scaffold protein SIN3 (Salas-Armenteros et al., 2017), we wondered whether UAP56 also interacted with SIN3. For this purpose, we performed co-immunoprecipitation (co-IP) assays with an anti-UAP56 antibody. SIN3 was detected in in the immunoprecipitated of HEK293T cells (Figure R2A) revealing the *in vivo* interaction between UAP56 and SIN3.

We confirmed this physical interaction *in situ* by Proximity Ligation Assay (PLA) (Soderberg et al., 2006). High levels of PLA signal were detected after the addition of anti-UAP56 and anti-SIN3 specific antibodies highlighting a close association between these two proteins. Importantly, this physical proximity is detected only in the nucleus, where both proteins are known to function (Figure R2B). This result is consistent with the idea that UAP56 as THO and likely other RNA binding factors participating in the assembly of the nascent mRNP.

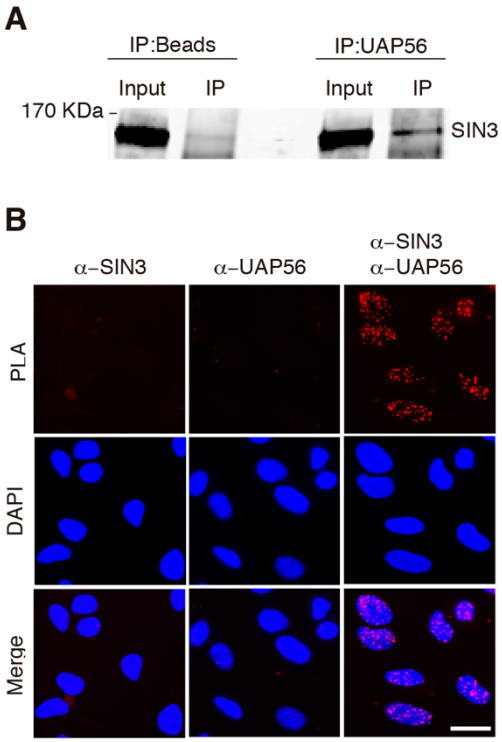

Figure R2. Interaction analysis of UAP56 and SIN3.
(A) Co-IP analysis of whole cell extracts of HEK293T with anti-UAP56 antibody showing the interaction between UAP56 and SIN3. Western blot using SIN3 antibody of input extract and total immunoprecipitated (IP). **(B)** PLA experiments corroborating the physical proximity of UAP56 and SIN3 endogenous proteins. Red spots are representative of a positive PLA signal. The use of only one antibody is used as a negative control. Scale bar, 25 μm.

1.3. Genome instability in UAP56-depleted cells

Once established the connection among these proteins, we hypothesized that the role of UAP56 in the maintenance of genome integrity could be related to that of THOC1 (Dominguez-Sanchez et al., 2011) and SIN3A (Salas-Armenteros et al., 2017). We first showed that transient depletion of UAP56 in HeLa cells (Figure R1) leads to an accumulation of DNA breaks, as detected by single-cell electrophoresis (comet assay) and γH2AX foci monitored by immunofluorescence (IF) in comparison with siC control cells, consistent with previous results (Dominguez-Sanchez et al., 2011). Both SSBs and DSBs were detected by alkaline and neutral comet assays. UAP56-depleted cells lead to a

significant increase in tail moment (Figure R3A,B). To determine whether this DNA break accumulation in siUAP56 cells was dependent on transcription, we performed alkaline comet assay in cells in which transcription was inhibited with the adenosine antagonist 3' deoxyadenosine (cordycepin), a specific inhibitor of RNA chain elongation (Tuduri et al., 2009). The addition of cordycepin fully suppressed the increase in DNA breaks (Figure R3A). We next assayed whether the increase in DNA damage was also dependent on RNA-DNA hybrids. For this purpose, we overexpressed human RNase H1 and analyze the γH2AX foci as a marker of DNA damage. We found that these foci were significantly reduced in siUAP56 cells (Figure R3C), indicating that DNA damage was R loop-dependent.

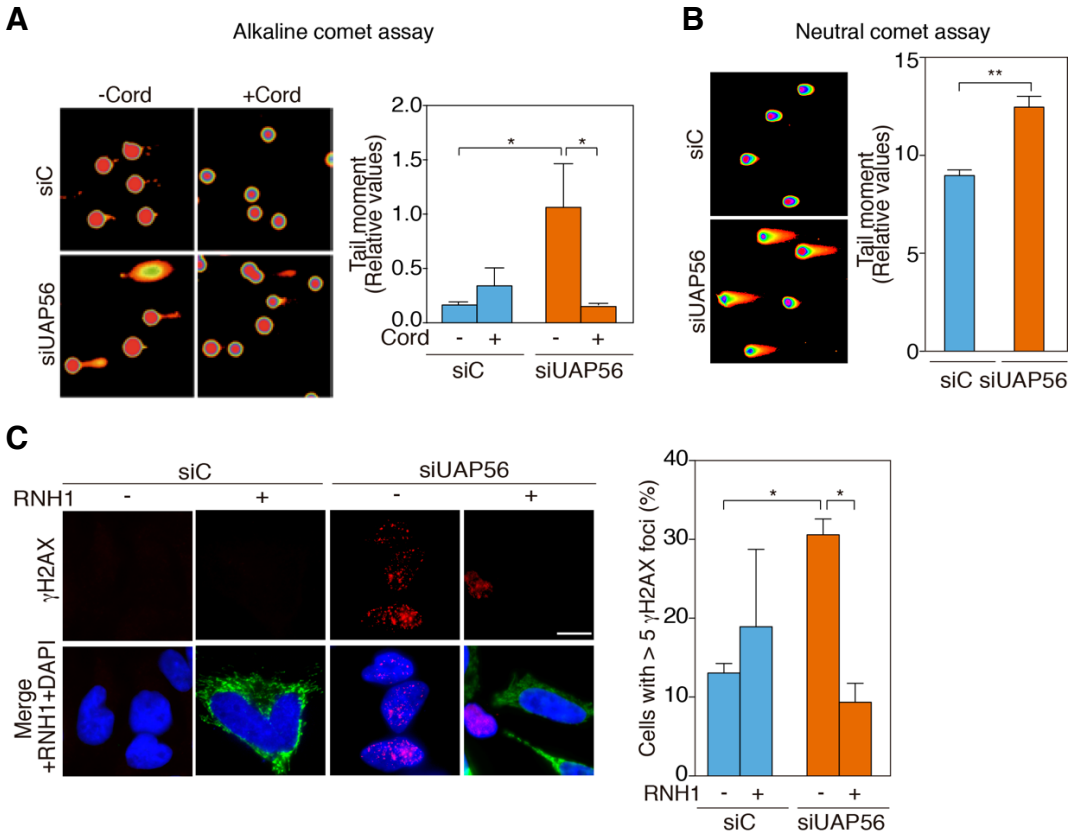

Figure R3. Accumulation of DNA breaks in UAP56-depleted cells.
(A) Alkaline comet assay of siC and siUAP56-depleted HeLa cells untreated or treated with 50 μM of cordycepin for 4 hours. **(B)** Neutral comet assay of siC and siUAP56-depleted HeLa cells. **(C)** γH2AX immunofluorescence in siC control and UAP56-deprived cells. Percentage of cells with > 5 γH2AX foci was shown. Nuclei were stained with DAPI. Comet-tail moments and γH2AX foci are represented as means and SEM (n=3). *, $P < 0.05$; **, $P < 0.01$(Student T-test). Scale bar, 25 μm.

1.4. R loop accumulation in UAP56-depleted cells

Next, we assayed whether R loops were increased, as a way to explain the described phenotypes. We first assayed R-loops by IF using the anti-RNA-DNA hybrid S9.6 monoclonal antibody and observed a significant increase in the S9.6 nuclear signal in siUAP56 cells (Figure R4A). To confirm this result with a more reliable technique that eliminated the possibility of mixed signals of RNA-DNA hybrids and putative dsRNAs that the S9.6 might be able to detect in IF experiments (Hartono et al., 2018; Silva et al., 2018), we analyzed hybrid accumulation by DRIP-qPCR in a set of genes that have been previously validated for this purpose (Bhatia et al., 2014). As can be seen in Figure R4B, RNA-DNA hybrids increased in UAP56-depleted cells up to 2-fold above the siC control levels in the analyzed genes (*APOE, RPL13A and EGR1*). Consistently, the RNA-DNA hybrid signals were completely removed by *in vitro* RNase H treatment as a confirmation of the specificity of the assay. Altogether, the data indicate that UAP56 depletion leads to a significant increase of R loops and R-loop-mediated genome instability at cellular and molecular levels.

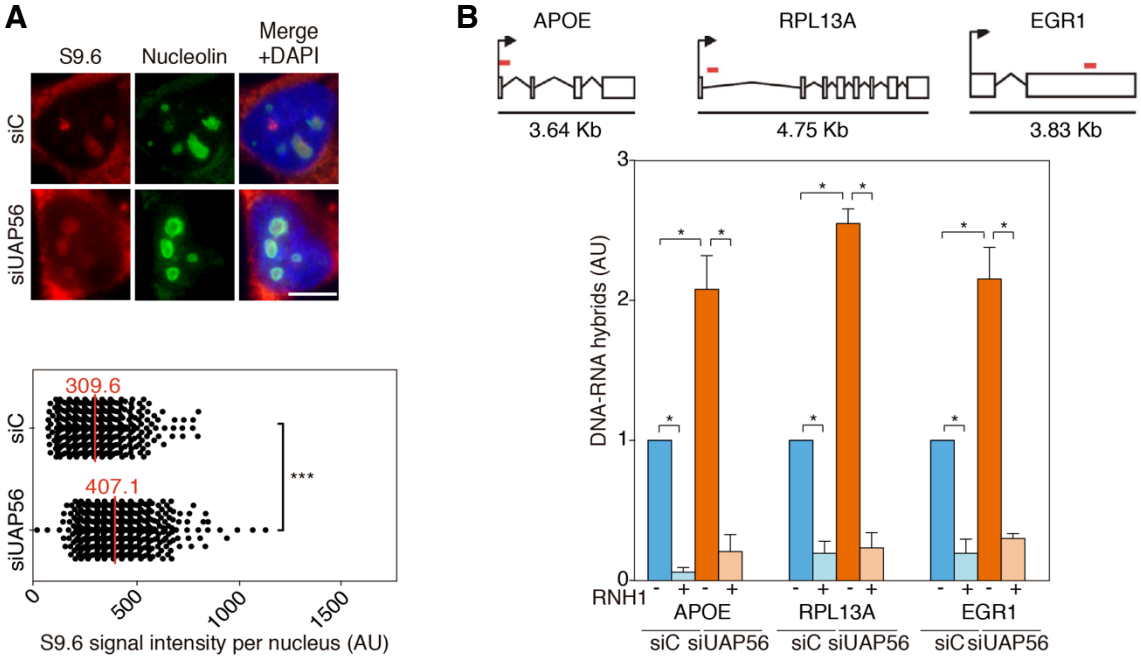

Figure R4. R loop accumulation in UAP56-depleted cells.
(A) Immunofluorescence of S9.6 (red) and anti-nucleolin (green) in siC and siUAP56-transfected HeLa cells. The median of S9.6 signal intensity per nucleus after nucleolar signal removal is represented (n=3). ***, $P < 0.001$ (Mann-Whitney U test, two-tailed). Scale bar, 10 μm. **(B)** DRIP-qPCR in siC and siUAP56-transfected cells at indicated regions (red lines). Samples were treated or not with RNase H prior immunoprecipitation. Values normalized respect to the siC control are plotted (n=3) as means and SEM. *, $P < 0.05$ (Mann-Whitney U test).

Importantly, accumulation of γH2AX foci and S9.6 signal after UAP56 depletion was rescued by the transfection with a plasmid overexpressing UAP56, indicating that the DNA damage and R loop accumulation phenotypes in UAP56-depleted cells were specifically dependent on the reduction of UAP56 levels and not due to off-target effects (Figure R5A, B).

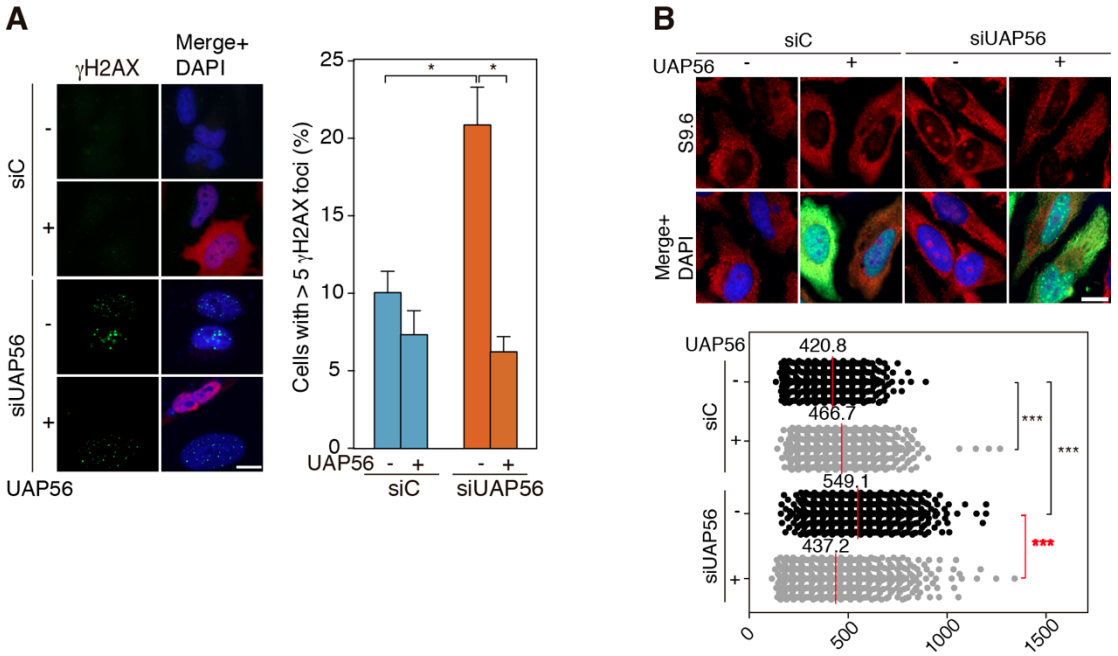

Figure R5. Ectopic expression of UAP56 in UAP56-depleted cells.
(A) Immunofluorescence of HeLa cells stained with antibodies anti-γH2AX and anti-FLAG (for UAP56 detection). After siRNA transfection for 72 hours, cells were also transfected with the empty plasmid or the UAP56 plasmid for UAP56 siRNA-resistant expression. More than 100 cells expressing UAP56 (positive-stained) or of mixed population transfected with the empty plasmid were counted in each experiment. Percentage of cells with > 5 γH2AX foci are plotted (n=3) as mean and SEM. *, $P < 0.05$ (Student T-test, two tailed). **(B)** Immunostaining of HeLa cells using the S9.6 antibody (red) and anti-FLAG (for UAP56 detection, green) in siC and siUAP56-transfected cells followed by transfection with the empty plasmid or the UAP56 plasmid for UAP56 siRNA-resistant expression. More than 100 cells expressing UAP56 (positive-stained) or of mixed population transfected with empty plasmid were counted in each experiment. The median of S9.6 signal intensity per nucleus (n=3). The red asterisks indicate the significant decrease in the S9.6 signal. ***, $P < 0.001$ (Mann-Whitney U test, two-tailed).

To discard that the alteration of the cell cycle progression was the responsible of the observed phenotypes in siUAP56-depleted cells, we analyze the cell cycle distribution of asynchronously growing siRNA-transfected HeLa cells. Cells were collected and incubated with Propidium Iodide, and then subjected to FACS analysis. We could not observe any significant different in the percentages of cells in G1, S or G2. (Figure R6).

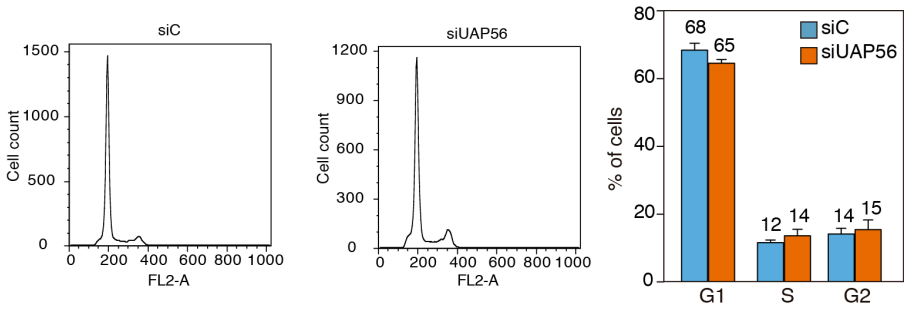

Figure R6. Cell cycle progression analysis in UAP56-depleted cells.
FACS analysis of asynchronously growing HeLa cells control or depleted of UAP56 incubated with Propidium Iodide to separate cells based on their DNA content.

1.5. Replication impairment in UAP56-depleted cells

Given the accumulated evidence indicating that RF stalling is a major cause of R loop-dependent DNA damage (Aguilera and Garcia-Muse, 2012; Hamperl et al., 2017), next we determined the impact of UAP56 depletion on replication in HeLa cells. First, we analyzed the levels of FANCD2 foci by IF, provided that Fanconi Anemia factors accumulate at sites of putative RF blockages caused by R loops (Garcia-Rubio et al., 2015). As can be seen in Figure R6A, a significant increase of FANCD2 foci was observed in UAP56-depleted cells as compared to the siC control. Importantly, overexpression of RNase H1 in these cells drastically reduced this increase of FANCD2 foci, suggesting that R-loop accumulation in UAP56-depleted cells leads to RF blockage that requires the action of Fanconi Anemia pathway for its processing.

To investigate more accurately whether RF progression was affected in UAP56-depleted cells, we performed single-molecule DNA combing assays. For this, two thymidine analogues Iododeoxyuridine (IdU) and Cloro-deoxyuridine (CldU) were added sequentially to the cell media and subsequently incorporated into the DNA during replication. Afterwards, these analogues were immuno-detected over the stretched of isolated DNA. These experiments in HeLa cells depleted of UAP56 via siRNA for 72 hours revealed a significantly slower RF progression in siUAP56 cells than in the siC control cells (Figure R6B). This reduction in RF velocity was paralleled by an increase in the frequency of RF stalling as measured by RF asymmetry (Figure R6B). This was calculated as the

distance that is longer a track compared to the other for each pair of sister RFs (see Materials and Methods 12.2), suggesting that RF stalling can also contribute to reduce the RF velocity in these cells. Then, we wondered whether replication failures were associated with R loops. Analysis of RF progression of DNA combing after RNase H1 overexpression showed the recovery of RF velocity and asymmetry (Figure R6B). Therefore, our results indicate that silencing of UAP56 promotes slower RF progression and RF stalling that are mediated by R-loops, suggesting that these are a primary cause of the increased DNA damage.

Finally, given that UAP56 interacts with both THOC1 and SIN3, we also studied RF progression in HeLa cells depleted of these proteins for 72 hours. Interestingly, the experiments revealed a faster replication velocity (Figure R8) accompanied by an increase in the frequency of RF stalling as measured by RF asymmetry (Figure R8). Then, we considered the possibility that these RF phenomenon alterations were also R loop-dependent. To asses that, RNase H1 was overexpressed in the cells deprived of THOC1 or SIN3. Curiously, both phenotypes, fork velocity and asymmetry, were suppressed upon RNase H1 overexpression. Hence, as happened in UAP56-depleted cells, R loops are the main responsible of the alteration in the RF progression in these cells.

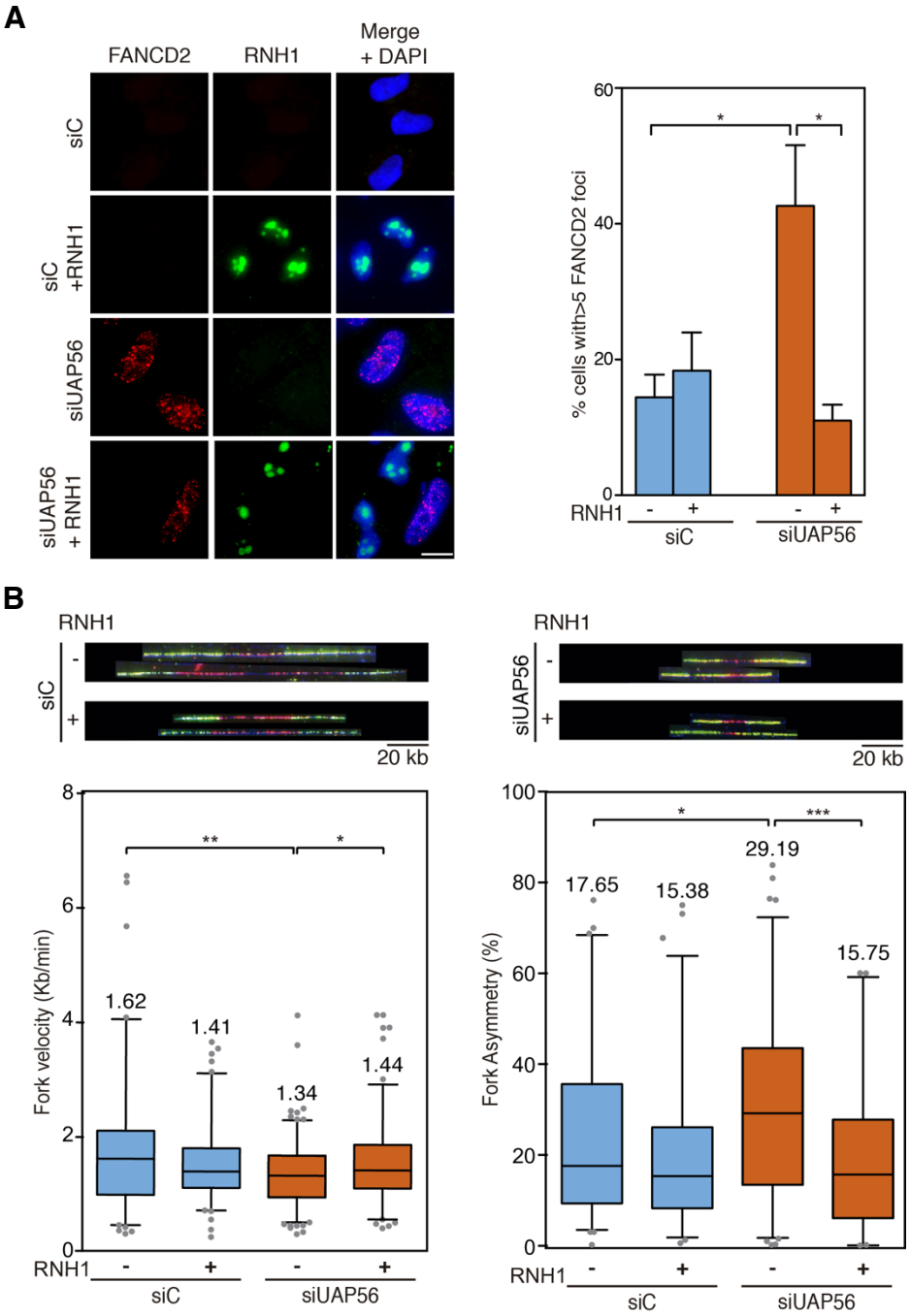

Figure R7. Replication analysis of UAP56-depleted cells.
(A) Immunofluorescence of FANCD2 in siC and siUAP56 HeLa cells with or without RNase H1 overexpression. The graph shows the quantification of the percentage of cells containing >5 FANCD2 foci. More than 100 cells overexpressing RNase H1 (pcDNA3-RNaseH1) (positive-stained) or more than 100 cells of mixed population transfected with the empty vector (pcDNA3) were counted in each of the three experiments. **(B)** Effect of UAP56 depletion on DNA replication detected by single molecule DNA combing assay. Representative picture of DNA fibers labeled by IdU and CIdU for single DNA molecule analysis in HeLa cells. Profiles of RF velocity and asymmetry of siC and siUAP56 HeLa cells transfected with the empty vector pcDNA3 or pcDNA3-RNaseH1 (+RNH1) for RNase H1 overexpression are shown. Data are plotted as box and whiskers (5-95 percentile) where median values are indicated (n=2). *, $P < 0.05$; **, $P < 0.01$ (Mann-Whitney U test, two-tailed).

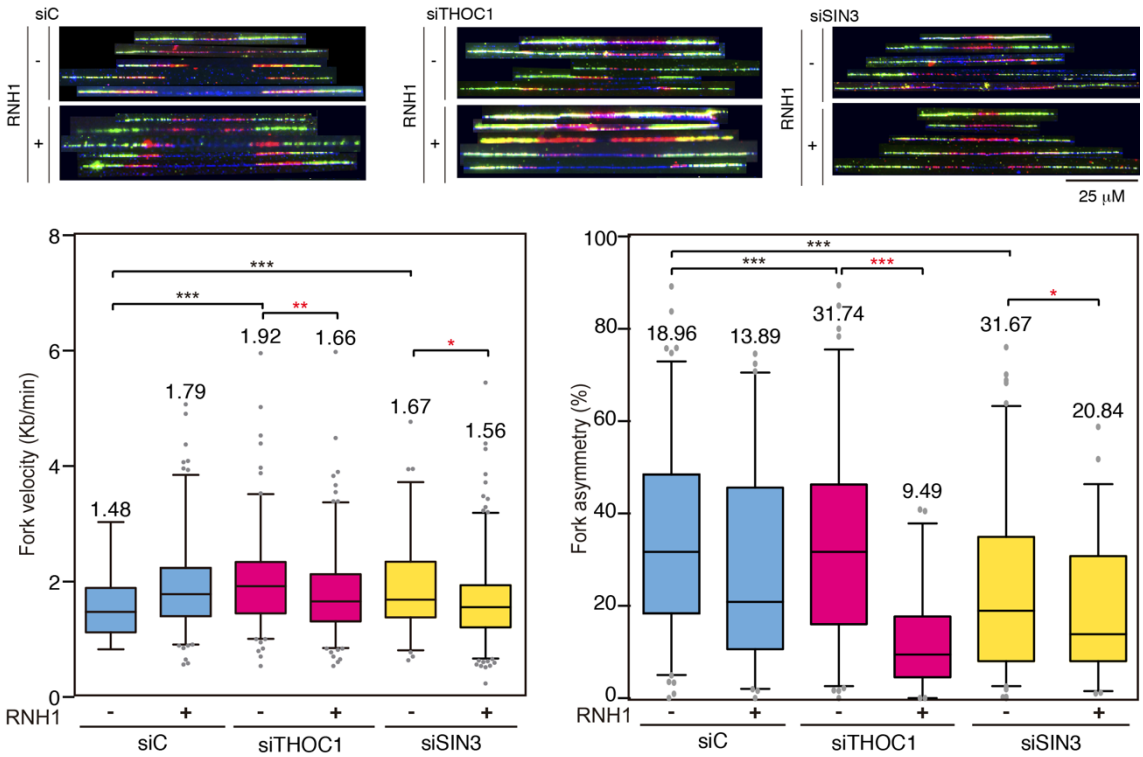

Figure R8. Replication analysis in THOC1- and SIN3-depleted cells.
Effect of THOC1 and SIN3 depletion on DNA replication detected by single molecule DNA combing assay. Profiles of RF velocity (left) and asymmetry (right) of siC, siTHOC1 and siSIN3 HeLa cells transfected with the empty vector pcDNA3 or pcDNA3-RNaseH1 (+RNH1) for RNase H1 overexpression are shown. Red asterisk refer to the significant decrease of the parameter studied. Data are plotted as box and whiskers (5-95 percentile) where median values are indicated (n=2). *, $P < 0.05$; **, $P < 0.01$; *** < 0.001 (Mann-Whitney U test, two-tailed).

1.6. Chromatin condensation by UAP56 depletion

Recent reports have proposed that R loops that are linked to genome instability are associated with histone H3 phosphorylation at serine 10 (H3S10-P)(Castellano-Pozo et al., 2013) and the importance of the chromatin reorganizing complex FACT preventing R loop-dependent transcription-replication conflicts (Herrera-Moyano et al., 2014). In this line, since the mark of chromatin condensation H3S10-P has been linked to R loops in SETX- and THOC1-depleted cells, we wondered whether UAP56 depletion could lead also to an increase in H3S10-P. For this, we performed immunofluorescence with anti-H3S10-P antibody in control, UAP56- and THOC1-depleted HeLa cells in EdU-containing media. As previously reported, we observed an increase in the

percentage of cells with more than 5 H3S10-P foci in THOC1-depleted cells (3.6%), as well as in UAP56-depleted cells (2.36%) (Figure R9). This result suggests that UAP56 could work as THOC1 in the prevention of R loop accumulation that triggers chromatin compaction that could lead to genome instability. However, further studies need to be addressed to clarify the role of UAP56 in this issue.

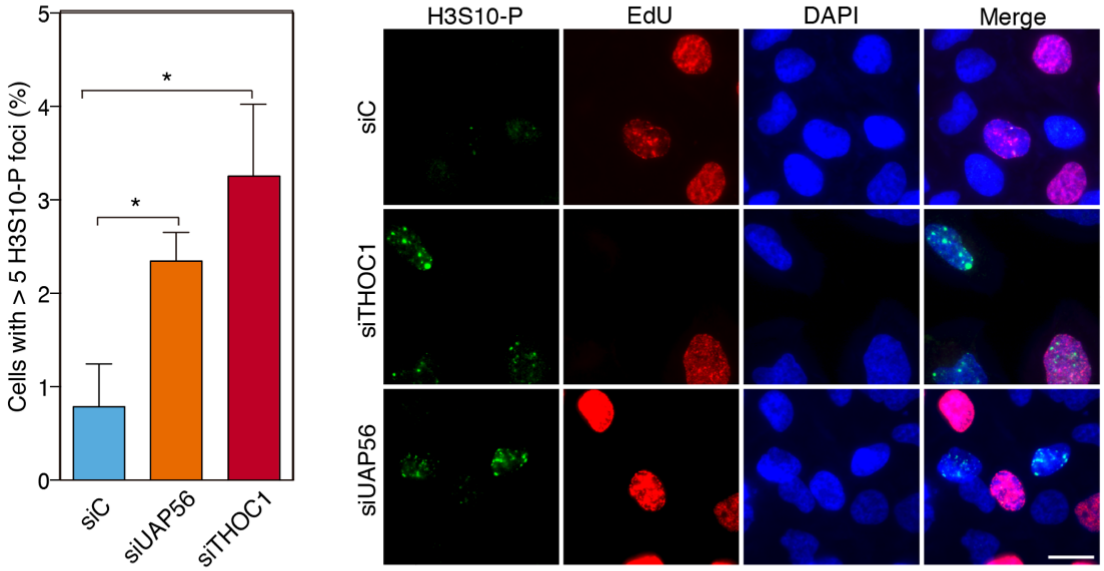

Figure R9. Analysis of H3S10-P in UAP56-depleted cells.
Immunofluorescence of H3S10-P in HeLa cells deprived of THOC1 or UAP56. Percentage of cells containing > 5 H3S10-P foci excluding S-phase and mitotic cells, identified by EdU labeling or DAPI staining, respectively. Data are represented as means and SEM (n=4). Scale bar, 25 μm. *, $P < 0.05$ (Student's t-test).

1.7. UAP56 *in vitro* activity

Given that UAP56 is a DEAD-box RNA dependent ATPase (Shen et al., 2007), we wondered whether it possesses RNA-DNA unwinding activity that could explain the strong R loop accumulation of siUAP56 cells. For this, we collaborated with Xue Xiaoyu and Patrick Sung in Yale University. UAP56 was purified from WT and two mutants, UAP56-K95A and E197A (Figure R10A), that lack ATPase activity (Figure R10B). Using a blunt-ended RNA duplex (dsRNA) of 13 base pairs, it could be observed that UAP56 unwinds this substrate in a protein concentration-dependent manner, consistent with previous results (Shen et al.,

2007) (Figure R10C). Similar results were obtained using other dsRNA substrates with either a 5' or 3' overhang (Figure R10D).

Next, unwinding of RNA-DNA hybrid with a 5' or 3' RNA overhang was tested. UAP56 could unwind both substrates in a protein concentration and ATP-dependent manner (Figure R11A). In contrast, UAP56 was unable to unwind dsDNA (Figure R11B). Importantly, the percentage of unwound product with the RNA-DNA hybrids was up to 4 fold of that obtained for dsRNA (Figure R11C). Therefore, UAP56 is more adept at unwinding RNA-DNA hybrids than dsRNA. To confirm the molecular identity of this unwinding activity we constructed new plasmids to purify mutant UAP56-K95A and UAP56-E197A proteins that have been previously reported to be deficient for the ATPase activity and, therefore, for its helicase activity (Shen et al., 2007). We confirmed that neither UAP56-K95A nor UAP56-E197A could unwind the RNA-DNA substrates (Figure R11A). Finally, UAP56 activity was tested with a 5' RNA-DNA flap structure that resembles a branch migratable R-loop (Schwab et al., 2015). As shown in Figure R11D, UAP56, but not the UAP56-K95A or UAP56-E197A mutant, could dissociate the flap structure to yield a dsDNA product. Therefore, we can conclude that UAP56 resolves RNA-DNA hybrids as well as R-loop-mimicking structures.

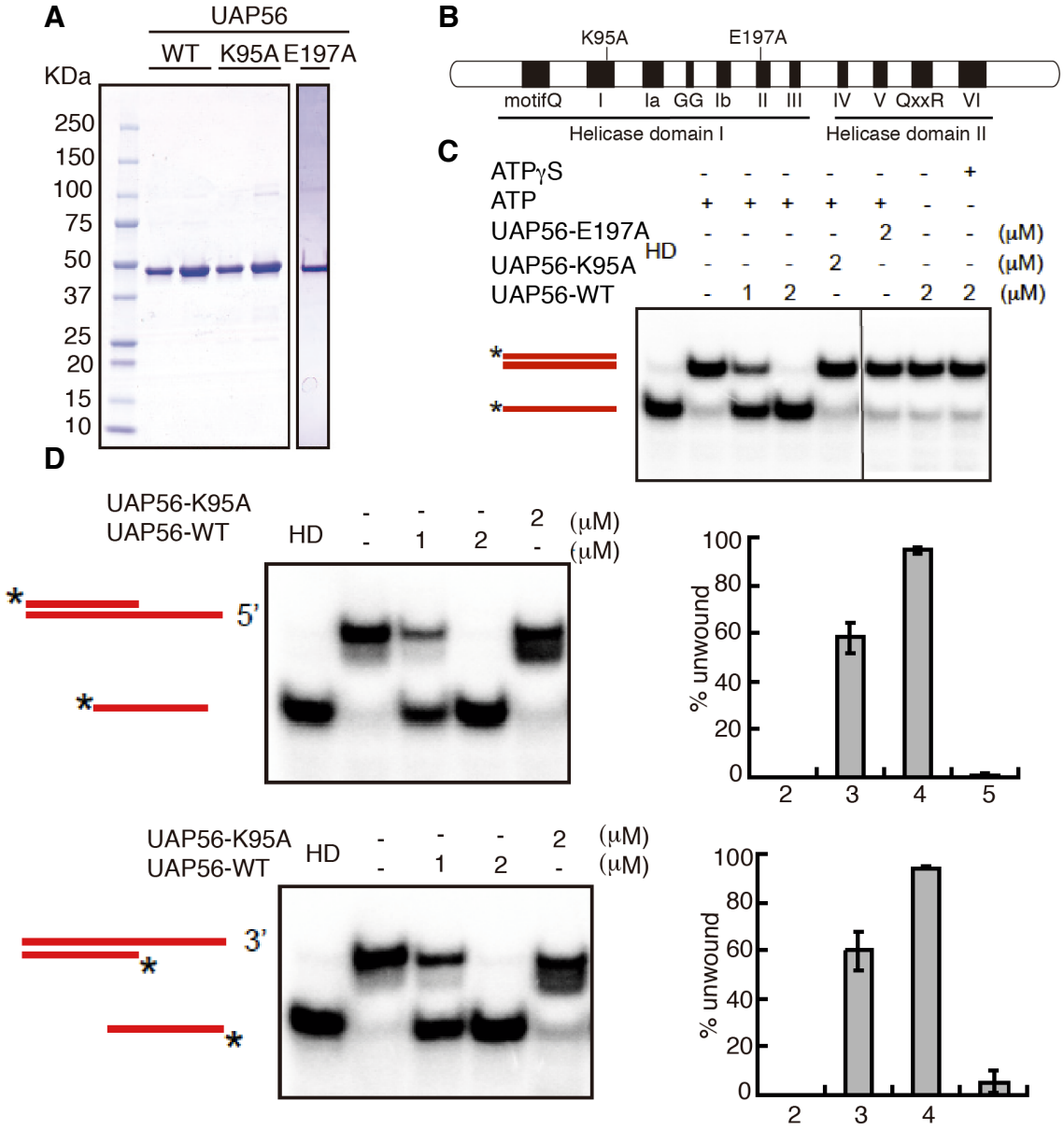

Figure R10. UAP56 RNA helicase in vitro analysis.
(A) UAP56-WT and UAP56 mutants protein purification. Purified wild type and UAP56 mutants were analyzed on SDS-polyacrilamide gel and stained with Coomassie Blue. First two lines representing UAP56-WT, the next two lines UAP56-K95A mutant and last line UAP56-E197A mutant. **(B)** Schematic representation of mutations in the helicase core of UAP56 analyzed in this study. **(C)** UAP56 RNA-RNA unwinding activity. RNA-unwinding assay was performed using a blunt-ended RNA duplex (dsRNA) as substrate with different amounts of UAP56-WT, UAP56-K95A and UAP56-E197A. **(D)** UAP56 RNA-RNA unwinding activity. RNA-unwinding assay was performed using a dsRNA with a 5' or 3' overhang as substrates with different amounts of UAP56-WT and UAP56-K95A. The positions of duplex substrate and unwound products are indicated at the left, where the stars show the position of the radiolabel. Gels were dried and subject to phosphorimaging analysis. Performed in collaboration with Patrick Sung's group.

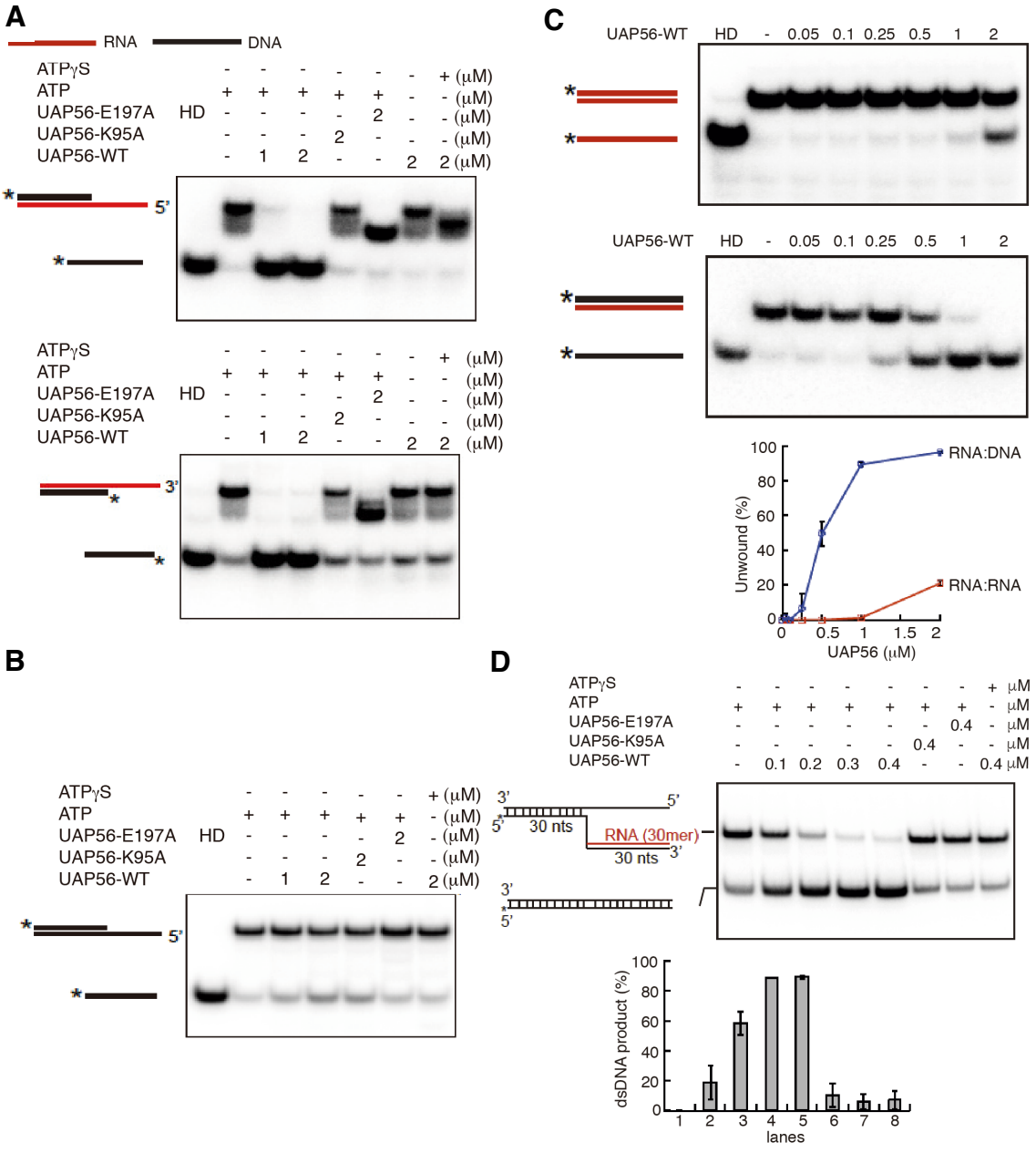

Figure R11. UAP56 RNA-DNA helicase in vitro analysis.
(A) Unwinding of RNA-DNA hybrids or dsRNA structures by UAP56 depends on its helicase activity. RNA-unwinding assay with UAP56-WT, UAP56-E197A and UAP56-K95A using a dsRNA or a RNA-DNA duplex as a substrate. The positions of duplex substrate and unwound products are indicated at the left, where the stars show the position of the radiolabel. Gels were dried and subject to phosphorimaging analysis. **(B)** UAP56 DNA-DNA unwinding activity. DNA-unwinding assay with UAP56-WT, UAP56-K95A and UAP56-E197A using 5' overhang DNA duplex as a substrate. Other details as in (A). **(C)** Comparison between UAP56 RNA helicase and RNA-DNA helicase activity using same amount of dsRNA or RNA-DNA duplex with a serial dilution of UAP56-WT protein. Other details as in (A). Graph shows the percentage of unwound product respect to the UAP56 concentration-dependent manner. **(D)** UAP56 unwinds RNA-DNA flap structures mimicking R-loops. RNA-DNA unwinding assay with UAP56-WT, UAP56-E197A and UAP56-K95A using RNA-DNA flap structures mimicking R-loops as substrates. Other details as in (A). Graph shows the percentage of dsDNA product recovered after the reaction. Concentrations of UAP56-WT of 0.3-0.4 μM exhibit almost 90% of dsDNA recovery (R loop resolution). Performed in collaboration with Patrick Sung's group.

1.8. UAP56 *in vivo* activity

In the last years a number of known RNA helicases like DDX19 or DDX21 have been shown to have RNA-DNA unwinding activity *in vitro* (Hodroj et al., 2017a; Song et al., 2017). According to the way of action of DEAD-box RNA helicases (Yang et al., 2007), it may not be surprising that any RNA helicase so far tested is able to unwind *in vitro* the RNA strand regardless of whether paired with an RNA or a DNA strand. For this reason, we assayed whether overexpression of WT and helicase-dead mutants of UAP56 suppressed the R loop-accumulation and R loop-mediated genome instability of a number of unrelated conditions, such as those created by depletion of three RNA helicases DDX23, SETX and AQR and two different factors FANCD2 and THOC1, all of which accumulate R loops by different mechanisms (Dominguez-Sanchez et al., 2011; Garcia-Rubio et al., 2015; Skourti-Stathaki et al., 2011; Sridhara et al., 2017).

First, we checked the efficiency of the new siRNA pools against DDX23, SETX and AQR by RT-PCR after 72 hours of transfection (Figure R12). Subsequently, we analyzed R loop accumulation via IF with the S9.6 antibody and DNA damage via γH2AX foci. Depletion of all these factors via siRNA (Figure R12) led to an increase in S9.6 signal (Figure R13A) and γH2AX foci (Figure R13B), as expected. Notably, wild-type UAP56 overexpression rescued both phenotypes in all cases (Figure R13A,B).

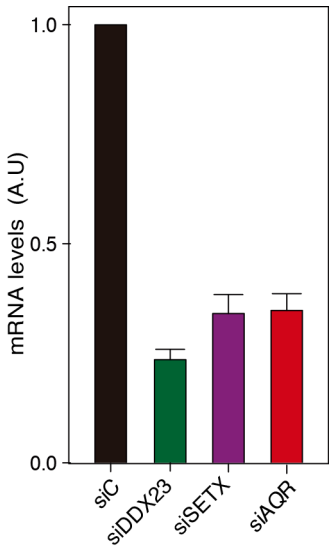

Figure R12. siRNA silencing of DDX23, SETX and AQR in human cells.
Efficiency of siRNA depletion against *DDX23*, *SETX* and *AQR*. Graph showing the mRNA levels by qPCR of siC (control), siDDX23-, siSETX- and siAQR-depleted cells. mRNA expression values of the indicated genes were normalized with mRNA expression of the HPRT housekeeping gene. Data are plotted as mean and SEM (n=3).

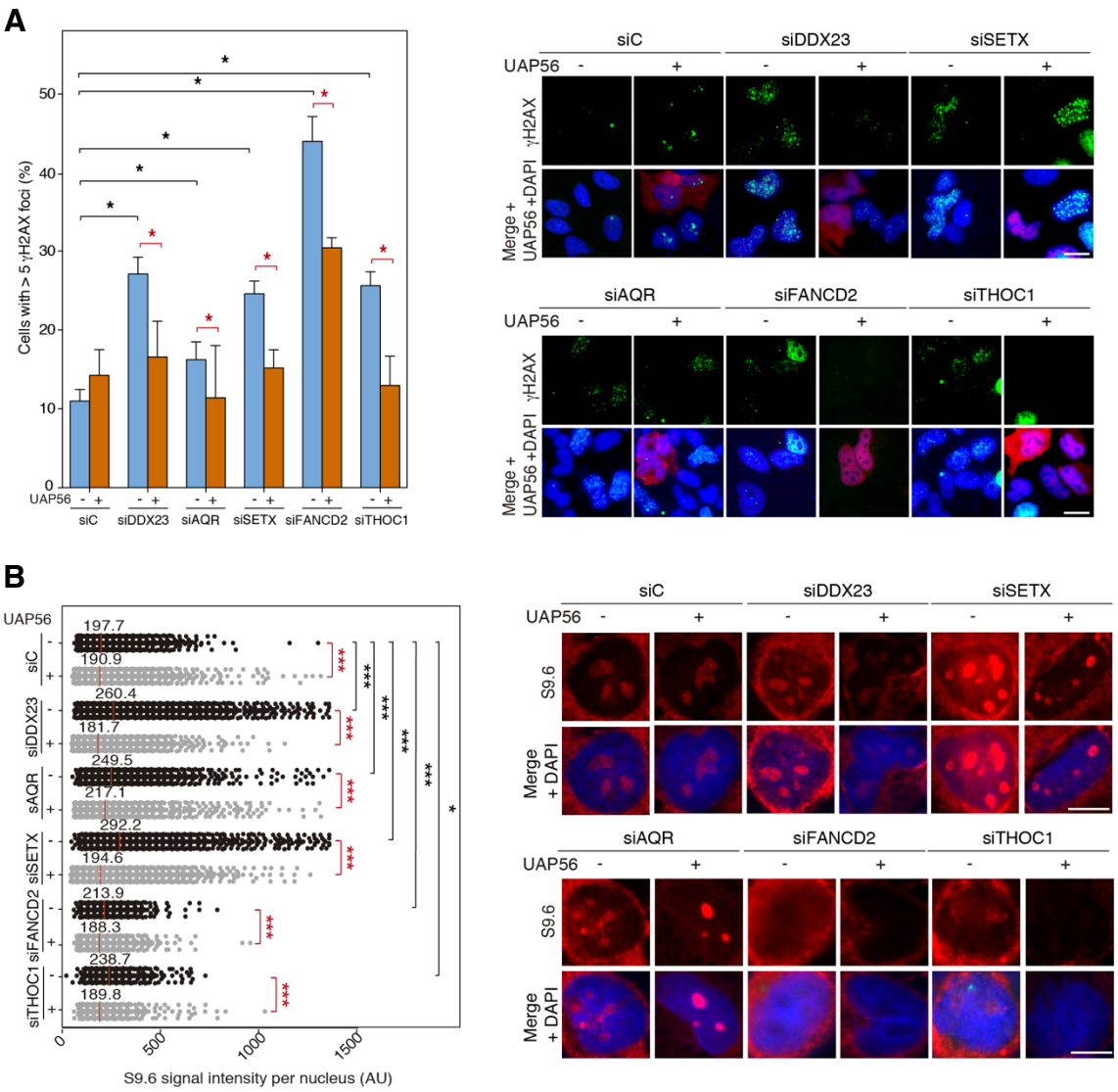

Figure R13. Analysis of R loop accumulation and DNA damage in DDX23-, SETX-, AQR-, FANCD2- and THOC1-depleted cells upon UAP56 overexpression.
(A) Detection of γH2AX foci by IF in siC, siDDX23, siAQR, siSETX, siFANCD2 and siTHOC1 HeLa cells transfected with pFLAG (-UAP56) or pFLAG-UAP56 (+UAP56) overexpressing UAP56. Immunostaining with anti-γH2AX antibody (green), anti-FLAG antibody (red) to detect UAP56 overexpression and DAPI (blue) are shown. The graph shows the quantification of cells containing >5 γH2AX foci. More than 100 cells overexpressing UAP56 (pFLAG-UAP56) (positive-stained) or more than 100 cells of mixed population transfected with the empty vector (pFLAG) were counted in each of the three experiments. Data are plotted as mean ± SEM (n≥5). Red asterisks refer to the comparative statistical analysis of each siRNA depletion sample with and without UAP56 overexpression. *, $P < 0.05$ (Student's t-test, two-tailed). **(B)** Quantification of S9.6 immunofluorescence signal in siC, siDDX23, siAQR, siSETX, siFANCD2 and siTHOC1 HeLa cells transfected with the empty vector pFLAG (-UAP56) or pFLAG-UAP56 (+UAP56) for UAP56 overexpression. Immunostaining shows S9.6 monoclonal antibody (red), anti-FLAG antibody (green) to detect UAP56 overexpression and DAPI (blue).The graph shows the median of the S9.6 signal intensity per nucleus. More than 100 cells overexpressing UAP56 (pFLAG-UAP56) (positive-stained) or more than 100 cells of mixed population transfected with the empty vector (pFLAG) were counted in each experiment (n=3). The red asterisks refer to the comparison of each siRNA depletion sample versus its own UAP56 overexpression sample. Scale bar, 10 μm. *, $P < 0.05$; ***, $P < 0.001$ (Mann-Whitney U test, two-tailed).

Next, we overexpressed the two UAP56 helicase-dead mutants UAP56-K95A and E197A in siTHOC1-depleted cells to assay whether the *in vivo* ability to suppress R loops resided in the active sites. Importantly, none of the two mutant forms were able to suppress the R loop accumulation, as detected by IF with S9.6, and the increased DNA damage, as detected by γH2AX foci (Figure R14A,B). Altogether, our results indicate that UAP56 has the *in vivo* ability to use its RNA-DNA helicase and R loop-resolving activity to remove R loops regardless of the origin of its accumulation.

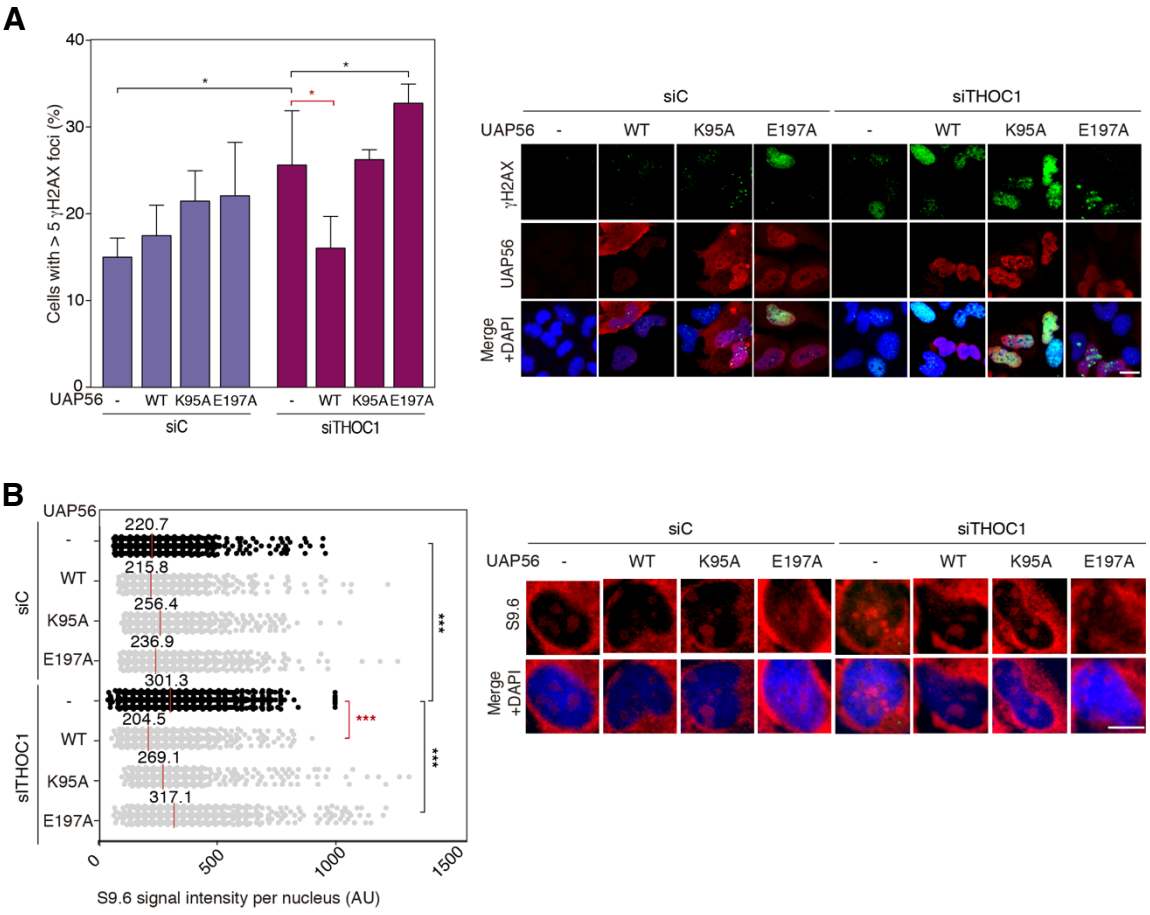

Figure R14. Analysis of R loop accumulation and DNA damage in THOC1-depleted cells transfected with UAP56 WT and two-helicase-dead mutants.
(A) Detection of γH2AX foci by IF in siC and siTHOC1 HeLa cells transfected with pFLAG (-UAP56), pFLAG-UAP56 (+UAP56) for UAP56 overexpression, pFLAG-UAP56-K95A (+UAP56-K95A) and pFLAG-UAP56-E197A (+UAP56-E197A) for UAP56 mutant overexpression. Other details as in Figure R13A. Data are plotted as mean and SEM (n=4). The red asterisks refer to the comparison of siTHOC1 sample versus its own UAP56 non-mutated overexpression sample. Scale bar, 25 μm. *, $P < 0.05$ (Student's t-test, two-tailed). **(B)** Quantification of S9.6 immunofluorescence signal siC and siTHOC1 HeLa cells transfected with pFLAG (-UAP56), pFLAG-UAP56 (+UAP56) for UAP56 overexpression, pFLAG-UAP56-K95A (+UAP56-K95A) and pFLAG-UAP56-E197A (+UAP56-E197A) for helicase-dead UAP56 overexpression. The graph shows the median of the S9.6 signal intensity per nucleus (n≥3). Other details as in Figure R13B. The red asterisks refer to the comparison of siTHOC1 sample versus its own UAP56 non-mutated overexpression sample. Scale bar, 10 μm. ***, $P < 0.001$ (Mann-Whitney U test, two-tailed).

1.9. URH49

In humans, an additional UAP56 related helicase named URH49/DDX39a was found. This protein shares 90% amino acid sequence homology with UAP56, conserving completely the DEAD/H box RNA helicase motifs. Consequently, URH49, as UAP56, is also able to complement *SUB2* deletion in yeast (Pryor et al., 2004). Respect to its role, URH49 has been shown to interact with the mRNA export factor ALY and CIP29 (Pryor et al., 2004). Its preferential association with CIP29 has been proposed to be part of an alternative mRNA export complex termed AREX. However, both helicases are expressed at different levels and regulated the export of different sets of mRNAs (Yamazaki et al., 2010). Given the similarities between both proteins, we explored the possible implications of URH49 in the maintenance of genome integrity, as we tested in the case of UAP56.

First, we wondered whether URH49 depletion leads to an increase in DNA damage measured by γH2AX foci. siURH49 transfected HeLa cells for 72 hours exhibit an increase in γH2AX foci respect to the siC control cells. Then, we assayed whether the observed DNA damage was R loop-dependent, as happened for UAP56. For this purpose, RNase H1 was overexpressed in URH49-depleted cells. Although RNase H1 overexpression seems to partially rescue this phenotype, after three independent experiments, our results remained statistically inconclusive, because of the high variability between replicates (Figure R15A). Then, we assayed directly R loop accumulation via immunofluorescence using the S9.6 antibody. Quantification of the nuclear S9.6 signal intensity revealed a non-significant mild increase in URH49-depleted cells after the evaluation of three independent replicates (Figure R15B). Even though, these results can be explained by specific functions of both helicases, further studies are needed to know whether or not URH49 has any role in R loop homeostasis.

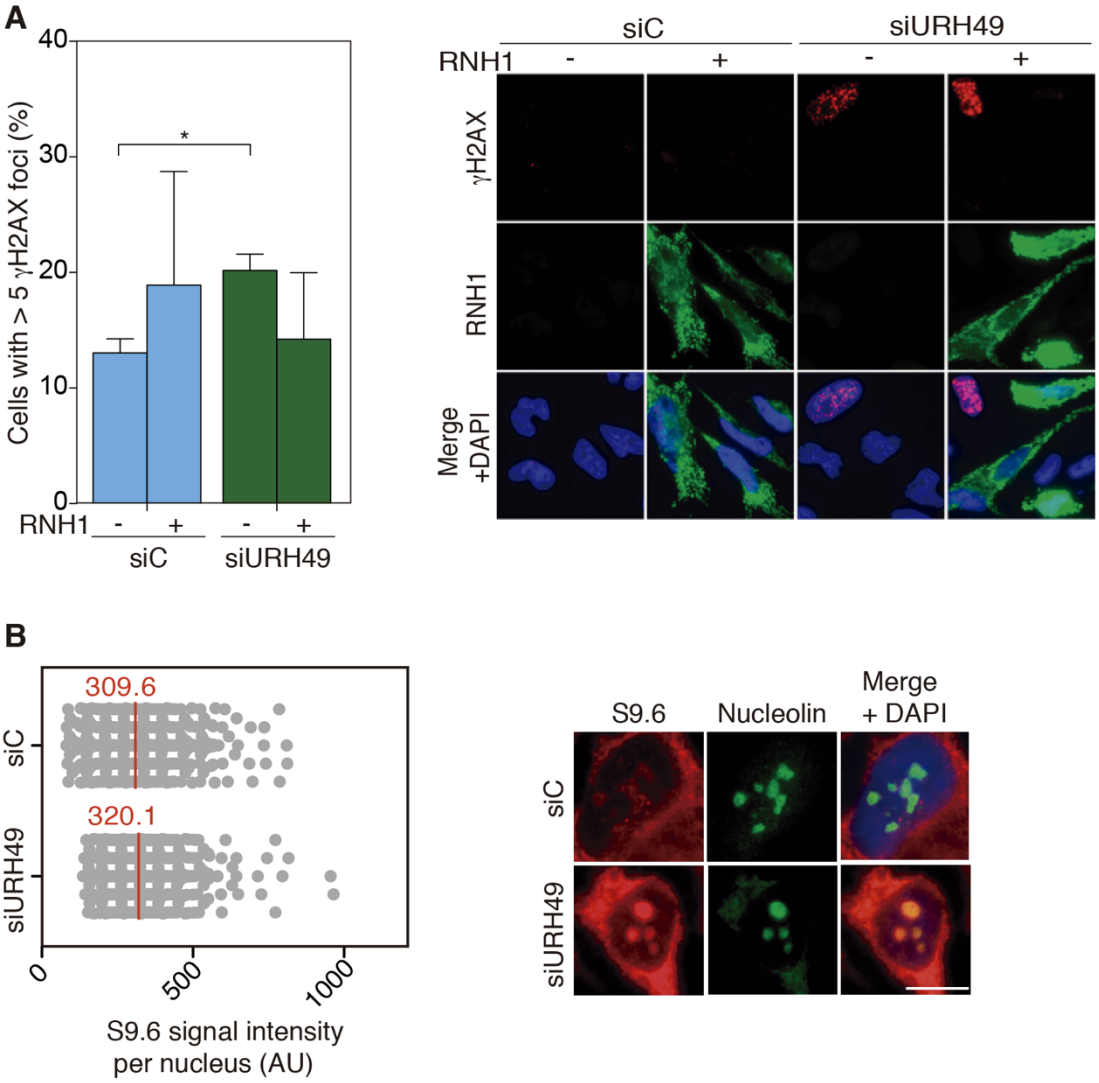

Figure R15. Accumulation of DNA breaks and R loop in URH49-depleted cells.
(A) Immunofluorescence of HeLa cells stained with antibodies anti-γH2AX and anti-RNase H1. After URH49 siRNA transfection for 72 hours, cells were also transfected with the empty plasmid or the RNase H1 plasmid. More than 100 cells expressing RNase H1 (positive-stained) or of mixed population transfected with the empty plasmid were counted in each experiment. Percentage of cells with > 5 γH2AX foci are plotted (n=3) as mean and SEM. *, $P < 0.05$ (Student T-test, two tailed). **(B)** Immunostaining of HeLa cells using the S9.6 antibody (red) and anti-nucleolin in siC and siURH49-transfected cells. More than 100 cells were counted in each experiment. The median of S9.6 signal intensity per nucleus is plotted (n=3).

2. CONTRIBUTION OF UAP56 TO THE MAINTENANCE OF GENOME STABILITY THROUGHOUT THE GENOME

Given the role of UAP56 in the maintenance of genome integrity, we wondered next whether UAP56 exerts it function genome-wide or it is restricted to a specific subset of genes.

2.1. Transcriptome of UAP56-depleted cells

Firs, we wondered what would be the effect of silencing UAP56 on gene expression levels. For this purpose, we performed total RNA-seq in cells transfected with siC and siUAP56 for 72 hours. From the total genes analyzed, we identified 9704 genes whose expression changed upon UAP56 depletion. Among them, 4683 genes were up-regulated and 5021 genes were down-regulated (Figure R16A). Globally, when the fold change in gene expression levels in siUAP56 cells are plotted regarding their expression levels in siC control cells, we observed a general downregulation effect of gene expression. In particular, highly expressed genes were the ones more strongly affected as can be seen in Figure 16B. Despite that more biological replicates are required, these data are in the same line as previous reports in yeast, where a reduction of total mRNA levels was observed as a consequence of mutations in SUB2 (Jimeno et al., 2002; Libri et al., 2002; Zenklusen et al., 2002), *Drosophila*, in which the overall reduction of mRNA levels was shown (Herold et al., 2003) and *C. elegans* (MacMorris et al., 2003).

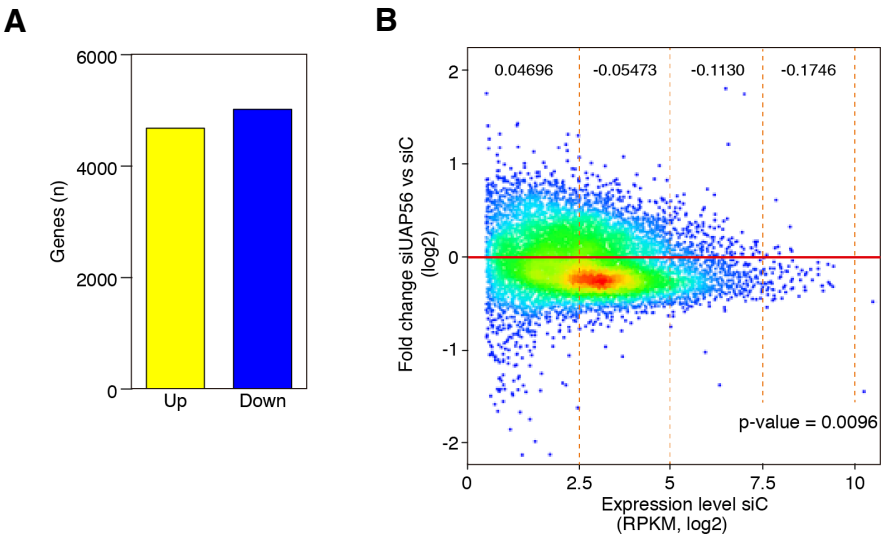

Figure R16. Gene expression analysis by RNA-seq in UAP56-depleted cells.
(A) Analysis of number of genes up- and down-regulated after UAP56 depletion. **(B)** Density scatterplot showing log2 fold change for siUAP56 against siC as function of log2 siC expression levels. The red line (y = 0) indicates no change between samples in expression. Orange dot lines separate different expression ranges in which their fold change median are indicated (n=1). Median Pearson correlation associated p-value indicated in the bottom right.

2.2. Genome-wide chromatin-associated action of UAP56

To analyze whether UAP56 was present all over the genome, as would be expected by a general co-transcriptional RNA-binding and processing factor, we performed Chromatin immunoprecipitation coupled with DNA sequencing (ChIP-seq) in the K562 cell line. This line is regularly used in genome-wide occupancy analysis of different transcription factors, secondary DNA structures and chromatin modifications, so that there are an increasing set of data to which compare any genome-wide analysis (Sloan et al., 2016). UAP56 ChIP-seq data were subjected to computational analysis revealing a global distribution of this protein (Figure R17).

We compared UAP56 ChIP-seq results with transcription related data available at ENCODE and GEO databases. We crossed data from different datasets such as the Precision nuclear run-on sequencing (PRO-seq) (GSE104800), which map RNAP active sites, RNAPII ChIP-seq (ENCSR000BMR) and RNAPII-S2P ChIP-seq (ENCSR000EGF), which marks transcription elongation regions and our RNA-seq data from siC control cells. As can be seen in Figure R18A, the majority of UAP56 clusters mapped in ORFs, where a general coincidence of the distinct tracks is observed. As can be seen in Fig. 6A, the majority of UAP56 clusters coincided with those from PRO-seq and RNAPII ChIP-seq. These data are in concordance with an UAP56 global co-transcriptional function all over the transcribed genome. Indeed, UAP56 could be found associated with chromatin in the majority of RNAPII active sites (97%), according to the overlap between UAP56 ChIP-seq and PRO-seq data (Figure R18A,B). Furthermore, to analyze the distribution of UAP56 along the length of all ORFs, we performed metagenomic analysis along all these genes and their flanking regions. The binding profile of UAP56 reveals that UAP56 peaks at promoters and it is increased in a gradient manner towards the end of ORFs (Figure R18C). This result is consistent with the previously reported genome-wide occupancy of the yeast ortholog Sub2, where it is recruited in a continuous manner towards the 3' end of the transcribed genes of the yeast genome (Gomez-Gonzalez et al., 2011). Additionally, to verify that the two biological

replicates display high reproducibility, we obtained correlation plots showing reasonable good correlation (Figure R18D). Thus, we can conclude that UAP56 acts in active chromatin all over the genome (Figure R18).

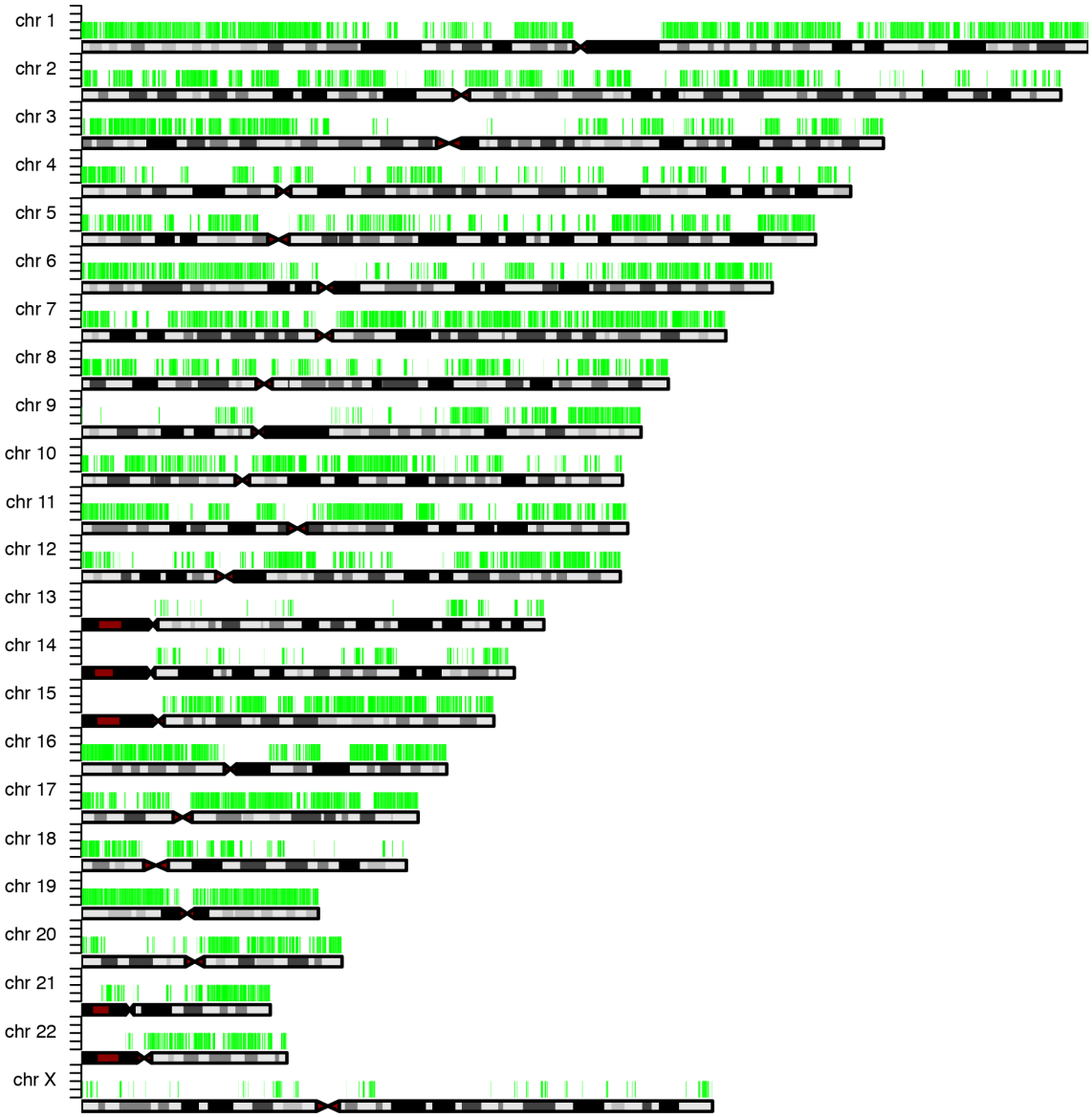

Figure R17. Genomic view of UAP56 recruitment in K562 cell line.
Genome-wide occupancy of UAP56 in K562 cell line. Histogram bars show the signal of loci enriched in the immunoprecipitated fraction.

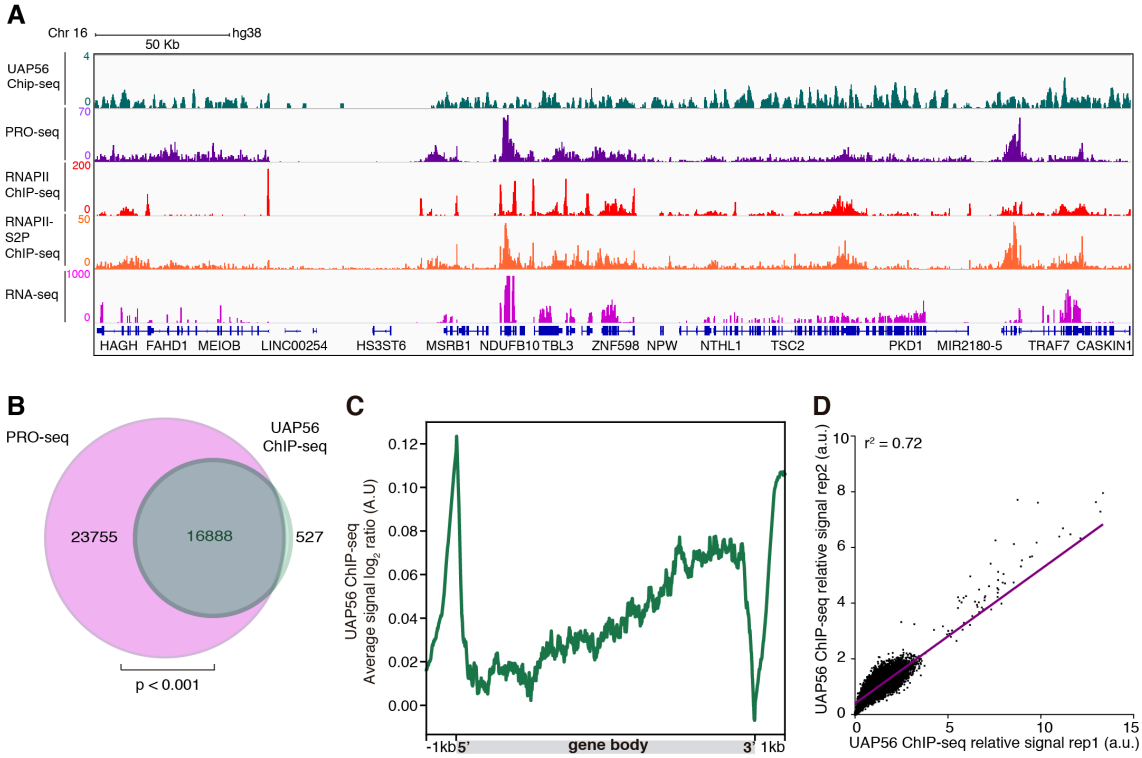

Figure R18. UAP56 occupancy within genes and expression levels in K562 cells.
(A) Analysis of the distribution of chromatin-bound UAP56, PRO-seq, RNAPII ChIP-seq, RNAPII-S2P ChIP-seq and RNA-seq. Representative screenshots of UAP56 (green), PRO-seq (purple), RNAPII ChIP-seq (red), RNAPII-S5P ChIP-seq (orange) and RNA-seq (magenta) in K562 cells. A representative screenshot is shown. **(B)** Venn diagram showing the overlap between RNAPII active sites detected by PRO-seq (magenta) and UAP56 chromatin-bound genes detected by ChIP-seq (green). $P < 0.001$ (Hypergeometric test). **(C)** Analysis of the distribution of UAP56 ChIP-seq data throughout gene body. Metaplot analysis of the distribution of the UAP56 ChIP-seq signal (IP-Input) along gene body. **(D)** *xy* correlation plot between UAP56 ChIP-seq replicates in K562 cells. (r^2, Pearson correlation).

2.3. Genome-wide accumulation of RNA-DNA hybrids in UAP56-depleted cells

To investigate the global impact of UAP56 depletion on R loop accumulation, we performed DRIPc-seq (DRIP followed by cDNA conversion coupled to high-throughput sequencing) in siC control and siUAP56 silenced K562 cells. Since, the use of the S9.6 monoclonal antibody to detect explicitly RNA-DNA hybrids have represented always a concern in the field, due to the residual affinity for dsRNA (Phillips et al., 2013). We first performed DRIP-seq in K562 cells with and without RNase H treatment, as a proof of the ability of the S9.6 antibody to specifically precipitate RNA-DNA hybrids. As can be seen in Figure R19A, the DRIP-seq signal was highly sensitive to RNase H pre-treatment, that is, strongly

reduced in RNase H-treated DRIP-seq samples. This excludes the possibility of mixed dsRNA and RNA-DNA signals from the S9.6 immunoprecipitation. Indeed, in mammalian systems this has never been encountered.

Once S9.6 was confirmed to specifically detect RNA-DNA hybrids, we proceeded to perform the more accurate approach that permits high-resolution and strand-specific R loop mapping genome wide, DRIPc-seq. Whereas DRIP-seq is a powerful technique that enables robust genome-wide profiling of R loop formation, it suffers from limited resolution and lack of strand specificity (Sanz and Chedin, 2019). Subsequently, in the DRIPc-seq methology the RNA-DNA hybrids from siC control cells and UAP56-depleted cells were immunoprecipitated with the S9.6 antibody and subjected to DNase I treatment, so that only the RNA strands of hybrids remained. Thus, the resulting RNA strands were purified and retrotranscribed to cDNA to build the libraries, which were then sequenced in the Illumina platform. However, following protocol guidelines, we first checked the efficiency of the siRNA pool against UAP56 by western blot analysis in K562 cells, where undetectable levels of UAP56 were shown (Figure R19B). Moreover, before DNAse I treatment and sequencing, DRIP efficiency was checked by qPCR in the *RPL13A* gene (Figure R19C). This locus has been previously established as a hotspot for R loop accumulation (Sanz and Chedin, 2019). Remarkably, when we attempted to obtain RNase H treated samples, we noticed that DRIPc-seq was so sensitive to RNase H pretreatment that the samples presented insufficient material to build sequencing libraries, as has been reported before (Sanz and Chedin, 2019). In the same line, this result confirmed that actually the material sequenced indeed derives from RNA-DNA hybrids. Therefore, we used RNase H treated DRIP-seq data as an indicator of hybrid-prone regions when possible, since it exhibits lower resolution capacity than DRIPc-seq.

Sequencing results were quality-checked and aligned to the *H. sapiens* hg38 reference genome using BWA-MEM (Zhu et al., 2013). Resulted BAM files were analyzed with different tools such as MACS2 (Zhang et al., 2008) for peak

calling of positive regions or deeptTools (Ramirez et al., 2016) for the generation of profiles. To identify hybrid-prone regions, MACS2 Peak caller was used. siC samples were used as a control and mutant samples as treatment files, considering as a statistically difference those with a p-value ≤ 0.05. Global inspection of generated tracks revealed that DRIPc-seq technique gave comparable results to those of DRIP-seq, although DRIPc-seq permitted the detection of hybrids at both DNA strands. Indeed, this feature is a clear sign of the S9.6 specificity in RNA-DNA hybrid detection, since otherwise dsRNA would resulted in the same signal detected in both strands. In addition, the global analysis indicated a predominant correlation between positive regions identified in the siC control and siUAP56 cells, with either new and more-intense interval regions after UAP56 depletion, as expected (Figure R20).

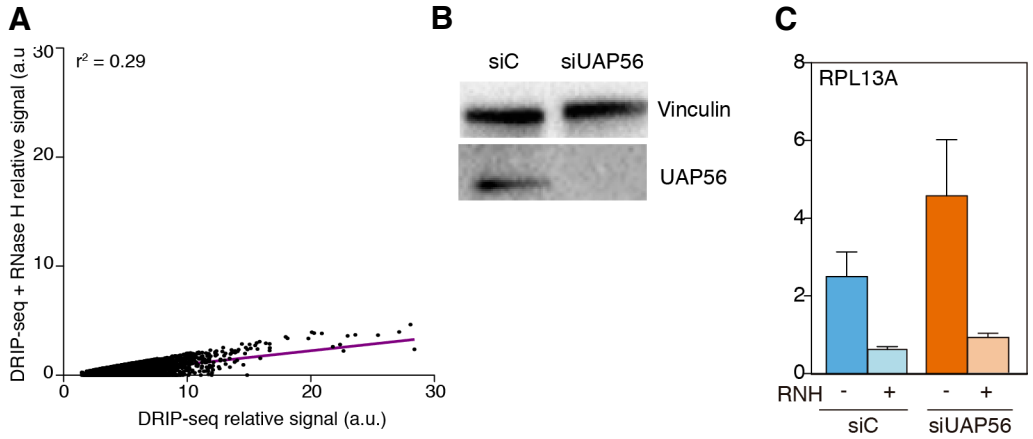

Figure R19. Previous DRIPc-seq validations.
(A) xy correlation plot between the DRIP-seq RNase H-treated (y axis) and untreated (x axis) (r2, Pearson correlation) samples. **(B)** Western blot analysis of UAP56-depleted K562 cell line. **(C)** Genomic samples from siC and siUAP56 transfected cells were treated (+) or not (-) *in vitro* with RNase H and subjected to DRIP-qPCR in the RPL13A gene.

It is generally accepted that R loops in the cell appears as co-transcriptional byproducts that occurs with high frequency in certain regions (Sanz et al., 2016). Therefore, further analysis was focused on the ORFs identified as hybrid-prone genes. As can be seen in Figure R21, analysis of RNA-DNA hybrids along a gene metaplot revealed a similar distribution for siC control and UAP56-depleted cells. The intensity of RNA-DNA hybrid signal, measured

as mean coverage of DRIPc-seq across an average gene body, for the corresponding template in each case (sense transcription) revealed an specific increase towards the 3' end in both strands (Watson and Crick strand). A specific enrichment at promoters corresponding to antisense transcription was also observed in both strands when the non-template strand was analyzed.

Next, we analyzed the correlation of DRIPc-seq signal with other annotated features available in ENCODE project. We could see that ORFs represent approximately 65% in UAP56-depleted cells with respect to the total number of positive regions identified (Figure R22A). Interestingly, these genes were longer than the median of the genome (Figure R22B). We then determined whether hybrid-prone genes in siUAP56 cells, as deduced from the DRIPc-seq data, coincided with the UAP56-positive genes obtained from the ChIP-seq data of siC control cells. The comparative analysis highlights that the vast majority (approximately 97%) of R loop-prone genes in siUAP56 cells are those that recruit UAP56 in the siC control (Figure R22C). Altogether our data demonstrate that UAP56 is located genome-wide primarily in genes that are being transcribed and at which UAP56 co-transcriptionally functions. Moreover, when UAP56 ChIP-seq signals were plotted throughout genes according to its R loop content, a significant enrichment of UAP56 was observed reinforcing this conclusion (Figure R22D). The protective role of UAP56 preventing RNA-DNA hybrid accumulation is also supported by the fact that in a large proportion of genes, a DRIPc-seq signal was only detected after siUAP56 depletion (Figure R22C). Consequently, DRIPc-seq results demonstrate that the increase in R loop accumulation, previously detected by DRIP-qPCR and IF (Figure R4A,B), was indeed genome-wide. Altogether, our data unveils that UAP56 is an RNA-DNA helicase that unwinds co-transcriptional non-scheduled R loops that could sporadically form at transcribed genes all over the genome.

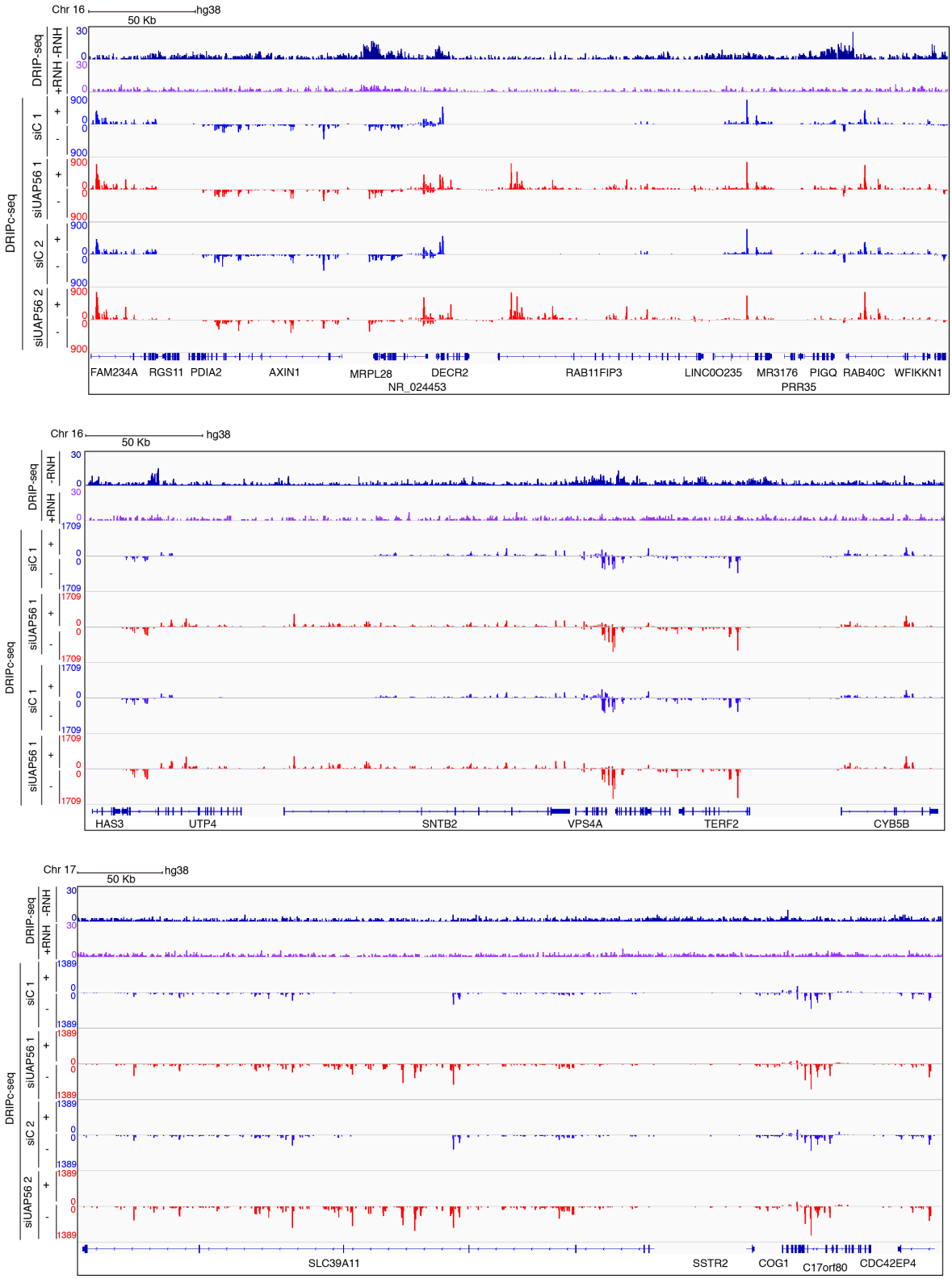

Figure R20. Genome-wide analysis of RNA-DNA hybrids in control and UAP56-depleted K562 cells.

Representative screenshots of different genomic regions showing the DRIP-seq signal profile for untreated (blue) and RNase H-treated (purple) K562 cells, as well as the DRIPc-seq signal profiles for siC (blue) and siUAP56 (red) in plus and minus strand (two independent replicates).

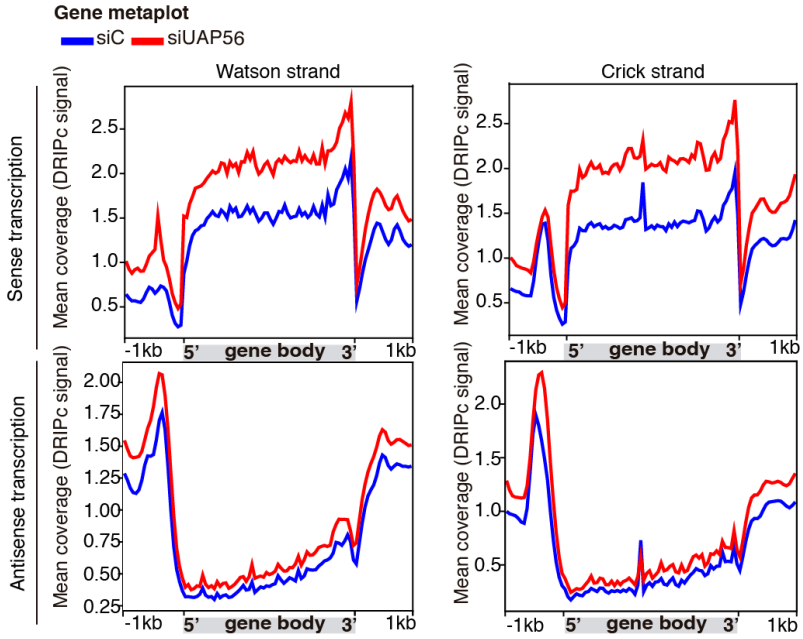

Figure R21. RNA-DNA hybrids distribution over genes in UAP56-depleted cells.
DRIPc-seq analysis of siUAP56-depleted cells. Distribution of DRIPc signals (mean coverage) along a gene metaplot for siC control (blue) and siUAP56 (red) cells over Watson (left) and Crick strand (right) in sense and antisense transcription.

A

	Genome	DRIPc-seq	ChIP-seq
ORFs	19951	10550	17415
lncRNA	8777	1527	4921
ncRNA	7119	683	2071
Antisense	5583	148	672
Other	17345	2837	7724
Total	58735	15732	34984

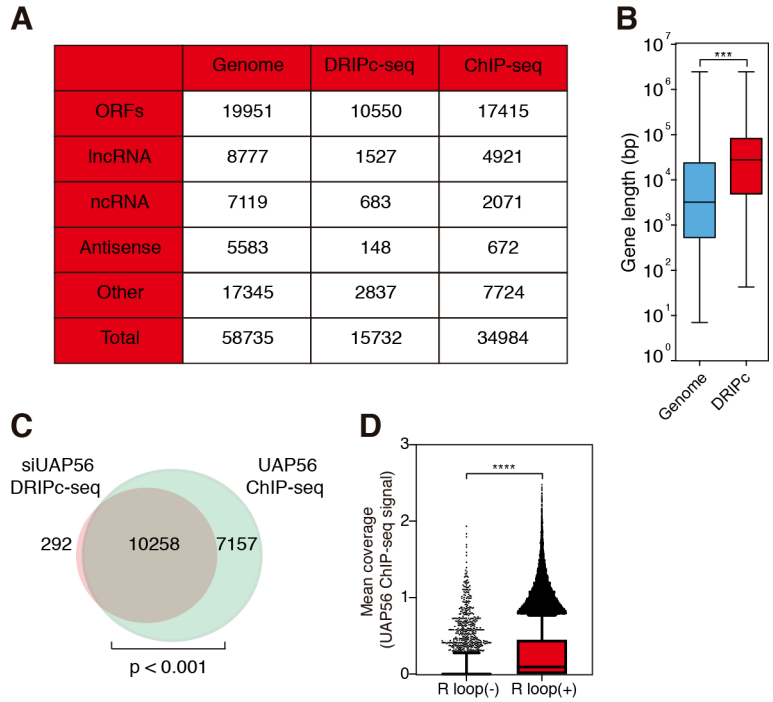

Figure R22. Analysis of RNA:DNA hybrid positive features in UAP56-depleted cells.
(A) Table showing the different RNA-DNA hybrid positive genomic features mapped in siUAP56 cells and positive genomic features identified in UAP56 ChIP-seq. **(B)** Statistical analysis of length values for R loop-enriched protein coding genes in UAP56-depleted cells. Median values are represented. ***, $P < 0.001$ (Mann-Whitney U-test, two tailed). **(C)** Venn diagrams showing the overlap between hybrid-prone genes after UAP56 depletion (red) and UAP56 chromatin-bound genes as detected by ChIP-seq (green). $P < 0.001$ (Hypergeometric test). **(D)** UAP56 ChIP-seq signal (mean coverage) over genes according to its R loop content. R loop (-) refers to genes that do not accumulate R loops, while R loop (+) those accumulating them in siC control cells. ****, $P < 0.0001$ (Mann-Whitney U test, two-tailed).

Finally, to complete the genome data analysis we asked whether those genes enriched in R loop after siUAP56 depletion possess specific predictive chromatin features. For this purpose, we crossed our data with the available ChIP-seq data for H3K9Ac (ENCSR000AKV) and H3K4me2 (ENCSR000AKT), histone modifications associated with active transcription, and with DNase-seq data (ENCSR000EKS) for nucleosome positioning from the same K562 cells (ENCODE). Interestingly, as can be seen in Figure R23, H3K9Ac and H3K4me2 histone marks were enriched all over the genome at promoters in genes that accumulate hybrids upon UAP56 depletion. Regarding DNase accessibility, as observed from DNase-seq data, these genes showed also higher levels at the TSSs, consistent with high expression.

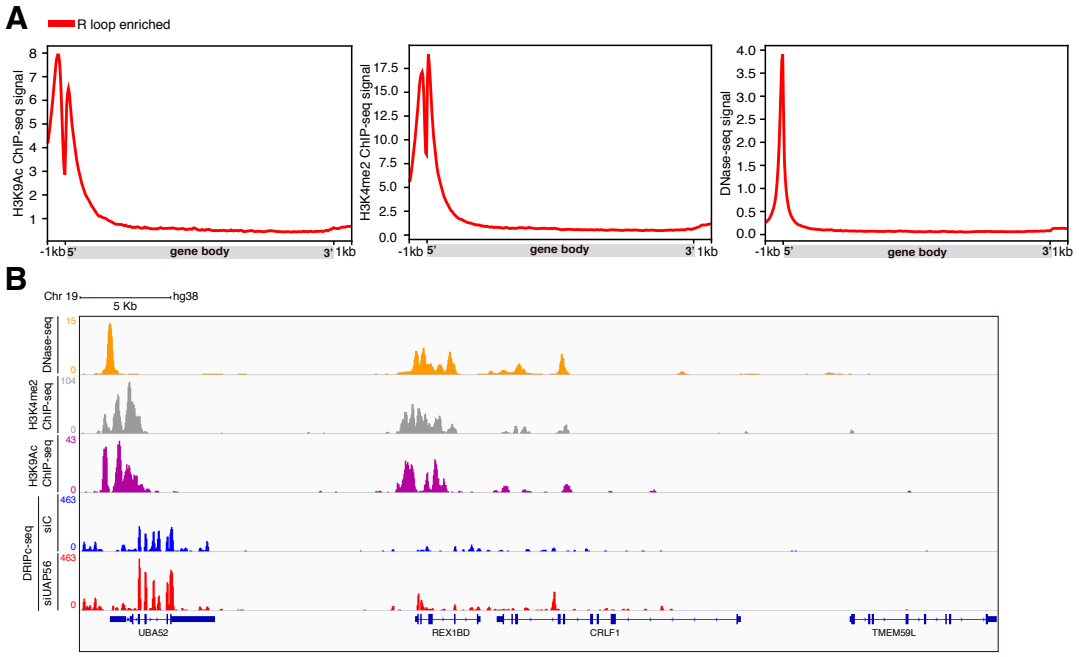

Figure R23. Chromatin features associated to hybrid-prone genes in UAP56-depleted cells.
(A) Genes accumulating R loop upon UAP56 depletion correlate with different active chromatin marks. Metaplots of ChIP-seq signals (mean coverage) for H3K9Ac, H3K4me2 and DNase-seq. **(B)** Representative screenshot of a genomic region showing DNase-seq signal (orange), H3K4me2 (grey) and H3K9Ac ChIP-seq signal (purple) and DRIPc-seq signal for siC control (blue) and siUAP56 (red) cells.

To verify the reliability and reproducibility of the experiments, we performed correlation plots of the two DRIPc-seq biological replicates. Importantly, the regression analysis of the data (Figure R24A), as well the

comparison of all hybrid-prone genes in the two DRIPc-seq experiments performed (Figure R24B) corroborated the high reproducibility of these experiments.

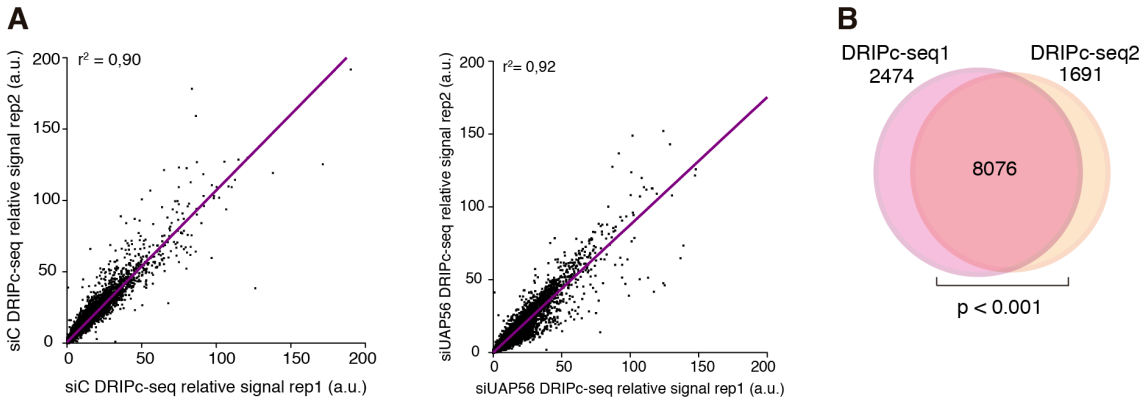

Figure R24. DRIPc-seq reproducibility between different biological replicates.
(A) (Left) *xy* correlation plot between two siC control samples DRIPc-seq replicates. (Right) *xy* correlation plot between two siUAP56 samples DRIPc-seq replicates (r^2, Pearson correlation). **(B)** Venn diagram showing the overlap between first DRIPc-seq replica (pink) and the second one (orange). P < 0.001 (Hypergeometric test).

2.4. Genome-wide accumulation of RNA-DNA hybrids in DDX5-depleted cells

Due to the increasing number of reports that have linked different DDX RNA helicases with R loop metabolism, we wondered whether the global R loop distribution pattern of two different DDX RNA helicases would be similar, suggesting redundant functions, or different. As have been detailed before, we have analyzed the RNA-DNA hybrid distribution along the entire genome in cells deprived of the UAP56 DEAD-box RNA helicase. To compare the results with those of another DDX helicase, we did the same analysis in cells depleted of DDX5. DDX5 (yeast Dbp2) acts as a RNA chaperone in multiple steps of RNA metabolism such as alternative splicing, regulation of lncRNA activities in transcription, mRNA export or miRNA processing. However, this protein was specially compelling since a BRCA2 interactome performed by Aura Carreira's group revealed that this protein boosted the helicase activity of DDX5. Indeed, they also reported that DDX5 unwinds RNA-DNA hybrids and R loops *in vitro* and *in vivo* (unpublished results). This link could be particularly striking since our laboratory previously reported the involvement of BRCA2 in R loop metabolism,

suggesting a direct connection of R loops with DSB repair and cancerous processes (Bhatia et al., 2014).

We performed DRIPc-seq in siC control and DDX5 silenced K562 cells. DRIPc-seq data revealed R loop accumulation in siDDX5-transfected cells in the whole genome, as can be seen in the genomic regions selected for its visualization. Globally, whereas a mild DRIPc-seq signal in siC control cells was observed, an increased RNA-DNA hybrid signal intensity was observed after DDX5 depletion (Figure R25A). To ensure the reproducibility of the experiments, we performed correlation plots and comparative analysis of the two biological replicates of DRIPc-seq in siDDX5 cells. The regression analysis of the data confirmed the good correlation between replicates (Figure R25B). In the same line, the comparative analysis by Venn diagram confirmed the significant overlap between replicates (Figure R25C). After peak calling analysis, we identified hybrid-prone regions that correlate with distinct genomic features. Among them, ORFs represented the largest category covering the 74% of these regions (Figure R26A). DRIPc metaplot analysis of all protein coding genes revealed that the RNA-DNA hybrid signal, measured as mean coverage of DRIPc-seq across the average gene body for the corresponding template in each case (sense transcription), showed an specific increase towards the 3' end in both strands (Watson and Crick strands). It was also observed a specific enrichment at promoters corresponding to antisense transcription in both strands when the non-template strand was analyzed. Thus, general distribution of RNA-DNA hybrids along gene bodies were not significantly different in siDDX5 cells (Figure R26B).

Finally, we asked whether those genes prone to accumulate hybrids after DDX5 depletion possess specific predictive chromatin features. As we did before, we crossed our data with different dataset of ChIP-seq for H3K9Ac (ENCSR000AKV) and H3K4me2 (ENCSR000AKT), histone modifications associated with active transcription, and with DNase-seq data (ENCSR000EKS) for nucleosome positioning from the same K562 cells (ENCODE). Accordingly to our previous data, as can be observed in Figure R27, H3K9Ac and H3K4me2

histone marks were enriched at promoters all over the genome. Regarding DNase accessibility, inferred from DNase-seq data, these genes showed also higher levels at the TSSs.

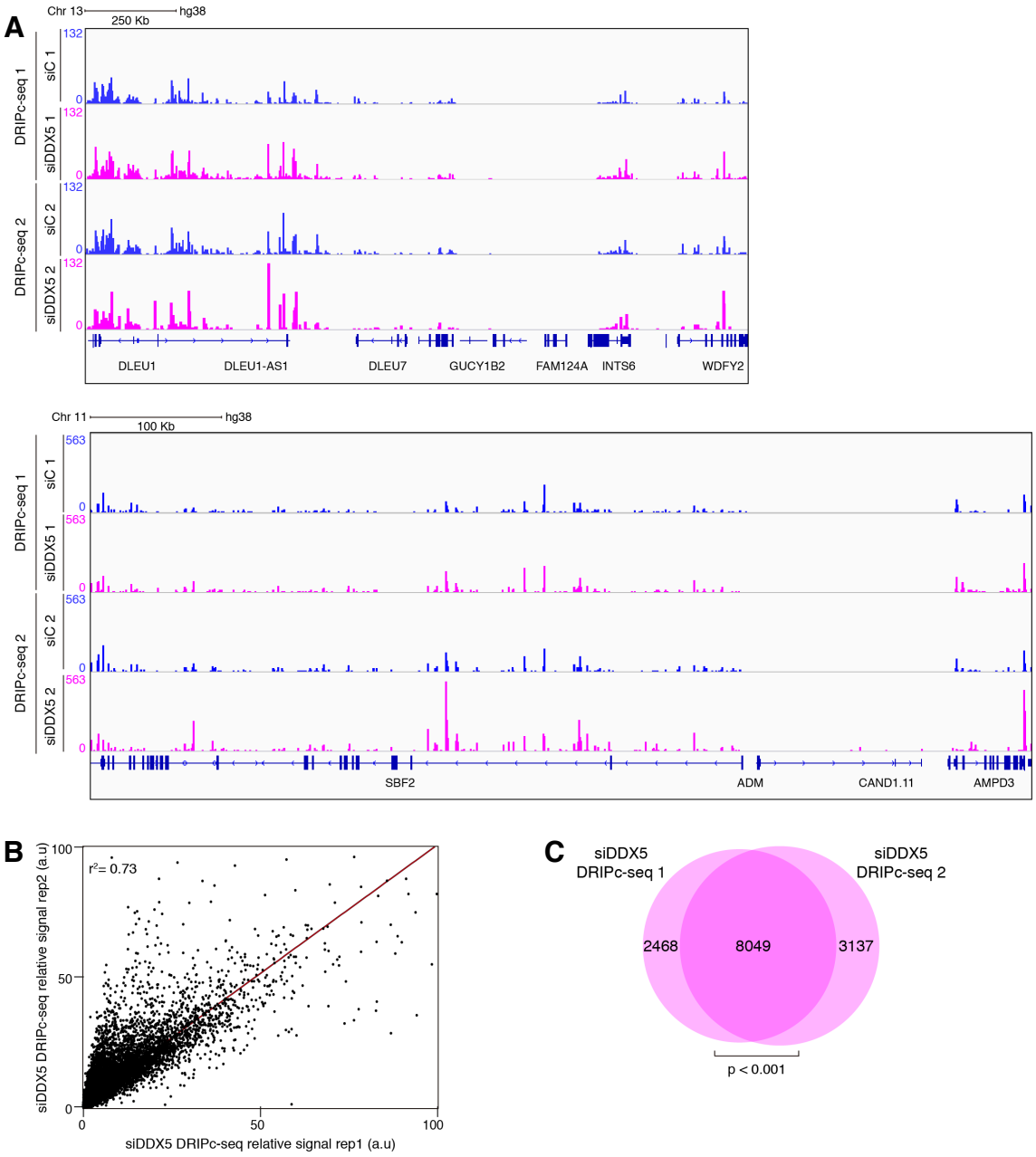

Figure R25. Genome-wide analysis of RNA-DNA hybrids in control and DDX5-depleted K562 cells.
(A) Representative screenshots of different genomic regions showing the DRIPc-seq signal profiles for siC (blue) and siDDX5-transfected cell (pink) in two biological replicates. **(B)** *xy* correlation plot between two siDDX5 samples DRIPc-seq replicates (r^2, Pearson correlation). **(C)** Venn diagram showing the overlap between first siDDX5 DRIPc-seq replica and the second one. $P < 0.001$ (Hypergeometric test).

A

	ORFS	lncRNA	ncRNA	Antisense	Other	Total
siDDX5 DRIPc-seq	10517	1059	484	99	2087	14246
Genome	19951	8777	7119	5583	17345	58735

B

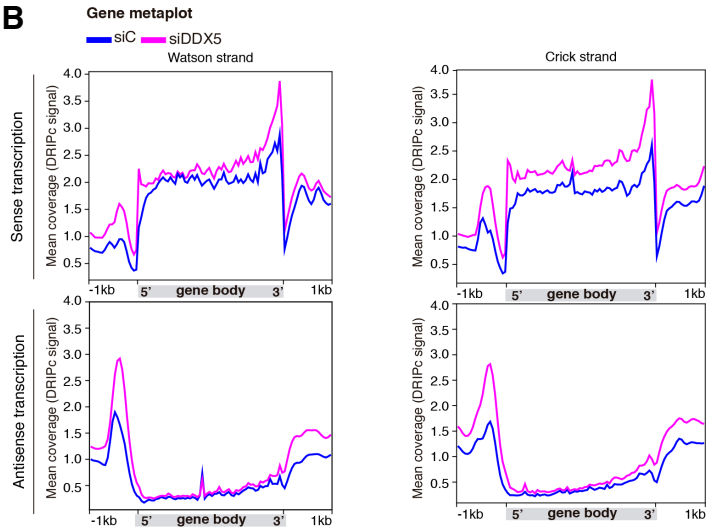

Figure R26. Analysis of RNA:DNA hybrid positive features in UAP56-depleted cells.
(A) Table showing the different RNA-DNA hybrid positive genomic features mapped in siDDX5 cells. **(B)** Distribution of DRIPc signals (mean coverage) along a gene metaplot for siC control and siDDX5 cells over Watson (left) and Crick strand (right) in sense and antisense transcription.

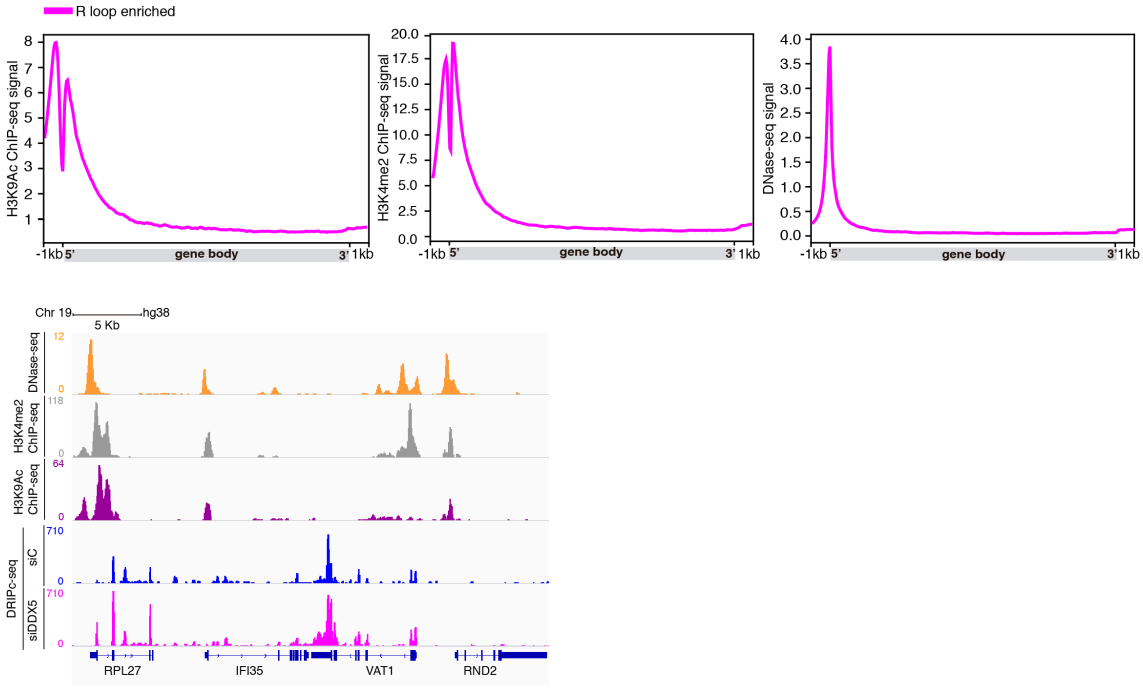

Figure R27. Chromatin features associated to hybrid-prone genes in DDX5-depleted cells.
(A) Genes accumulating R loop upon DDX5 depletion correlate with different active chromatin marks. Metaplots of ChIP-seq signals (mean coverage) for H3K9Ac, H3K4me2 and DNase-seq. **(B)** Representative screenshot of a genomic region showing DNase-seq signal (orange), H3K4me2 (grey) and H3K9Ac ChIP-seq signal (purple) and DRIPc-seq signal for siC control (blue) and siDDX5 (pink) cells.

Then, we wondered whether our data fit with the possibility that DDX5 resolved R loops at DSBs sites. With that aim in view, we crossed γH2AX ChIP-seq (GEO, GSE104800) (Kim et al., 2018) available data from the GEO database, which would mark the fragile sites in this cell line, with the R loop distribution data obtained from our DRIPc-seq results in DDX5 knock-down cells (Figure R28A). When the DRIPc-seq signal was plotted through γH2AX ChIP-seq peaks, an enrichment of RNA-DNA hybrids was found at DSBs in control cells and DDX5-depleted cells, being the second more pronounced (Figure R28B). In addition, we detected that the proportion of the RNA-DNA hybrids detected by DRIPc-seq that coincided with γH2AX positive sites (γH2AX+) was significantly higher ($p<0.001$, as determined by $\chi 2$ statistical analysis) in siDDX5-treated cells (9.4%) than in siC-treated cells (7.9%) (Figure R28C).

To investigate whether the activity of DDX5 would be specific or not at DSBs, we performed the same analysis this time using the data from the DRIPc-seq of UAP56-depleted cells. We displayed the general tracks of the distribution of the signal from γH2AX ChIP-seq and siUAP56 DRIPc-seq (Figure R28D). Plotting DRIPc-seq signal from siUAP56 cells through γH2AX ChIP-seq peaks revealed the same pattern than before. Indeed, the RNA-DNA signal enrichment observed in siUAP56 cells at DSBs sites was even higher than in siDDX5 cells (Figure R28E). Moreover, the proportion of the RNA-DNA hybrids detected by DRIPc-seq in UAP56-depleted cells that overlapped with γH2AX positive sites (γH2AX+) was significantly higher ($p<0.001$, as determined by χ^2 statistical analysis) in siUAP56-treated cells (10.8%) than in siC-treated cells (8.9%) (Figure R28F).

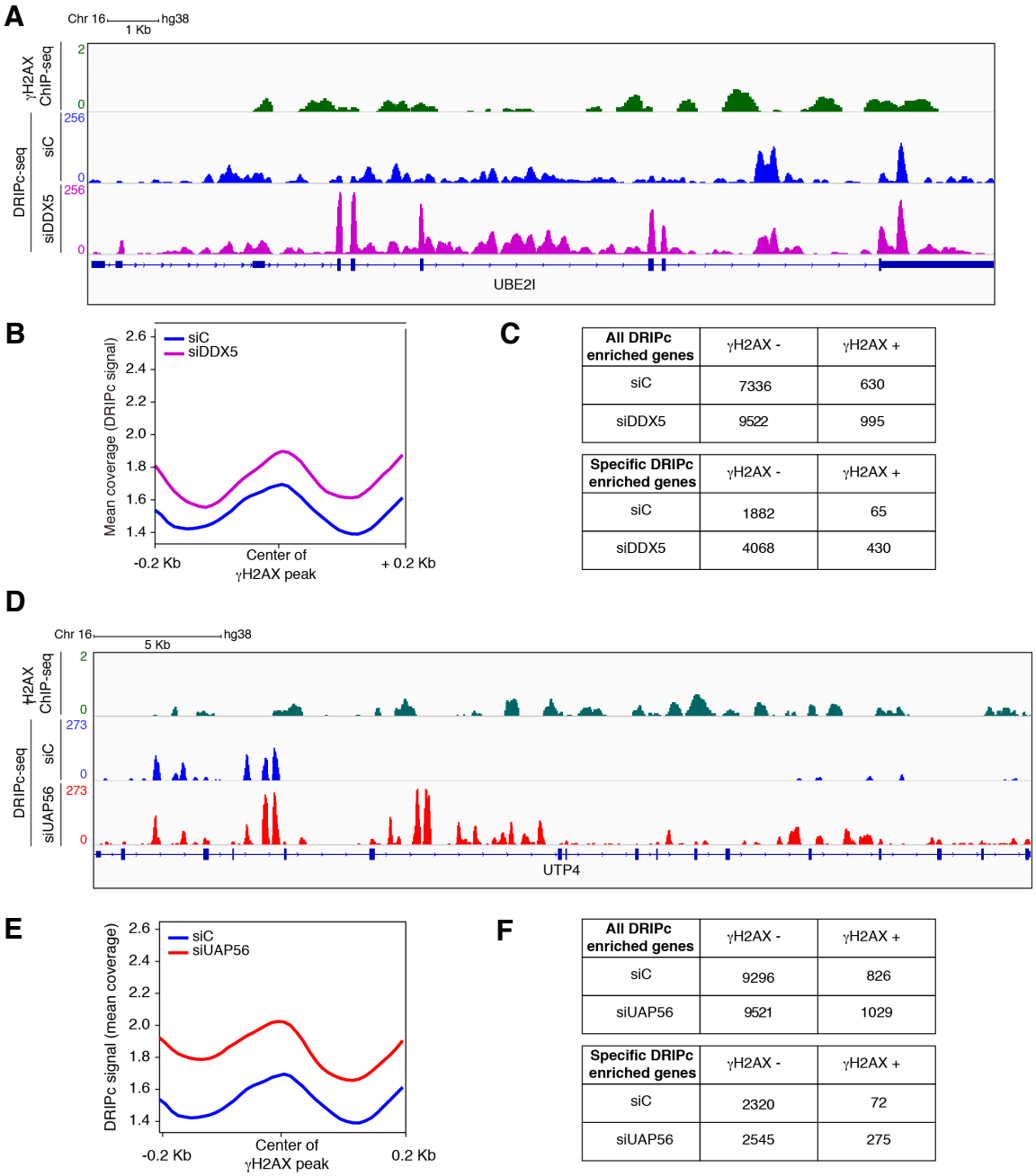

Figure R28. Correlation analysis of γH2AX and R loop distribution genome-wide.
(A) Representative screenshot of a representative genomic region showing the γH2AX signal profile of K562 cells (green) and DRIPc-seq signal profiles for siC- (blue) and siDDX5- (pink) transfected K562 cells along the *UBE2I* gene. **(B)** Distribution of DRIPc signals (mean coverage) along a gene metaplot for siC- (blue) and siDDX5- (pink) treated cells throughout the γH2AX peaks in the first biological replicate. **(C)** Comparative analysis between DRIPc-seq enriched genes overlapping a region with positive signal for γH2AX (γH2AX +) or not (γH2AX -) in siC- or siDDX5- transfected K562 cells in the first biological replicate. **(D)** Representative screenshot of a representative genomic region showing the γH2AX signal profile of K562 cells (green) and DRIPc-seq signal profiles for siC- (blue) and siUAP56- (red) transfected K562 cells along the *UTP4* gene. **(E)** Distribution of DRIPc signals (mean coverage) along a gene metaplot for siC- (blue) and siUAP56- (red) treated cells throughout the γH2AX peaks in the first biological replicate. **(F)** Comparative analysis between DRIPc-seq enriched genes overlapping a region with positive signal for γH2AX (γH2AX +) or not (γH2AX -) in siC- or siUAP56- transfected K562 cells in the first biological replicate.

To investigate the particular pattern changes in R loop distribution upon knock-down of different DDX helicases, we compared the DRIPc-seq profiles of the UAP56- and DDX5-depleted cells. As can be seen in Figure R29A, general inspection of the tracks showed similar profiles in the siC control, siUAP56 and siDDX5 cells. However, cells deprived of these RNA helicases presented higher signal intensity of DRIPc-seq as well as new peaks respect to control cells. Indeed, there were many regions across the genome in siUAP56-treated cells in which new specific DRIPc-seq peaks arose when compare to control and siDDX5 cells (Figure R29A). Moreover, analysis of hybrid-prone genes identified in both conditions indicated that they were significantly longer than the median of the genome (Figure R29B). To compare those hybrid-prone genes identified after the depletion of each DDX helicase, we tested the overlap between them. Venn diagram revealed that indeed the 77% of hybrid-prone genes were identified in both conditions, consistent with the global role as RNA chaperones of both proteins (Figure R29C). This is also supported by the existing correlation between DRIPc-seq data from siUAP56 and siDDX5 cells (Figure R29D). Altogether, these data suggest a global function of these factors in the prevention of R loop accumulation and highlight the importance of the RNA metabolism in this process.

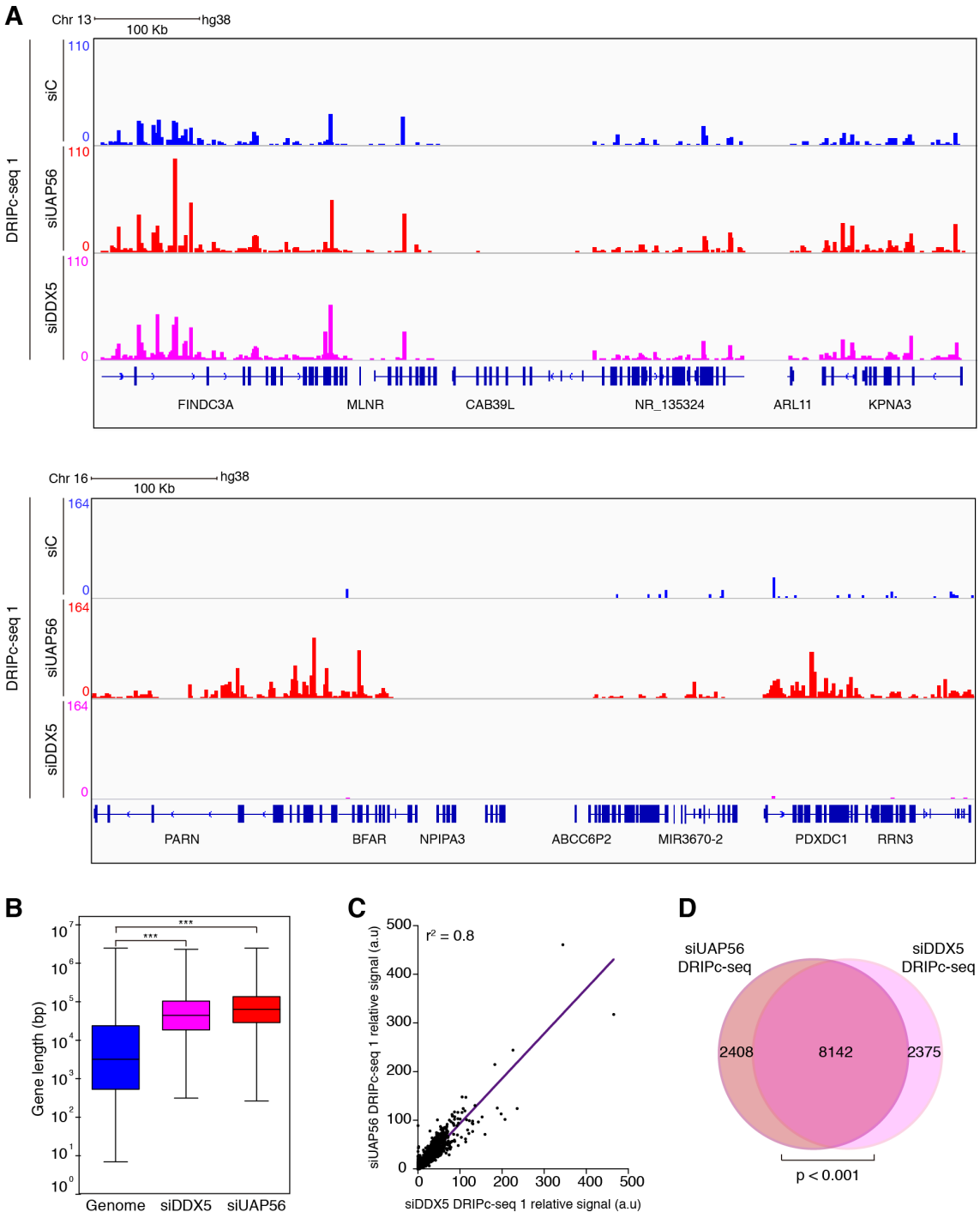

Figure R29. Comparison of hybrid-prone genes in UAP56- and DDX5-depleted cells.
(A) Representative screenshots of different genomic regions showing the DRIP-seq signal profile for the DRIPc-seq signal profiles for siC (blue), siDDX5-transfected cell (pink) and siUAP56-transfected cells (red). **(B)** Statistical analysis of length values for hybrid-prone protein coding genes in DDX5- and UAP56-depleted cells. Median values are represented. ***, $P < 0.001$ (Mann-Whitney U-test, two tailed). **(C)** *xy* correlation plot between siUAP56 and siDDX5 DRIPc-seq samples (r^2, Pearson correlation). **(D)** Venn diagram showing the overlap between hybrid-prone protein coding genes in siUAP56 and siDDX5 cells. $P < 0.001$ (Hypergeometric test).

3. ROLE OF SNAIL1 IN THE MAINTENANCE OF GENOME INTEGRITY

3.1. Snail1 is required for the maintenance of genome stability

The transcriptional factor Snail1 is widely known for its critical role in the control of EMT and cell invasion (Batlle et al., 2000). During this process cells undergo changes in chromatin organization, given the new characteristics and expression patterns that cells acquire after this transition (McDonald et al., 2011). Snail1 has been proposed to have a regulatory role in heterochromatinic transcription through the control of the expression of noncoding pericentromeric RNAs in mice (Millanes-Romero et al., 2013). Given this, together with the emerging role of the co-transcriptional R loops in gene expression and chromatin structure, made us wonder about the possible role of Snail1 in R loop-dependent genome instability and R loop homeostasis.

3.2. Genome instability in Snail1-depleted cells

First, we checked Snail1 depletion in HeLa cells via siRNA. As shown in Figure R30A, siRNA-transfected HeLa cells exhibit a clear reduction in Snail1 mRNA levels. Next, we tested whether the transient depletion of Snail1 in HeLa cells leads to an accumulation of DNA breaks, as detected by comet assay and by IF of γH2AX foci in comparison with siC control cells. Both SSBs and DSBs were detected by alkaline comet assays. Snail1-depleted cells lead to a significant increase (2.9 fold) in tail moment (Figure R30B). To determine whether this DNA break accumulation in siSnail1 cells was dependent on transcription, we performed alkaline comet assays in which transcription was inhibited with cordycepin. As can be seen in Figure R30B, the addition of cordycepin suppressed the increase in DNA breaks as detected by alkaline comet assay. Given the transcription-dependency of the increase in DNA damage, we then asked whether this was also dependent on R loops. We determined γH2AX foci, as a marker of DNA damage, in HeLa cells depleted of Snail1 after RNase H1 overexpression. Importantly, the number of cells containing > 5 foci of γH2AX was reduced in Snail1-depleted cells overexpressing RNase H1 down to the siC-control levels (Figure R30C). Therefore, the DNA damage accumulated in siSnail1 cells was R loop-dependent.

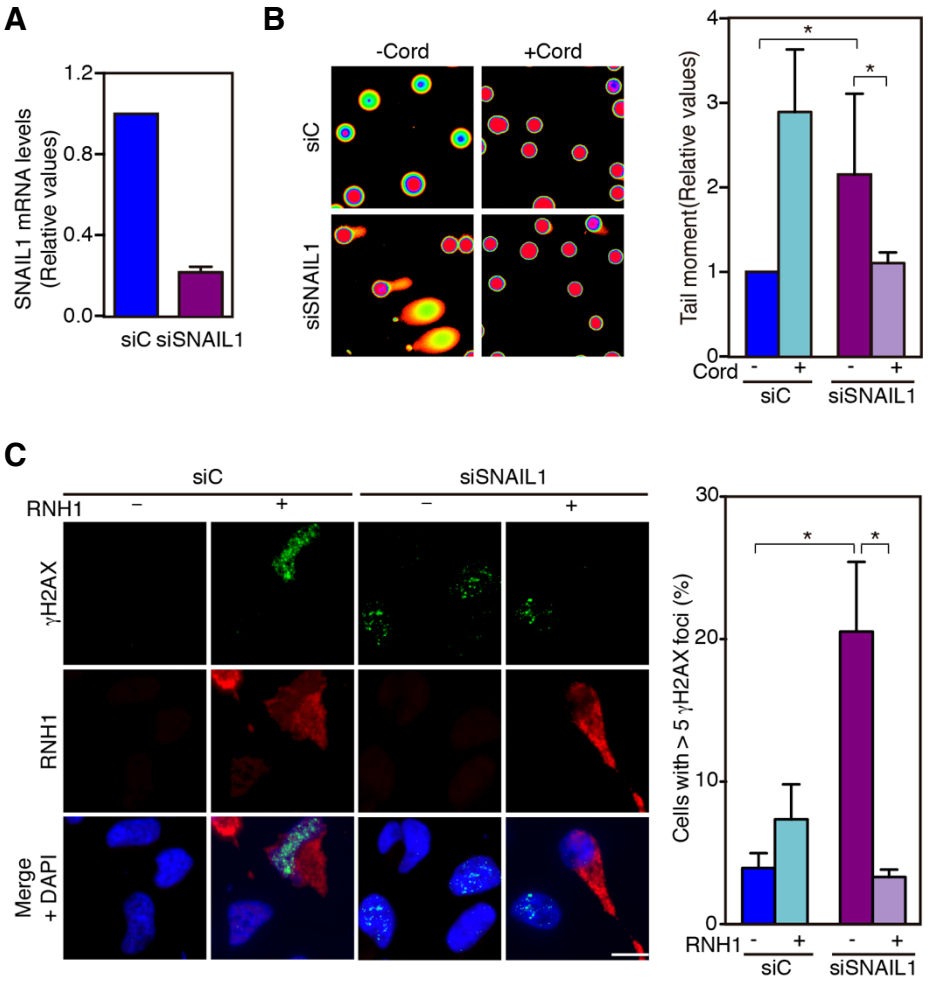

Figure R30. Accumulation of DNA breaks in SNAIL1-depleted cells.
(A) RT-qPCR in siRNA transfected HeLa cells to measure the relative levels of *SNAIL1* mRNA, using the HPRT housekeeping gene to normalize those values. Plotted values represented as means and SEM (n=3). **(B)** Alkaline comet assay of siC and Snail1-depleted HeLa cells untreated or treated with 50 μM of cordycepin for 4 hours. Relative comet-tail moments are represented as means and SEM (n=3). *, $P < 0.05$ (Mann-Whitney U test). **(C)** γH2AX immunofluorescence in siC control and Snail1-depleted cells. Percentage of cells with > 5 γH2AX foci was shown. Nuclei were stained with DAPI. γH2AX foci are represented as means and SEM (n=3). *, $P < 0.05$ (Student T-test). Scale bar, 25 μm.

3.3. Snail1-depleted cells accumulate R loops

Next, we assayed directly whether R loop accumulation was increased in siSnail1 cells by IF using the S9.6 monoclonal antibody. Quantification of the S9.6 nuclear signal revealed a significant increase after Snail1 knock-down (Figure R31A). Then, as previously described, we further analyzed this RNA-DNA hybrid accumulation with the more reliable technique, DRIP in two genes that have been previously validated for this purpose (Bhatia et al., 2014; Garcia-Rubio et al.,

2015; Herrera-Moyano et al., 2014). As can be seen in Figure R31B, R loops significantly accumulate in Snail1-depleted cells in the analyzed genes (*APOE* and *RPL13A*). Consistently, RNA-DNA hybrid signal were completely removed by *in vitro* RNase H treatment as a confirmation of the specificity of the assay (Figure R31B). Given that Snail1 can alter the transcription pattern of different genes, we tested whether the increased levels of RNA-DNA hybrids were caused by an increase in the transcription of those genes. We found, as corroborated by RT-qPCR in siC and siSnail1 cells, no significant differences in mRNA levels of those genes (Figure R31C). Altogether, these data indicate that Snail1 depletion leads to a significant increase of R loops at the cellular and molecular levels.

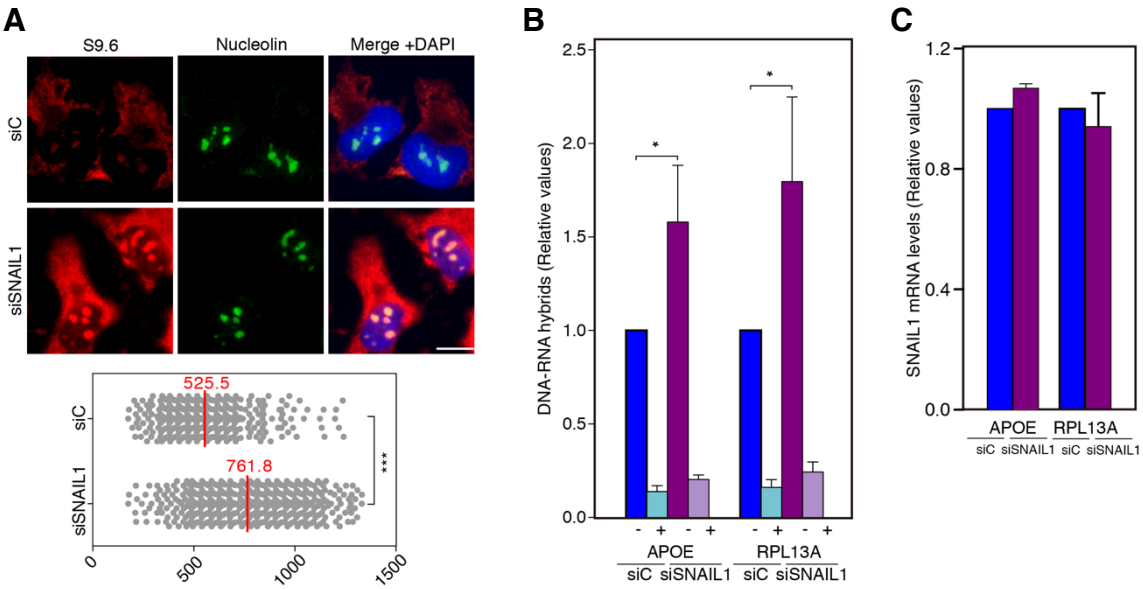

Figure R31. R loop accumulation in Snail1-depleted cells.
(A) Immunofluorescence of S9.6 (red) and anti-nucleolin (green) in siC and siSnail1-transfected HeLa cells. The median of S9.6 signal intensity per nucleus after nucleolar signal removal is represented (n=3). ***, $P < 0.001$ (Mann-Whitney U test, two-tailed). Scale bar, 25 μm. **(B)** DRIP-qPCR using the anti-RNA-DNA hybrid S9.6 monoclonal antibody in siC and siSnail1-transfected cells at indicated regions. Samples were treated or not with RNase H prior immunoprecipitation. Values normalized respect to the siC control are plotted (n=3) as means and SEM. *, $P < 0.05$ (Mann-Whitney U test). **(C)** RT-qPCR in siSnail1-transfected HeLa cells to measure the relative levels of *APOE and RPL13A* mRNA, using the HPRT housekeeping gene to normalize those values. Plotted values represented as means and SEM (n=3).

3.4. Replication impairment in Snail1-depleted cells

As reasoned before, R loops can represent an obstacle for RF progression at regions of putative transcription-replication conflicts (Aguilera and Garcia-Muse, 2012). Consequently, we wondered whether RF progression in siSnail1-

transfected cells was altered. To investigate it using an accurate technique, we performed DNA combing assay in HeLa cells to analyze single DNA fibers. As already described, both subsequent thymidine analogues (IdU and ClU) were added to the media and incorporated into the DNA during replication permitting its immuno-detection on isolated DNA once it has been stretched. Combing in HeLa cells after Snail1 depletion for 72 hours revealed that replication velocity was reduced (Figure R32). Notably, this reduction in RF velocity was accompanied by an increase in the frequency of RF stalling as measured by RF asymmetry (Figure R32). Importantly, in agreement with the hypothesis that R-loops are the main responsible of these phenotypes, overexpression of RNase H1 recovered both phenotypes in Snail1-depleted cells restoring fork velocity and asymmetry (Figure R32). Therefore, our results indicate that silencing of Snail1 promotes slower RF progression and RF stalling that are mediated by R-loops, suggesting that these are a primary cause of the increased DNA damage.

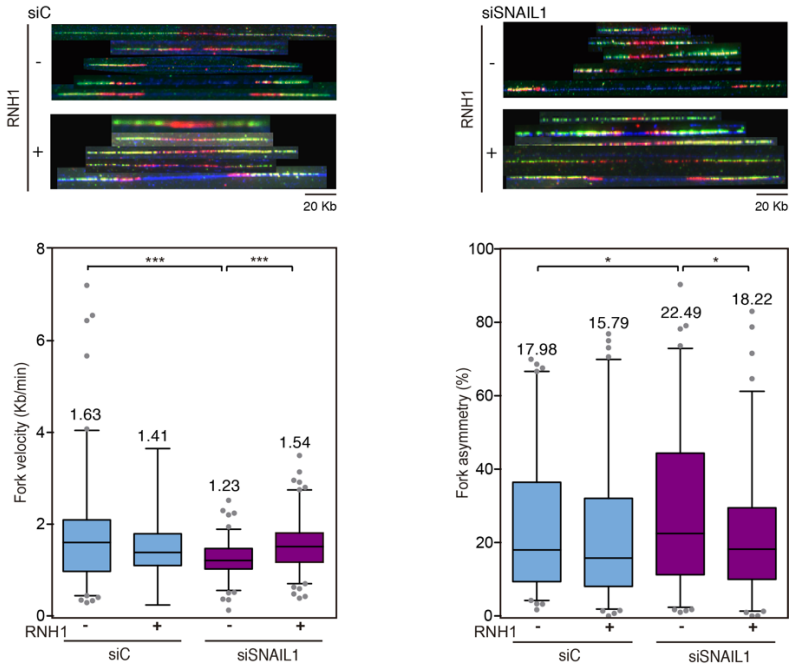

Figure R32. Replication analysis of Snail1-depleted cells.
Effect of Snail1 depletion on DNA replication detected by single molecule DNA combing assay. Representative pictures of DNA fibers labeled by IdU and CIdU for single DNA molecule analysis in HeLa cells. (Left) Profile of RF velocity and (right) asymmetry of siC and Snail1-depleted HeLa cells transfected with the empty vector pcDNA3 or pcDNA3-RNaseH1 (+RNH1) for RNase H1 overexpression are shown. Data are plotted as box and whiskers (5-95 percentile) where median values are indicated (n=2). *, $P < 0.05$; ***, $P < 0.001$ (Mann-Whitney U test, two-tailed).

DISCUSSION

In this thesis we have analyzed in detail the role of UAP56 in the maintenance of genome stability. We have observed that, on one hand, depletion of UAP56 caused R loop-dependent genome instability and replication defects. On the other hand, UAP56 overexpression rescued R loop accumulation and DNA damage phenotypes. *In vitro* analysis shows that UAP56 has a novel function as an RNA-DNA helicase and R loop resolvase in addition to its previously reported RNA-RNA helicase activity. Inactivation of the helicase activity led to R loop accumulation and genome instability *in vivo*. Moreover, we show that UAP56 not only interacts with THOC1, a subunit of the THO complex, but also with the Sin3A histone deacetylase complex. Importantly, we provide genome-wide data of global UAP56 recruitment to actively transcribed genes and the R loop distribution in UAP56-depleted cells, supporting a general function of UAP56 all over the active genome. We have also evaluated the role of another RNA helicase, DDX5, in RNA-DNA hybrid homeostasis and found that it also presented a global function in the prevention of such structures. Finally, to evaluate the possible implication of other transcription factors on R loops metabolism, we have analyzed the depletion of Snail1, a master transcription factor crucial in the EMT. Interestingly, we have underscored that Snail1 depletion leads to R loop accumulation, R loop-dependent genome instability and replication alterations phenotypes suggesting a new role for Snail1 in R loop control.

1. ROLE OF UAP56 IN R LOOP PREVENTION AND RESOLUTION

1.1. UAP56 as an RNA chaperone that warrants genome integrity

During transcription, many factors with a role in RNA metabolic steps are loaded to active chromatin via the RNAPII or the nascent RNA, thus progressing through the ORF of genes from 5' to 3' together with the RNAPII and transcription elongation factors (Maniatis and Reed, 2002). Among them, the THO complex interacts with the RNA helicase UAP56/DDX39B and the export factor ALY/REF constituting the so-called THO/TREX complex that couples transcription and export (Strasser et al., 2002). UAP56 has been shown to perform a central role in the THO/TREX assembly facilitating the ATP-dependent interaction of several

RBPs with THO. The involvement of UAP56 RNA-dependent ATPase activity in this process suggests that this DDX helicase could be an RNA chaperone that unwinds RNA secondary structures and at the same time is capable of adding/removing RBPs to assemble an export-competent mRNP. In agreement, UAP56 is necessary for the export of most of the mRNAs, as has been shown in yeast, *Drosophila, C. elegans* and human cells (Gatfield et al., 2001; Herold et al., 2003; Jensen et al., 2001; Kapadia et al., 2006).

The observation that THO/TREX was necessary for mRNA export (Jimeno et al., 2002; Strasser et al., 2002) and the fact that yeast THO mutants presented increased levels of RNA-DNA hybrids (Huertas and Aguilera, 2003) led to propose a connection between RNA export and genome stability. Thus, work in yeast and mammals has revealed that mRNP biogenesis is also crucial to maintain genome integrity. Mutations in different mRNP factors that affect the proper assembly of the mRNP result in genome instability (Luna et al., 2005; Paulsen et al., 2009; Stirling et al., 2012; Wahba et al., 2011), which has been associated with RNA-DNA hybrids (Huertas and Aguilera, 2003; Li and Manley, 2005). These findings suggest that a sub-optimally assembled mRNP would propitiate R loop formation (Aguilera, 2005b). In this thesis, we have unveiled the role of UAP56 in the maintenance of genome integrity. In an exhaustive characterization of the resultant phenotype derived from the lack of UAP56 in human cells, we have demonstrated that the observed siUAP56-driven genome instability (Dominguez-Sanchez et al., 2011) is indeed transcription- and R loop-dependent (Figure R3 and R4), as occurred in the case of the THO-depleted cells (Dominguez-Sanchez et al., 2011; Salas-Armenteros et al., 2017). These data are consistent with Sub2 studies in yeast, where mutations of *SUB2* led to similar defects in transcription and genome instability to those of THO mutants, indicating a similar function. In the current view, the R loop accumulation phenotype of UAP56 knock-down cells would be mainly attributed to the defects in mRNP biogenesis. This is supported by an increasing number of reports where the presence of R loops were confirmed after the silencing of other mRNP processing factors, helicases and RNA binding factors such as SRSF1, DDX19,

DDX23, SETX/Sen1 or AQR (Hodroj et al., 2017a; Li and Manley, 2005; Paulsen et al., 2009; Sollier et al., 2014; Sridhara et al., 2017) (Figure D1A).

1.2. UAP56 as an RNA-DNA helicase and R loop resolvase

R loops have been considered to constitute a major barrier for the RF progression either by themselves or by their ability to trap the RNAPII at the DNA. Such R loop mediated transcription-replication conflicts could derive in DNA breaks and in the end, genome instability and chromosome fragility (Garcia-Muse and Aguilera, 2016; Hamperl and Cimprich, 2016). Consistently, we showed DNA replication impairment in UAP56-depleted cells that is suppressed by RNase H (Figure R7). These data are in agreement with the fact that yeast and human cells with defective THO complex exhibited R loop-mediated hyper-recombination linked to an increase in transcription-replication conflicts (Gomez-Gonzalez et al., 2009; Gomez-Gonzalez et al., 2011; Huertas and Aguilera, 2003; Salas-Armenteros et al., 2017; Wellinger et al., 2006). In agreement, we have shown an R loop-dependent DNA replication impairment in THOC1-depleted human cells, as indicated by an increased asymmetry as a measurement of RF stalling detected by DNA combing (Figure R8). However, whereas THOC1 knock-down led to faster RF progression, UAP56 depletion causes a slow-down of forks. This could be explain attending to the different nature of these proteins. While THOC1 does not possess any helicase activity, the previous reported helicase activity of UAP56 (Shen et al., 2007) suggests a possible direct action of UAP56 over RNA-DNA hybrids beyond its role in mRNP biogenesis (Figure R7 and R8).

By testing this hypothesis, we demonstrate that UAP56 is able to unwind RNA-DNA hybrids and structures that resemble an R loop *in vitro* (Figure R10 and R11). In parallel, we also show that overexpression of UAP56 in different genetic backgrounds, which accumulate high levels of R loops, suppressed R loops and R loop-mediated genome instability, confirming the relevance of its RNA-DNA unwinding activity *in vivo* (Figure R13). These data ratify that the ability of UAP56 to eliminate hybrids is additional to its role in mRNA processing and export (Figure D1B). Such results are coherent with studies in yeast, where

overexpressed Sub2 showed also the ability to suppress the growth defect and genome instability of *hpr1* mutants (Jimeno et al., 2002). Moreover, these conclusions are supported by the fact that helicase-dead UAP56 mutant proteins are unable to unwind RNA-DNA hybrids *in vitro*. By contrast, they cause high levels of R loops and genome instability *in vivo* (Figure R11 and R14), likely indicating that the helicase-dead proteins bind and stabilize the hybrid strengthening its negative impact on genome integrity, as it has been shown for nuclease-dead RNase H or RBPs such as Yra1 (Chen et al., 2017; Garcia-Rubio et al., 2018). Mutational analysis of Sub2 strengthened these findings, since overexpression of certain Sub2 helicase-dead mutants resulted in growth deficiency and severe hyper-recombination phenotypes (Saguez et al., 2013). Indeed, there are precedents of negative effects caused by the overexpression of mutant RNA helicases. Previous studies in rabbit reticulocyte lysates showed that the eukaryotic initiation factor-4A (eIF4A)-driven translation was inhibited when defective eIF4A was added (Pause et al., 1994). In the same line, ATPase-dead mutant UPF1 abrogated NMD in human cells (Sun et al., 1998). Considering that UAP56/Sub2 mutants proteins are not able to hydrolyze the ATP to facilitate their co-transcriptional action, it is also possible that failures in the binding or the release of their key interaction partners could trigger genome instability via its inability to resolve RNA-DNA hybrids or even by increasing R loop formation. Therefore, this discovery could be used as a tool to stabilize R loops, as previously reported for yeast Yra1 overexpression or the GFP fused to the hybrid-binding domain of RNase H1 (Bhatia et al., 2014; Garcia-Rubio et al., 2018). This would replace the need of the depletion of any R loop homeostasis-related factor by generating a high R loop basal level to work with.

1.3. Functional association of UAP56 with THO and Sin3A complexes in R loop prevention

Chromatin has emerged as another factor implicated in R loop homeostasis. Studies in *S. cerevisiae* revealed the existence of certain histone H3 and H4 mutants that presented high levels of R loop accumulation (Garcia-Pichardo et al., 2017). In this line of thought, correlation analysis between R loops and

chromatin state have uncovered an R loop association with DNase I hyper-accessibility (Chen et al., 2017; Sanz et al., 2016). Here we show that promoters of R loop-enriched genes in siUAP56 cells associate with active chromatin marks such as H3K4me2 and H3K9Ac (Figure R23) suggesting an open chromatin state. Such findings are in agreement with studies of R loop accumulation observed in human cells deprived of the histone deacetylase complex Sin3A and cells treated with histone deacetylase inhibitors, such as TSA, where a more accessible DNA is thought to favor RNA-DNA hybridization (Salas-Armenteros et al., 2017). We have previously demonstrated that THO not only prevents R loop formation by ensuring an optimal structure of the mRNP but also via the interaction with Sin3A promoting local co-transcriptional histone deacetylation and thus, transiently closing the chromatin (Salas-Armenteros et al., 2017). Now, we introduce another actor in this scenario, UAP56, which interacts with both, the THO and Sin3A complexes. During transcription, THO, UAP56 and other RBPs bind to the nascent RNA, as it emerges from the RNAPII, warranting an appropriate mRNP structure to prevent R loop formation. Additionally, THO also interacts with the Sin3A complex likely to promote its role on chromatin and to avoid the arising of such harmful structures. Finally, the RNA-DNA helicase UAP56 would remove unscheduled co-transcriptional hybrids formed behind the transcription machinery, thus potentially releasing the intact nascent RNA molecule for further processing and export (Figure D1).

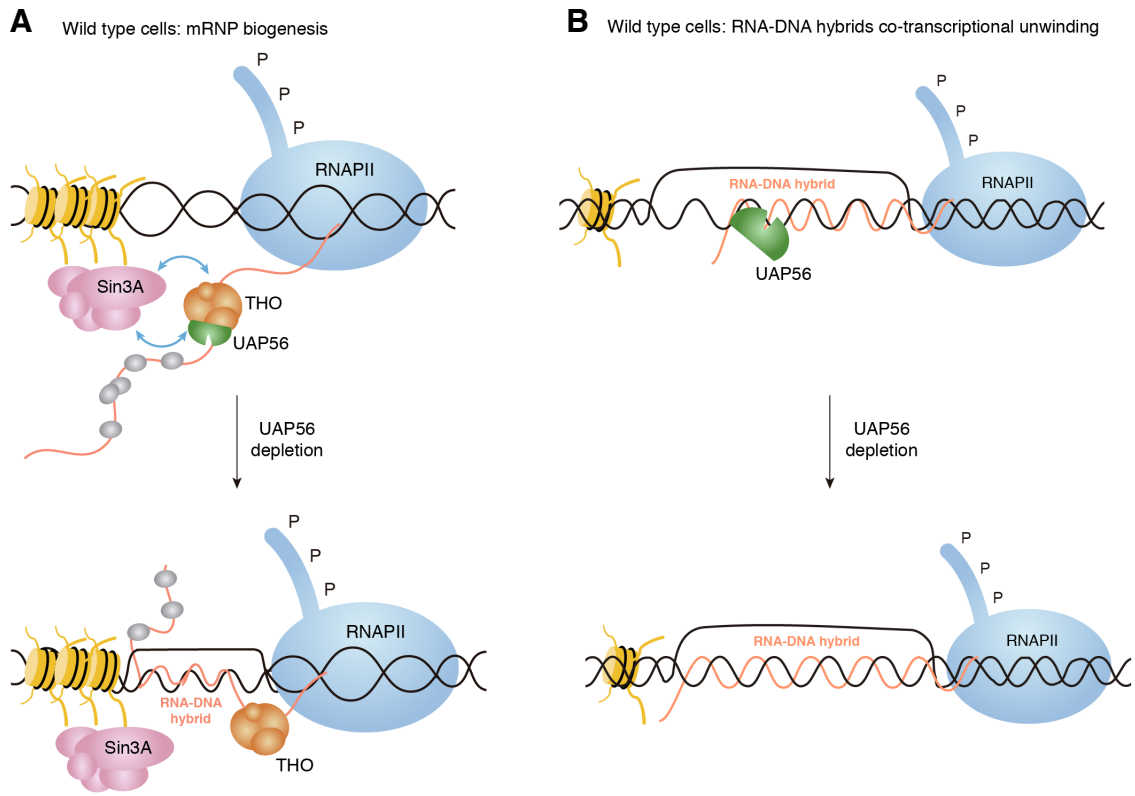

Figure D1. A dual role of UAP56 in the maintenance of genome integrity.
(A) In wild type cells, the co-transcriptional process of mRNP biogenesis and several RNA binding factors ensure an optimal structure of the mRNP to avoid the hybridization of the mRNA with its DNA template preventing the R loop formation. **(B)** Under normal circumstances, UAP56 is also able to unwind co-transcriptionally R loops using its R loop resolvase activity.

2. UAP56 WARRANTS GENOME STABILITY GENOME-WIDE

2.1. Genome-wide chromatin-associated action of UAP56

As anticipated for a general co-transcriptional RNA-binding and processing factor, we have observed that the action of UAP56 is extended all over the genome and not restricted to specific regions or to a subset of genes according to function or structure. UAP56 is located in the majority of the transcribed regions of genes in a gradient manner from 5' to 3' (Figure R18). This is consistent with the expected function of UAP56 in mRNP biogenesis and export, which are intimately linked to transcription. Moreover, its interaction with the Sin3A histone deacetylase complex (Figure R2) also supports the function of UAP56 in chromatin during transcription. The reported interaction between UAP56 and THO and genome-wide studies of the Sub2 and Hpr1 yeast homologues, which also showed a recruitment of both factors to RNAPII-transcribed genes with a

tendency to accumulate at the 3' of the transcribed region, endorse our results (Gomez-Gonzalez et al., 2011; Strasser et al., 2002). Additionally, we have found a downregulated transcriptome for UAP56-depleted cells (Figure R16) in agreement with the proposed role of UAP56 in mRNP biogenesis. Similar effects have been reported in yeast, where a reduction of total mRNA levels was observed as a consequence of mutations in Sub2 (Jimeno et al., 2002; Libri et al., 2002; Zenklusen et al., 2002), *Drosophila*, in which the overall reduction of mRNA levels was shown (Herold et al., 2003) and *C. elegans* (MacMorris et al., 2003). These results exemplifying that high transcription levels are not indispensable for the occurrence of RNA-DNA hybrids. In fact, RNA-DNA hybrids also appeared in transcription defective mutants, as is the case of THO (Huertas and Aguilera, 2003). Actually, RNA-DNA hybrids have been shown to affect transcription elongation (Tous and Aguilera, 2007). In addition, defects in RNA export that lead to an RNA accumulation in the nucleus, as could be the case of siUAP56 cells, have been demonstrated not to be sufficient either to induce RNA-DNA hybrids by themselves (Garcia-Rubio et al., 2018) corroborating that R loop are not just the result of high transcription rates. Altogether, these data fit with the idea of the existence of a multi-protein platform that would be formed at active transcription sites as an intrinsic part of the transcription activity. It is feasible that these proteins would assemble this structure to further process and export the nascent RNA co-transcriptionally. Thus, UAP56 would work at the site of transcription interacting with other RBPs such as THO or ALY. Indeed, the recent resolution of the crystal structure of UAP56 in complex with these factors supports this hypothesis (Ren et al., 2017).

2.2. UAP56 prevents R loop formation genome-wide

Concomitantly, we reasoned that cells lacking UAP56 would be defective firstly in mRNP biogenesis, as is the case of cells deprived of the THO complex, and secondly in the removal of co-transcriptional unscheduled R loops, due to the lack of its helicase activity. In agreement, we found that UAP56-depleted cells accumulate hybrids essentially at RNAPII transcribed genes all over the genome, being the largest fraction of R loops observed over gene bodies (Figure R20).

The RNA-DNA signal distribution peaks at promoters and then spreads from 5' to 3', with a weak enrichment towards the latter (Figure R21). These profiles are consistent with previous studies where similar RNA-DNA distribution has been shown in human (Manzo et al., 2018; Sanz et al., 2016) and wild type yeast cells (Wahba et al., 2016), and are in agreement with the co-transcriptional nature of those R loops.

Although the mechanistic implications of R loops in these regions remains to be clarified, it is possible that these unscheduled R loops may have consequences for gene expression. Indeed, there are several reports that show the role R loops in gene expression. R loops have been linked to unmethylated CpG islands at many gene promoters of mammalian cells protecting them from methylation and thus, from transcription silencing (Ginno et al., 2012; Grunseich et al., 2018). It seems that RNA-DNA hybrids are less preference for the binding of the DNA methyl-transferase 1 than the dsDNA (Grunseich et al., 2018). Moreover, R loops can also serve as a guide for the binding of transcription regulator factors, as is the case of the regulation driven by lncRNAs. This is exemplified in the human VIM promoter, where antisense transcription leads to the generation of a lncRNA that forms an R loop around this promoter region permitting the recruitment of transcription factors. Thus, VIM expression is avoided by the depletion of this lncRNA or RNase H overexpression that would degrade this R loop (Boque-Sastre et al., 2015). Analogously, the lncRNA TARID (resulting from the antisense transcription of the tumor suppressor gene TCF21) forms an R loop at TCF21 promoter that mediates the binding of the stress response protein GADD45A that, in turn, recruits the methylcytosine dioxygenase TET1 triggering DNA demethylation and TCF21 expression (Arab et al., 2019). On the contrary, at termination regions, the capability of R loops to hamper transcription could be used as an initial pause signal to slowdown RNAPII (Skourti-Stathaki et al., 2011) that would facilitate the co-transcriptional splicing process or the correct termination and polyadenylation of the nascent mRNA (Proudfoot, 2016; Wahba et al., 2016). In this context, a role for SETX has been proposed in removing R loops downstream of the gene poly(A) signal. It seems

that the di-methylation of an RNAPII CTD arginine residue recruits the Tudor-domain protein SMN which, in turn, interacts with SETX to resolve these R loops allowing the access of the exonuclease Xrn2 and termination factors (Skourti-Stathaki et al., 2011; Zhao et al., 2016). Importantly, R loop metaplot analyses obtained from our DRIPc-seq after UAP56 depletion are very similar to the UAP56 binding profile detected by ChIP-seq. Both profiles peak at promoters and accumulate towards the 3' end of genes, consistent with the proposed role of UAP56 in the removal of co-transcriptional RNA-DNA hybrids (Figure R18 and R21). This is supported by the high coincidence between regions that accumulate R loops after UAP56 depletion and those that accumulate UAP56 in WT cells, as well as by the fact that hybrid-prone genes in WT cells present increased UAP56 binding (Figure R22).

2.3. DDX5 as another RNA-dependent ATPase that prevents R loop formation genome-wide

During the last years, it is noteworthy that the number of reports identifying RNA-dependent ATPases involved in R loop homeostasis have exponentially increased. Attending to this striking fact, we have assessed a comparative R loop analysis with another RNA-dependent ATPase, as is the case of DDX5. This protein is specially compelling since recent studies have evidenced its interaction with BRCA2, in which this factor boosted DDX5 helicase activity to unwind RNA-DNA hybrids *in vitro* (S. Gaetana and A. Carreira, unpusblished results). As formerly noted for UAP56, cells lacking DDX5 are also deficient in a proper mRNP biogenesis and accumulate R loops due to the absence of this RNA chaperone. Accordingly, DDX5- and UAP56-depleted cells share similar R loop distribution and DRIPc gene metaplot profiles (Figure R21 and R26). This analysis in siDDX5 cells repeats an RNA-DNA hybrid accumulation genome-wide, rather to be succinct to a subset of genes. Thus, these data extend the recently reported role of Dbp2 (yeast DDX5) in the resolution of R loops on lncRNA in conjunction with Sen1 (Tedeschi et al., 2018) at transcription termination sites. Similarly, studies in human cells also propose a role for DDX5 in removing RNA-DNA hybrids at transcriptional termination regions downstream of poly(A) sites through its

interaction with the exonuclease Xrn2 (Mersaoui et al., 2019). This would be in agreement with a more pronounced enrichment towards the 3' end of the DRIPc signal observed for DDX5- respect to UAP56-depleted cells (Figure R26). Our DRIPc-seq data from this two different helicases revealed that both share many common regions where they can act preventing RNA-DNA hybrid accumulation. This suggests a global function of these proteins possibly due to their roles as RNA chaperones. In agreement with the general role of DDX5 in mRNP formation, studies on *S. cerevisiae* have reported an interaction between Dbp2 and other RBPs such as Yra1 (Ma et al., 2013; Ma et al., 2016). Whereas reports in human cells also suggested an interaction of DDX5 with the THO complex (Katahira et al., 2019). These data fit with the idea of a general action of the DEAD-box helicases as RNA chaperones to guarantee R loop prevention and genome stability by ensuring a proper mRNP biogenesis. This could be the case of DDX5, which would work during the mRNP biogenesis and whose action would be specially required at termination sites.

As we mentioned before, unpublished data from the lab of A.Carreira suggest that DDX5 could have a role in R loop removal at DSBs due to its interaction with BRCA2. This would be in agreement with our data showing an increased correlation between γH2AX recruitment and R loop-enriched genes in DDX5-depleted cells (Figure R28). However, a similar association was observed when analyzing UAP56-depleted cells (Figure R29). Consequently, it is possible that DDX5 would work together with other RBPs during mRNP biogenesis and at DSB. Given the accumulating evidence that shows that RNA-DNA hybrids can form at DSB (Aguilera and Gomez-Gonzalez, 2017), it is tempting to speculate that these or other helicases would be required for RNA-DNA hybrid removal allowing DSB repair. If a DSB occurs, BRCA2 assists its repair as a part of the HR pathway. Under this circumstance, the fact that BRCA2 interacts with DDX5 and boosts its RNA-DNA helicase activity suggests that this two factors would work together to prevent and resolve R loops at DSBs. However, given its similarities with UAP56, it is also conceivable that BRCA2 could work in association with other RNA helicases and RBPs involved in the mRNP

biogenesis and export, as could be the case of UAP56. Indeed, previous reports have shown the interaction between BRCA2 and the TREX-2 complex, also involved in mRNP biogenesis and export (Bhatia et al., 2014). Further experiments would be required to test these hypotheses. It would be also interesting to test the effects of DDX5 overexpression on R loop-dependent genome instability phenotype associated to the depletion of several factors involved in R loop homeostasis, such as the ones tested for UAP56.

3. PERSPECTIVES ON RNA HELICASES AS AN RNA-DNA RESOLVASES

Our study provides multiple pieces of evidence that support that UAP56 is a crucial RNA-DNA helicase able to co-transcriptionally remove R loops accumulated under different conditions *in vivo*. Given its genome-wide distribution all over the vast majority of transcribed DNA sequences, as detected by ChIP-seq, UAP56 emerges as a central RNA-DNA helicase removing unscheduled R loops formed during transcription. This has a key physiological relevance, because RNA-DNA hybrids need to be co-transcriptionally removed not only to avoid RF blockage and replication stress, but also to prevent transcription elongation impairment and premature transcription termination.

It is noteworthy that in the last years an increasing number of studies have demonstrated the RNA-DNA unwinding activity for different DDX RNA helicases. This is consistent with the ability of these proteins to act efficiently on short RNA-DNA heteroduplexes (Linder and Jankowsky, 2011) and their roles in gene expression as RNA chaperones. As a consequence, different reports showed an increase in RNA-DNA hybrids after depletion of such helicases including DDX19, DDX21, DDX23 or DDX5 (Hodroj et al., 2017a; Mersaoui et al., 2019; Song et al., 2017; Sridhara et al., 2017). The nucleopore-associated mRNA export factor DDX19 has been found to assist R loop removal via ATR/Chk1 upon DNA damage (Hodroj et al., 2017a). Instead, DDX23 is phosphorylated as a result of the R loop induced RNAPII pausing to resolve those structures (Sridhara et al., 2017). On the other hand, DDX21 promotes transcription elongation through the activation of the pTEFb elongation factor (Song et al., 2017). In addition, other

helicases such as DDX5 or FANCM have been also shown RNA-DNA unwinding activity *in vitro* and its depletion in cells lead to an increase in R loop accumulation (Mersaoui et al., 2019; Schwab et al., 2015). Therefore, in spite of the numerous studies about RNA helicases in this context, it remains unclear whether these helicases act directly unwinding the RNA-DNA hybrids or whether their capacity to deal with these structures consists in ensuring an optimal structure of the mRNP and its release. In this regard, the observation that certain RNA helicases could contribute to form R loop increases the skepticism about their role as R loop resolvases. This is the case of DDX1 which binds to G4 structures found in ncRNAs of immunoglobulin genes allowing the R loop formation necessary for class switch recombination (Ribeiro de Almeida et al., 2018), whereas it has also been shown to have RNA-DNA unwinding activity *in vitro* supposed to be required specially at DSB sites (Li et al., 2016). This also applies to the DHX9 helicase, whose capacity to unwind R loops *in vitro* is paralleled by its ability to promote R loop accumulation in spliceosome-defective conditions (Chakraborty et al., 2018).

Considering all the exposed, it is highly unlikely that different DDX proteins have redundant RNA-DNA unwinding abilities. It would certainly be possible that each DDX protein specifically works at a subset of R loops whether located in different DNA regions or nuclear structures (nucleolus, nuclear pore, away of pores) or whether formed by failures of different nuclear processes (transcription, splicing, export) or at different cell cycle stages, among other possibilities. Indeed, DDX21 and DDX23 seem to be specifically recruited at RNAPII stalling sites, whereas SETX could act at termination regions. However in this case, yeast Sen1 is expressed in the S-G2 phase of the cell cycle (Mischo et al., 2018), making it difficult to consider Sen1, and by extension SETX, a master co-transcriptional RNA-DNA unwinding factor.

Conversely, in the case of UAP56, we presupposed a more general role of this protein unwinding R loops during transcription. It is unlikely that cells rely only on RNases H to eliminate occasional co-transcriptional hybrids, because this would result in nascent RNA degradation, highly costly to cells. Instead, we

support an scenario in which a master transcription-coupled RNA-RNA and DNA-RNA helicase, such as UAP56, is able to release the nascent RNA from the DNA giving it a second chance to be properly coated into a full export-competent RNA -protein particle. We propose that in addition to its role as an RNA processing and mRNP biogenesis factor, UAP56 removes occasional hybrids that otherwise would block transcription and replication providing new insights into our understanding on how cells prevent and eliminate harmful RNA co-transcriptional structures.

4. SNAIL1 CONTRIBUTIONS TO MAINTAIN GENOME STABILITY

Snail1 is a master transcription factor that orchestrates the EMT. During this reversible biological process, epithelial cells lose their characteristics and acquire a mesenchymal phenotype which facilitates motility and thus, invasiveness. To achieve such a cellular remodeling, changes in the transcription pattern are required. Thus, there is a tightly control of the activation and repression of specific genes during EMT. In this context, Snail1 is considered the most important inductor of EMT by repressing the expression of diverse epithelial genes and, on the contrary, activating other mesenchymal genes. Interestingly, different reports have shown that chromatin reorganization occurs during EMT. It has been proposed a role for Snail1 and the co-repressor LOXL2 in regulating noncoding pericentromeric transcription and heterochromatin reorganization during EMT in mice (Millanes-Romero et al., 2013). Different analysis showed that many ncRNAs are involved in the regulation of high-order chromatin structure since they are supposed to function as a scaffold for silent chromatin assembly (Bernstein and Allis, 2005). Accordingly, studies in yeast also showed that ncRNAs transcribed from heterochromatin were associated with chromatin via the formation of RNA-DNA hybrids suggesting that R loops could play a role in chromatin ncRNA function (Nakama et al., 2012). Considering this precedent, we have studied the possible contribution of Snail1 in the maintenance of genome integrity in HeLa cells. Our analysis has shown that Snail1-depleted cells present an R loop-dependent genome instability phenotype characterized by an increase in DNA damage, R loop accumulation and replication defects (Figure R30, R31

and R32). Although these studies need to be expanded to more physiologically relevant cell lines with higher Snail1 expression levels or others used as EMT models, we provided here evidence linking Snail1 to R loop-dependent genome stability.

In HeLa cells, Snail1 ChIP-seq experiments (GSM3733671) available in the GEO database suggest that Snail1 is not only recruited to promoters as proposed in other cell lines, but also inside ORFs, as is the case of triple-negative breast cancer cells where Snail1 is also detected in intragenic regions (Maturi et al., 2018). This is consistent with other reports that propose that Snail1 occupies in a context-dependent manner different genomic locations in different cellular backgrounds (Beyes et al., 2019; Maturi et al., 2018; Millanes-Romero et al., 2013). Snail1 participates in regulating gene expression through its interaction with a wide range of transcriptional cofactors such as LOXL2, the Smad3/Smad4 complex, the histone deacetylase complex Sin3A, the protein Ajuba or the Polycomb repressive complex 2 (Ayyanathan et al., 2007; Herranz et al., 2008; Peinado et al., 2004; Peinado et al., 2005). Due to its diverse associations, Snail1 could help maintain chromatin organization linking transcriptional control with epigenetic modifications. In this context, the observed genome instability and replication defects are in concordance with reports in mouse cells where the lack of Snail1 drives alterations through heterochromatin replication and chromosomal instability (Millanes-Romero et al., 2013). To a large extent, our data suggest a possible involvement of R loops in these phenotypes, since in HeLa cells both phenotypes are rescued by RNase H1 overexpression. We consider three different ways by which Snail1 would protect from R loop accumulation, which in turn could lead to cell stress and thus, to genome instability. Firstly, Snail1 would act as a transcription repressor factor of specific genes through its interaction with different cofactors that promotes a repressive chromatin environment. In cells deprived of Snail1, those regions would become unrepressed favoring an open chromatin state more accessible to transcription complexes. This hyper-accessible state of the chromatin together with the fact that promoters are hotspots of R loop formation (Ginno et al., 2012) could facilitate that antisense

transcription favors the lncRNAs formation, which in turn would promote R loop formation. The accumulation of R loops would be also the result of an indirect effect caused by the unbalance between condensed and decondensed chromatin and of altered expression patterns (Figure D2A). Secondly, seeing that Snail1 has also been detected inside genes, it could be possible that Snail1 travel with the RNAPII favoring either directly or via other proteins transcription. In its absence, transcription would be compromised. A defective mRNP or RNAPII stalling would increase the possibility of hybridization of the mRNA with its DNA template leading to R loop accumulation. Indeed, previous reports have suggested the possible association between Snail1 and RNAPII at promoters (Wu et al., 2009) (Figure D2B). In short, the mechanism by which Snail1 preserve genome integrity is still unclear and further experiments are required for its understanding.

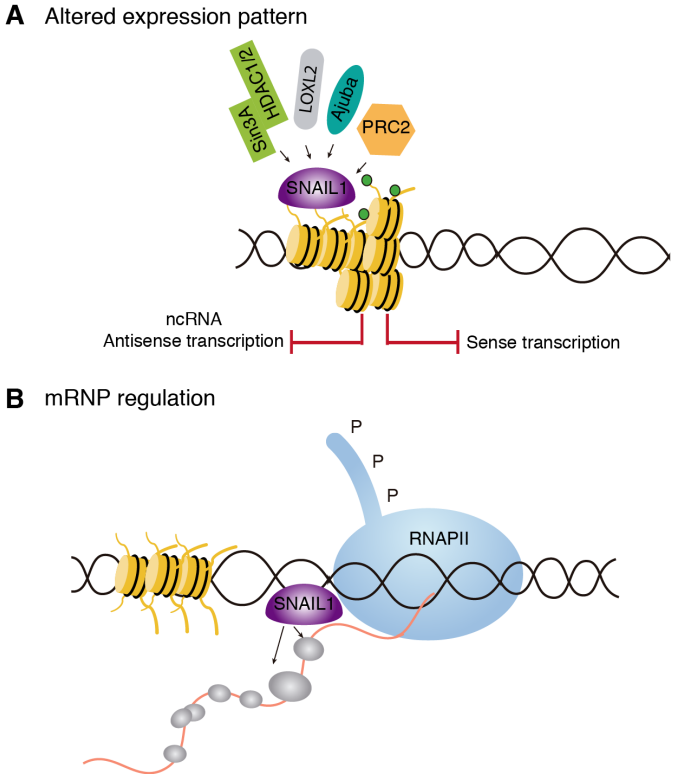

Figure D2. A model to explain the possible role of Snail1 in R loop-mediated genome instability.
(A) Snail1 through its interaction with different transcriptional cofactors such as Sin3A-HDAC1/2, LOXL2, Ajuba or Polycomb repressive complex 2 (PRC2) represses the expression of certain genes. Snail1 depletion leads to an altered transcription pattern and transcription deregulation which in turn, could lead to R loop formation. **(B)** Snail1 may travel with the RNAPII favoring, either directly or via other proteins, transcription. The production of a defective mRNP or even RNAPII stalling also increases the chance of R loop formation.

Altogether, the study of the transcription factor Snail1 has revealed a novel role of this protein in R loop metabolism and genome integrity. Snail1 has been studied due to its crucial function in the EMT, which is deregulated in tumor metastasis. Importantly, Snail1 has been shown to cooperate with chromatin enzymes and cofactors to modulate epigenetic information in favor of gene transcription activation or repression. The uncovered activity of Snail1 in R loop balance would support the crosstalk between R loops and epigenetic modifications of chromatin. However, we cannot disregard the possibility of Snail1 functioning in transcription directly with the RNAPII or via the recruitment of other proteins. Or even the possibility of R loop accumulation as a result of a more pleiotropic effect resulting from Snail1 depletion. Our results provide new hints to understand the role of this factor as a potential genome integrity guardian. Interestingly, Snail1 has been proposed as a target for the development of novel cancer therapeutics (Barrallo-Gimeno and Nieto, 2005; Kothari et al., 2014). Findings linking Snail1 and R loops open a new via to investigate the possible involvement of R loops in this process. For instance, it could be interesting to address how the overexpression of RNase H1 could affect the EMT and cell tumor features in cancer cell lines with high levels of Snail1 expression. To conclude, our study provides another putative link between R loops and cancer, whose further investigation could contribute to decipher the molecular basis of cancer-associated genetic marks.

CONCLUSIONS / CONCLUSIONES

CONCLUSIONS

1. Depletion of the DEAD/H box protein UAP56/DDX39B provokes a direct effect on R loop accumulation, genome integrity and replication. High levels of R loops are the main responsible for these effects.

2. UAP56 is an RNA-DNA helicase and R loop resolvase able to remove co-transcriptional R loops regardless of the origin of its accumulation, as shown *in vitro* and *in vivo*.

3. UAP56 is recruited to actively transcribed chromatin in order to prevent and unwind harmful R loops genome-wide.

4. The absence of the DEAD/H box protein DDX5, which interacts with BRCA2, leads to R loop accumulation genome-wide.

5. Depletion of the master transcription factor Snail1 compromises genome integrity in an R loop-dependent manner, supporting a novel connection between R loops and cancer-associated instability.

CONCLUSIONES

1. El silenciamiento de la proteína de la familia DEADH/box UAP56/DDX39B causa un efecto de acumulación de bucles R (*R loops*), inestabilidad del genoma y fallos de replicación. Siendo estas estructuras las principales responsables de dichos fenotipos.

2. UAP56 es una helicasa de ADN-ARN capaz de eliminar *R loops* de manera co-transcripcional e independientemente de su origen de acumulación, como se ha demostrado *in vitro* e *in vivo*.

3. UAP56 se recluta a cromatina activamente transcrita para prevenir y resolver *R loops* perjudiciales a nivel de todo el genoma.

4. La ausencia de la proteína de la familia DEAD/H box DDX5, que interacciona con BRCA2, causa un efecto de acumulación de *R loops* a nivel de todo el genoma.

5. El silenciamiento del factor de transcripción Snail1 compromete la integridad del genoma en función de los *R loops*, respaldando la relación entre los R loops y la inestabilidad genética asociada a cáncer.

MATERIALS AND METHODS

1. GROWTH MEDIA AND CONDITIONS

1.1. Bacteria cell culture

Bacteria were cultured at 37ºC in LB rich medium and supplemented with 100 μg/ml ampicillin or 25 μg/ml kanamycin when it was necessary for plasmid transfection.

LB: 0.5% yeast extract, 1% bacto-tryptone, 1% NaCl (and 2% agar for solid medium).

1.2. Human cell culture

HeLa (ECACC, 93021013) and HEK-293T cells were cultured in Dulbecco's modified Eagle's medium (DMEM; GIBCO, USA) supplemented with 10% heat-inactivated fetal bovine serum (SIGMA Aldrich, Germany), 2 mM L-glutamine and 1% antibiotic-antimycotic (Biowest, France). K562 (ATCC, CCL-243) cells were cultured in Iscove's Modified Dulbecco's medium (IMDM; GIBCO) supplemented with 10% heat-inactivated fetal bovine serum (Sigma Aldrich) and 1% antibiotic-antimycotic (Biowest). Cells were maintained at 37ºC and 5% CO_2.

2. ANTIBIOTICS, DRUGS, INHIBITORS, ENZYMES AND ANTIBODIES

2.1 Antibiotics

- *Ampicillin* (SIGMA): β-lactam antibiotic that inhibits cell wall synthesis in *Echerichia coli*. Used for plasmid selection in *E. coli* (Use: 100 μg/ml).
- *Kanamycin* (SIGMA): aminoglycoside antibiotic that inhibits cell growth by inducing mistranslation and inhibiting translocation during protein synthesis in *E.coli*. Used for plasmid selection in E.coli (Use: 25 μg/ml).
- *Penicillin, streptomycin and amphotericin B* (Biowest): penicillin inhibits bacterial cell wall synthesis (Use: 60 μg/ml). Streptomycin inhibits prokaryote protein synthesis by preventing the transition from initiation complex to chain-elongating ribosome and causes miscoding (Use: 100 μg/ml). Amphotericin B is used to prevent growth of bacteria, yeast and fungi in human cell culture since it interferes with fungal membrane permeability (Use: 0.25 μg/ml).

2.2 Drugs and inhibitors

- *Complete Protease Inhibitor Cocktail* (Roche): Mixture of several protease inhibitors including serine, cysteine and metalloproteases. It was used according to manufacturer's recommendations.
- *Phenylmethanesulfonyl fluride,* (PMSF) (SIGMA): Inhibitor of serine and cysteine proteases. (Use: 1 mM).
- *Dethyl pirocarbonate* (DEPC) (SIGMA): inhibitor of RNAses.
- *Cordycepin* (SIGMA): Adenosine antagonist 3' deoxyadenosine, inhibitor of chain elongation. (Use: 50 μM).

2.3. Enzymes and antibodies

- *iTaq universal SYBR Green supermix* (Bio-rad): 2x concentrated, ready-to-use reaction master mix optimized for dye-based quantitative PCR (qPCR). It contains antibody-mediated hot-start iTaq DNA polymerase, dNTPs, MgCl2, SYBR Green I dye, enhancers, stabilizers, and a blend of passive reference dyes (including ROX and fluorescein).
- *Q5 Hot Start High-Fidelity DNA Polymerase*: high-fidelity, thermostable, hot start DNA polymerase with 3´→ 5´ exonuclease activity, fused to a processivity-enhancing Sso7d domain to support robust DNA amplification. Used as a part of the Q5 Site-Directed Mutagenesis Kit.
- *Proteinase K* (Roche): very efficient serine protease from Pichia pastoris with no pronounced cleavage specificity.
- *Restriction enzymes* (New England and Takara): DNA endonucleases with specific DNA targets.
- *RNase A* (Roche): endoribonuclease that degrades single-stranded RNA.
- *Zymolyase 20T* (USB): mixture of enzymes from *Arthrobacter luteus* used for digestion of the cell wall of *S. cerevisiae*. (Use: 2 mg/ml).
- *Lysozyme* (SIGMA): enzyme purified from chicken egg white that hydrolyzes peptidoglycans.
- *Spermidine* (SIGMA): polyamine involved in cell metabolism. It binds and precipitates DNA and protein-bound DNA. (Use: 0.5 mM).

- *Dynabeads protein A/G* (Invitrogen): it binds specifically to the Fc portion of IgG. Used for immunoprecipitation experiments (co-IP, ChIP and DRIP).

Antibodies used are listed in Table M1 and Table M2 bellow.

Table M1. Primary antibodies used in this study

Antibody	Source	Epitope	Reference	Use
β-Actin	Mouse	Synthetic peptide conjugated to KLH derived from within residues 1-100 human beta-actin	ab8227 (Abcam)	WB (1:1000) TBS-T 5% milk
BrdU (clone B44)	Mouse	5-Bromo-2-deoxyuridine	347580(Becton Dickinson)	DNA combing (1/20)
BrdU (clone BU1/75)	Rat	5-Bromo-2-deoxyuridine	ABC1177513 (AbCys)	DNA combing (1/20)
ssDNA (poly dT)	Mouse	Poly dT	DSHB	DNA combing (1/50)
FANCD2	Mouse	Monoclonal antibody raised against the N-terminus of human FANCD2 fusion protein	sc-20022 (Santa Cruz Biotechnology)	IF (1:100)
FLAG	Rabbit	Polyclonal antibody recognizes the FLAG epitope located on FLAG fusion proteins	F7425 (Sigma)	IF (1:1000)
mSin3A	Mouse	Synthetic peptide corresponding to amino acids 1-19 of Mouse mSin3A	sc-5299 (Santa Cruz Biotechnology)	PLA (1:50) WB (1:200) odyssey buffer
Phospho-Histone H2AX.X (Ser 139), Clone JBW301	Mouse	Synthetic peptide Corresponding to amino acids 134-142 of human Histone H2A.X	05-636 (Milipore)	IF (1:1000)
Phospho-Histone H2AX.X (Ser 139), Clone 2F3	Mouse	Synthetic peptide Corresponding to amino acids 134-142 of human Histone H2A.X	613402 (Biolegend)	IF (1:1000)
Phospho-Histone H3 (Ser10) (H3S10p), Mitosis Marker	Rabbit	Linear peptide corresponding to human Histone H3 at Ser10. It recognizes Histone H3 when phosphorylated at Ser10	06-570 (Millipore)	IF (1:200)
S9.6	Mouse	Antibody that detects RNA-DNA hybrids	Hybridoma cell Line HB-8730	DRIP (20 μg) IF (1:500)

Antibody	Source	Epitope	Reference	Use
Nucleolin	Rabbit	Synthetic peptide conjugated to KLH, corresponding to N terminal amino acids 2-17 of Human Nucleolin with a C-terminal added cysteine	ab50279 (Abcam)	IF (1:1000)
RNase H1	Rabbit	Amino acids 1-286 RNASEH1 fusion protein	15606-1-AP (Proteintech)	IF (1:1000)
UAP56	Rabbit	Synthetic peptide corresponding to KLH derived from within residues 300-400 of human UAP56	ab47955 (Abcam)	IF (1:200) PLA (1:200) WB (1:1000) BB or odyssey buffer
UAP56	Rabbit	DDX39B fusion protein Ag6512	14798-1-AP (Proteintech)	ChIP (5 μg) IP (5 μg)
Vinculin	Mouse	Mouse monoclonal antibody derived from the hVIN-1 hybridoma	V9264 (Sigma)	WB (1:5000)

KLH: Keyhole Limpet Haemocyanin; WB: Western blot; IF: immunofluorescence; IP: immunoprecipitation; ChIP: Chromatin immunoprecipitation; DRIP: RNA-DNA immunoprecipitation; PLA: Proximity Ligation Assay; TBS-T: TBS-0.1 % Tween-20; BB: Blocking reagent (Roche).

Table M2. Secondary antibodies used in this study

Specificity	Conjugation	Reference	Use
Mouse	Horseradish peroxidase	SIGMA (A6154)	WB (1:5000)
Rabbit	Horseradish peroxidase	SIGMA (A6154)	WB (1:4000)
Mouse	IRDye 680RD	LI-COR (925-68074)	WB Odyssey (1:5000)/(1:15000)
Rabbit	IRDye 800CW	LI-COR (925-32211)	WB Odyssey (1:5000)/(1:15000)
Goat	IRDye 680RD	LI-COR (925-68070)	WB Odyssey (1:5000)/(1:15000)
Mouse	PLA probe (MINUS oligonucleotide)	Olink Bioscience	PLA (1:5)
Rabbit	PLA probe (PLUS oligonucleotide)	Olink Bioscience	PLA (1:5)
Mouse	Alexa fluor 488	Molecular Probes	IF (1:500)
Mouse	Alexa fluor 546	Molecular Probes	IF (1:500) DNA combing (1/50)
Mouse	Alexa fluor 594	Molecular Probes	IF (1:500)
Mouse	Alexa fluor 647	Molecular Probes	DNA combing (1/50)
Rabbit	Alexa fluor 488	Molecular Probes	IF (1:500)

Specificity	Conjugation	Reference	Use
Rabbit	Alexa fluor 488	Molecular Probes	IF (1:500)
Rat	Alexa fluor 488	Molecular Probes	DNA combing (1/50)

WB: Western blot; IF: immunofluorescence; PLA: Proximity Ligation Assay;

3. HUMAN CELL LINES

Human cells used in this study are listed in the Table M3.

Table M3. Cell lines used in this study

Cell line	Description	Medium	Source
HeLa	Human cervical adenocarcinoma epithelial cells	DMEM	ECACC
HEK293T	Human Embryonic Kidney 293 cells. It contains the SV40 T-antigen	DMEM	PhD. Amelia Nieto CNB-CSIC, Madrid (España)
K562	Human Caucasian chronic myelogenous leukemia lymphoblast cells	IMDM	ATCC

ECACC: European Collection of Authenticated Cell Cultures;

ATCC: American Type Culture Collection.

All experiments were performed using HeLa cells except co-immunoprecipitation experiments, which were performed using HEK293T cells and genome-wide studies, which were performed using K562 cells.

4. PLASMIDS

Plasmids used are shown in Table M4.

Table M4. Plasmids used in this study

Plasmid	Description	Resistance	Reference/Source
pCDNA3	Vector containing the P_{CMV} for expression in mammalian cells	Ampicillin	(ten Asbroek et al. 2002)
pCDNA3-RNaseH1	pcDNA3 containing the human RNase H1 gene under P_{CMV}	Ampicillin	ten Asbroek et al. 2002)
pFLAG-CMV-6a	Expression vector derivative of pCMV5 used to establish transient intracellular expression of N-terminal Met-FLAG fusion proteins in mammalian cells	Ampicillin	SIGMA

Plasmid	Description	Resistance	Reference/Source
pFLAG-UAP56	pFLAG containing the human UAP56 gene fussed to FLAG	Ampicillin	PhD. Irene Salas Armenteros
pFLAG-UAP56-K95A	pFLAG containing the K95A mutation in human UAP56 gene fussed to FLAG	Ampicillin	This study
pFLAG-UAP56-E197A	pFLAG containing the E197A mutation in human UAP56 gene fussed to FLAG	Ampicillin	This study
pGEX-KG-UAP56	Expression vector derivative of pGEX-2T used to establish transient intracellular expression of gutathione S-transferase (GST) UAP56 fusion protein in mammalian cells	Ampicillin	This study Patrick Sung lab
pGEX-KG-UAP56-K95A	pGEX-KG vector containing the the K95A mutation in human UAP56 gene fussed to GST	Ampicillin	This study Patrick Sung lab
pGEX-KG-UAP56-K95A	pGEX-KG vector containing the the E197A mutation in human UAP56 gene fussed to GST	Ampicillin	This study Patrick Sung lab

P_{CMV}: Cytomegalovirus promoter.

5. BACTERIAL TRANSFORMATION AND HUMAN CELLS TRANSFECTION

5.1. Bacterial transformation

Transformation of bacteria with exogenous DNA was carried out according to standard heat shock transformation protocol (Sambrook et al., 1989).

5.2. Human cells transfection

All assays were performed 72 hours after small interfering RNA (siRNA) transfection and 24 hours after plasmid transfection.

5.2.1. siRNA transfection

siRNA used are shown in Table M5.

Table M5. siRNAs used in this study

siRNA	Time	Source
ON-TARGETplus Non-targeting Pool (D-001810)	72 h	Dharmacon
ON-TARGETplus SMARTpool human UAP56 (L-003805-00)	72 h	Dharmacon

siRNA	Time	Source
ON-TARGETplus SMARTpool human THOC1 (L-016376-00)	72 h	Dharmacon
ON-TARGETplus SMARTpool human SETX (L-021420-00)	72 h	Dharmacon
ON-TARGETplus SMARTpool human DDX23 (L-19861-01)	72 h	Dharmacon
ON-TARGETplus SMARTpool human AQR (L-022214-01)	72 h	Dharmacon
ON-TARGETplus SMARTpool human FANCD2(L-016376-00)	72 h	Dharmacon
DDX5 siRNA: 5'-GCU CUU UAU AUU GUG UGU UAU dT-3'	72h	Sigma

Cells were transfected with siRNA using DharmaFECT 1 (Dharmacon) at 30-50% confluence. Transfection in a well of 6-well plate was performed using the following protocol:

- *Mixture A* (final volume 100 μl): 95 μl culture serum-free medium (medium without antibiotics or FBS) and 5 μl siRNA 20 μM (100 nM).
- *Mixture B* (final volume 100 μl): 95 μl culture serum-free medium (medium without antibiotics or FBS) and 5 μl of DharmaFECT1.

Each mixture was incubated at room temperature (RT) for 5 min. Then, *Mixture A* is added over *Mixture B*, mixed and incubated for 20 min. Meanwhile, medium was replaced by 800 μl antibiotic-free medium. Transfection solution was added carefully drop by drop to the cell culture and incubated for 2 hours. Afterwards, 2 ml of complete medium was added.

5.2.2. Plasmid transfection using Lipofectamine 2000 or Lipofectamine 3000

- For plasmid transfection using Lipofectamine 2000 (Invitrogen), cells were transfected at 80% confluence. 24 hours before transfection cell were cultured in antibiotic-free medium (2 ml for 6-well plates). Transfection in a well of a 6-well plate was performed using the following protocol:

- *Mixture A* (final volume 200 μl): 2 μg DNA in Opti-MEM (Gibco).
- *Mixture B* (final volume 300 μl): 4 μl Lipofectamine 2000 in Opti-MEM.

Each mixture was incubated at RT for 5 min, mixed and incubated for 5 min at RT. Transfection solution was added carefully drop by drop to the cell culture.

- For plasmid transfection using Lipofectamine 3000 (Invitrogen), cells were transfected at 80% confluence. 24 hours before transfection cell were cultured in antibiotic-free medium (2 ml for 6-well plates). Transfection in a well of a 6-well plate was performed using the following protocol:

- *Mixture A* (final volume 200 μl): 2 μg DNA and 4 μl of Enhancer Reagent in Opti-MEM (Gibco)
- *Mixture B* (final volume 300 μl): 4 μl Lipofectamine 3000 in Opti-MEM.

  Each mixture was incubated at RT for 5 min, mixed and incubated for 5 min at RT. Transfection solution was added carefully drop by drop to the cell culture.

6. *IN VITRO* ANALYSIS

These experiments were performed in collaboration with Patrick Sung lab in Yale University.

6.1. Purification of UAP56 wild-type and mutant proteins

The cDNAs that encode the wild type, K95A and E197A variants of UAP56 were introduced into the pGEX-KG vector to add an N-terminal GST tag to these proteins. The resulting UAP56 expression plasmids were introduced into *E. coli* BL21:DE3 Rosetta cells, which were grown at 37°C to OD600 = 0.8, and protein expression was induced by the addition of 0.2 mM IPTG and incubation at 16°C for 16 h. Cells were harvested by centrifugation and all the subsequent steps were carried out at 0-4°C. For lysate preparation, a cell pellet (20 g, from 4 L of culture) was suspended in 100 ml K buffer with 300 mM KCl and 5 μg/ml each of the protease inhibitors aprotinin, chymostatin, leupeptin and pepstatin, and then subject to sonication (three 1 min pulses). The crude cell lysate was clarified by ultracentrifugation (100,000Xg for 90 min) and then mixed gently with 2 ml of Glutathione Sepharose 4B resin (GE) for 1.5 h. The resin was washed sequentially with 50 ml K buffer containing 1 M KCl, 50 ml K buffer containing 300

mM KCl, 20 ml K buffer containing 300 mM KCl and 1 mM ATP, 20 ml K buffer containing 300 mM KCl and 5 mM $MgCl_2$, and 2 x 50 ml K buffer containing 300 mM KCl. UAP56 was eluted with 12 ml K buffer containing 300 mM KCl and 10 mM reduced glutathione and concentrated to 1 ml (Amicon 10K concentrator, Millipore). The GST tag was cleaved by incubating the concentrated protein pool with 100 μg of thrombin for 12 h. The reaction mixture was diluted with 2 ml of K buffer and applied onto to a 1-ml Mono Q column (GE), which was washed with 5 ml K buffer plus 150 mM KCl and then developed with a 25-ml linear gradient from 150 to 650 mM KCl. The peak of UAP56, eluting at ~350 mM KCl, was collected, concentrated to 0.5 ml, and fractionated in a Superdex 200 gel filtration column (24 ml, GE) in K buffer containing 300 mM KCl. Fractions containing highly purified UAP56 (1 mg protein) were pooled, concentrated to 1 mg/ml, and stored in small aliquots at -80°C. The UAP56 K95A and E197A mutants were purified using the same procedure with a similar yield.

K buffer: 20 mM KH_2PO_4, pH 7.4, 10% glycerol, 0.5 mM EDTA, 0.01% Igepal, 1 mM DTT.

6.2. Nucleic acid unwinding assays

RNA-RNA duplexes, without or with a 5' or 3' overhang, were prepared as described (Shen et al., 2007). RNA-DNA hybrids without and with a 5' or 3' overhang and DNA-DNA duplex with a 5' overhang were prepared by annealing oligonucleotides (with one of the oligonucleotides being labeled with ^{32}P) listed in Table M6. In the unwinding reaction, UAP56 (wild type or mutant at the indicated concentration) was incubated with 5 nM substrate in reaction buffer (1) and 100 nM of "trap" RNA or DNA (unlabeled version of the oligonucleotide that was labeled in the substrate) at 37°C (for the RNA-RNA substrates) or 30°C (for the RNA-DNA substrates) for 30 min or the indicated time. Reaction mixtures were deproteinized by treatment with SDS (0.1%) and proteinase K (0.5 mg/ml) for 10 min at 37°C and then resolved in 15% polyacrylamide gels in TAE buffer at 4°C. Gels were dried and subject to phosphorimaging analysis.

The 5' RNA-DNA flap structure that resembles a branch migratable R-loop structure was constructed as described (Schwab et al., 2015). UAP56 (wild type or mutant at the indicated concentration) was incubated with the substrate in reaction buffer (2) at 30°C for 20 min. Reaction mixtures were deproteinized before being resolved in 7% polyacrylamide gels in TAE buffer at 4°C and analyzed, as above.

Reaction buffer (1): 35 mM Tris-Cl, pH 7.5, 1 mM DTT, 3 mM ATP, 2 mM $MgCl_2$, 60 mM KCl.

Reaction buffer (2): 25 mM Hepes, pH 6.5, 1 mM DTT, 2 mM ATP, 2 mM $MgCl_2$, 60 mM KCl.

TAE buffer: 40 mM Tris, 20 mM Acetate acid and 1 mM EDTA.

Table M6. Oligonucleotides for unwinding assays used in this study

Oligo Name	RNA or DNA	Length	Sequence
R13	RNA	13	5'GCUUUACGGUGCU3'
R13C	RNA	13	5'AGCACCGUAAAGC3'
R23-5'	RNA	23	5'AAAACAAAAUAGCACCGUAAAGC3'
R23-3'	RNA	23	5'GCUUUACGGUGCUUAAAACAAAA3'
D13	DNA	13	5'GCTTTACGGTGCT3'
D13C	DNA	13	5'AGCACCGTAAAGC3'
D23-5'	DNA	23	5' AAAACAAAATAGCACCGTAAAGC3'
XX1	DNA	60	5'ACGCTGCCGAATTCTACCAGTGCCTTGCTAGGACA TCTTTGCCCACCTGCAGGTTCACCC3'
XX2	DNA	60	5'GGGTGAACCTGCAGGTGGGCAAAGATGTCCCAGC AAGGCACTGGTAGAATTCGGCAGCGT3'
R5'F	RNA	30	5'GGGUGAACCUGCAGGUGGGCAAAGAUGUCC3'

7. PROTEIN-PROTEIN INTERACTION METHODS

7.1. Co-immunoprecipitation (Co-IP)

Whole-cell extracts from a 10 cm petri dish of HEK293T cells at 80% confluence were obtained by lysing cells in 200 µl lysis buffer during 30 min on ice with occasionally gently pipetting up and down. The lysate was centrifuged 10 min at 16,000 g. For each immunoprecipitation, 50 µl Dynabeads Protein A (Invitrogen) were washed twice in 1 ml PBS-0.5%BSA and 5 µg antibody was bound to the beads in 200 µl PBS-0.5% BSA, 4h at 4 ºC. 20 and 180 µl od the lysate were diluted with 180 µl of dilution buffer (to obtain a 0.25% (vol/vol) final concentration of NP-40) and incubated with beads-antibody complexes for 2h at 4 ºC. The same amount of lysate was incubated with beads (without antibody) and was used as a control. Then, beads were washed twice in PBS, four times with wash buffer and bound proteins were eluted by boiling the beads for 10 min 25 µl of 2X Laemmli loading buffer. Finally the result was visualized by Western blot.

Lysis buffer: 10 mM Tris-HCl pH 7.5, 150 mM NaCl, 0.5 mM EDTA pH 8, 0.5% (vol/vol) NP-40, 1 mM PMSF, and protease inhibitor cocktail.
Dilution buffer: 10 mM Tris-HCl pH 7.5, 150 mM NaCl, 0.5 mM EDTA pH 8, 1 mM PMSF, and protease inhibitor cocktail.
Wash buffer: 10 mM Tris-HCl pH 7.5, 150 mM NaCl, 0.5 mM EDTA pH 8, 0.2% (vol/vol) NP-40, 1 mM PMSF, and protease inhibitor cocktail.

7.2. Proximity ligation Assay (PLA)

For detection of protein-protein interactions *in situ*, PLA was performed following manufacturer's instruction with reagents from Duolink In Situ Starter Kit (Olink Biosciences). Cells were cultured on glass coverslips and fixed in suitable conditions compatible with the two primary antibodies to be used (see Materials and methods 7). Coverslips were blocked with PBS-3% BSA for 1h at RT, incubated with primary antibodies diluted in PBS-3%BSA for 2h at RT (for antibodies dilution see Table M1), washed three times in 5 ml PBS for 5 min and incubated with PLA probes for 1 h at 37 °C. After two washed in 5 ml wash buffer A for 5 min, ligation reaction was performed for 30 min at 37 °C. Then, cells were

washed twice in 5 ml wash buffer A, incubated with the amplification reaction for 100 min at 37 °C in darkness, washed twice in 5 ml buffer B for 10 min and once in 5 ml 0.01X wash buffer B for 1 min. Finally, coverslips were dried in darkness, mounted with mounting medium with DAPI and images were acquired in a fluorescence microscope. For negative controls, everything was performed identically, except that only one of the primary antibodies was added.

For each coverslip:

- **PLA probes** (40 µl): 8 µl PLA probe anti-Mouse MINUS, 8 µl PLA probe anti-Rabbit PLUS, 24 µl PBS-3% BSA.
- **Ligation reaction** (40 µl): 8 µl of 5X Buffer ligase, 1 µl Ligase, 31 µl MQ H2O.
- **Amplification reaction** (40 µl): 8 µl of 5X Buffer amplification, 0.5 µl Polymerase, 31.5 µl MQ H2O.

PLA probes, buffers, enzymes and mounting media are provided in the Duolink In Situ Red Starter Kit.

8. CELL CYCLE ANALYSIS IN HUMAN CELLS

8.1. FACS analysis

After siRNA transfection for 72h, HeLa cells were harvested with trypsin, washed twice with cold PBS and centrifuged (3000 rpm 5 min). Pellet was resuspended in 300 µl cold PBS and cells were fixed by adding 700 ul cold 96% ethanol drop by drop and stored at -20 ºC. Before cell cycle analysis and sorting, cells were incubated with Propidium Iodide (50 µg/ml) and treated for RNA degradation with RNase A (250 µg/ml). After that, cells were examined by flow cytometry (FACSCalibur; BD). Three population of cells were analyzed based on their DNA content (1n=haploid or 2n=diploid DNA content of the genome).

9. IMMUNOFLUORESCENCE

Cell were cultured on glass coverslips and, if needed, transfected as indicated in Matherial and Methods 5.2. Cells were fixed in formaldehyde or methanol and selected target molecules were visualized in a fluorescence microscope after the

incubation with the corresponding primary antibodies and with the subsequent fluorophore-conjugated secondary antibodies.

Type of cell fixation used:

- Formaldehyde fixation: cells were fixed in 2% formaldehyde in PBS for 20 min or 4% formaldehyde in PBS for 10 min and permeabilized with 70% ethanol for 5 min at -20 ºC, 5 min at 4 ºC and washed twice in PBS. This fixation was used for immunofluorescence with γH2AX, pFLAG and H3Ser10P antibodies.
- Triton-Formaldehyde fixation: Cells were pre-permeabilized with cold 0.1% triton in PBS on ice for 1 min and then fixed in formaldehyde as previously described. This fixation was used for immunofluorescence with UAP56, pFLAG, SIN3
- Methanol fixation: Cells were fixed in cold absolute methanol for 7 min at -20 °C and washed twice in PBS. This fixation was used for immunofluorescence with S9.6 and nucleolin antibodies.

Immunofluorescence: Blocking, incubation with primary and secondary antibodies, DAPI staining and mounting conditions.

Cells were blocking using 3% bovine serum albumin (BSA) in PBS. Then, primary antibodies were diluted in 3% BSA in PBS for 1h at RT. For antibody dilutions see Table M1. Afterwards, cells were washed three times in PBS for 5 min. Secondary antibodies conjugated with Alexa Fluor diluted (1:500) in 3% BSA in PBS were also incubated for 1h at RT. Finally, coverslips were washed twice in PBS before and after the staining of the DNA with 1 µg/ml DAPI (2-(4-Amidinophenyl)-6-indolecarbamidine dihydrochloride) for 5 min. At the end, coverslips were washed in water and a drop of ProLong Gold Antifade reagent (Thermo) was used for mounting. For S9.6 and nucleolin immunofluorescence see Materials and Methods 8.3.

Detection of cells in S phase by immunofluorescence:

When necessary, detection of cells in S phase by immunofluorescence was performed by EdU detection using a Click-iT EdU Imaging Kit (Invitrogen) following manufacturer's instructions.

To perform this assay, cells were culture on glass coverslips and then, the modified thymidine analogue EdU (5-ethynyl-2'-deoxyuridine) is added for 20 min to the cell culture in order to be incorporated into DNA during active synthesis before its fixation. Afterwards, cells were fixed, cells were washed twice with 1 ml of 3% BSA in PBS, permeabilized with 1 ml of 0.5% Triton X-100 in PBS for 20 min at RT and washed again twice in 1 ml of 3% BSA in PBS. Finally cells were incubated with 50 µl/coverslip of Click-iT reaction cocktail (43 µl of 1X Click-iT reaction buffer, 2 µl of 100 mM CuSO4, 0.12 µl of Alexa Fluor azide, 5 µl of 1X reaction buffer additive) for 30 min at RT in darkness and washed once with 1 ml in 3% BSA.

10. GENOME INSTABILITY ANALYSIS

10.1. Analysis of γH2AX foci

Cells were culture on glass coverslips and transfected with siRNA as indicated in Materials and Methods 5.2., fixed in 2% formaldehyde and immunofluorescence was performed with mouse monoclonal anti-γH2AX (JBW301, 05-636 Millipore) or mouse monoclonal anti- γH2AX (2F3, 613402 Biolegend) (see Materials and Methods 7 and Table M1). More than 100 cells from each experiment were analyzed (see Materials and Methods 10).

10.2. Single cell gel electrophoresis (Comet assay)

Comet assay was performed using a commercial kit (Trevigen, Gaithersburg, MD,USA) following the manufacturer's protocol, 48 h after siRNA transfection. When it is indicated, 50 µM cordycepin was added to the culture 4 hours before the experiment.

10.2.1. Alkaline comet assay

Cells were collected using accutase, washed and resuspended in ice cold 1X PBS, combined with low melting agarose, immobilized on CometSlides (30 min at 4 °C, until agarose is solidified) and lysed for 30 min at 4 °C. Then, DNA was unwound and denatured in freshly prepared alkaline unwinding solution pH>13 for 30 min at RT and electrophoresis was performed in prechilled alkaline electrophoresis solution pH>13 at 21 V for 30 min. Next, slides were immersed twice in dH2O for 5 min each, then in 70% ethanol for 5 min and dried at RT. DNA was stained with SYBR Green at 4 °C for 5 min.

Alkaline unwinding solution/Alkaline electrophoresis solution pH>13: 200 mM NaOH, 1 mM EDTA.

10.2.2. Neutral comet assay

Cells were collected and immobilized on CometSlides as previously described. Cells were lysed for 1h at 4 ºC and immersed in prechilled 1X neutral electrophoresis buffer at 21V for 45 min and then immersed in DNA precipitation solution for 30 min at RT. Finally, slides were immersed in 70% ethanol for 30 min at RT and dried. DNA was stained with SYBER Green at 4 ºC for 30 min.

10X Neutral electrophoresis buffer (500 ml): 60.57 g Tris Base and 204.12 g of sodium acetate dissolved in H2O. Adjust to pH=9.0 with glacial acetic acid. 1X stock was obtained by diluting the 10X stock in dH2O.

DNA precipitation solution: 1 M NH4Ac in 70% ethanol.

For γH2AX foci and comet assays analyses at least three independent experiments were performed. More than 100 cells were scored in each experiment (see Materials and Methods 10).

10.3. RNA-DNA hybrids detection

10.3.1. RNA-DNA immunoprecipitation (DRIP-qPCR)

DRIP assays were performed by immunoprecipitating DNA–RNA hybrids using the S9.6 antibody from gently extracted and enzymatically digested DNA, treated or not with RNase H (New England Biolabs, USA) *in vitro* as described (Herrera-Moyano et al, 2014; Garcia-Rubio et al, 2015). After 72 h of siRNA transfection, pellet from a 6-cm plate of HeLa cells was collected using accutase, washed in PBS and resuspended in 800 µl of TE. Afterwards, 20.75 µl SDS 20% and 2.5 µl proteinase K (20 mg/ml) were added and pellet was incubated at 37 °C overnight. DNA was extracted gently with phenol-chloroform in phase lock tubes (VWR, USA). Precipitated DNA was spooled on a glass rod, washed 2 times with 70% EtOH, resuspended gently in TE and digested overnight with 50 U of HindIII, EcoRI, BsrGI, XbaI and SspI and 2mM spermidine. For the negative control, half of the DNA was treated with 3 *µ*l RNase H overnight. 5 *µ*g of the digested DNA were bound to 10 *µ*l of S9.6 antibody (1mg/ml) in 500 *µ*l 1X binding buffer in TE, overnight at 4ºC. DNA-antibody complexes were immunoprecipitated using Dynabeads Protein A (Invitrogen) during 2h at 4ºC and washed 3 times with 1X binding buffer. DNA was eluted in 180 µl elution buffer, treated 45 min with 7 *µ*l proteinase K at 55ºC and cleaned with the NucleoSpin Gel and PCR Clean-up (Macherey-Nagel, USA). Quantitative PCR of immunoprecipitated DNA fragments and input DNA was performed on a 7500 Fast & 7500 Real-Time PCR System SYBR qPCR Mix (Applied Biosystems, Thermo Fisher) with the primers listed in Table M7.

10X Binding buffer: 100 mM NaPO4 pH 7.0, 1.4 M NaCl, 0.5% triton X-100.
Elution buffer: 50 mM Tris pH 8.0, 10 mM EDTA, 0.5% SDS.

DRIP quantification and normalization: Input and immunoprecipitated (IP) were eluted in 150 µl of double-distilled H_2O. 4 µl of IP were used for qPCR. The relative abundance of RNA-DNA hybrid immunoprecipitated in each region was normalized to Input signal obtained.

10.3.2. S9.6 immunofluorescence

Cells were cultured on glass coverslips and fixed in methanol (see Materials and Methods 7). For S9.6 and nucleolin immunofluorescence, coverslips were blocked in 2% BSA in PBS overnight at 4°C and incubated with S9.6 mouse (1:500) and anti-nucleolin rabbit (1:1000, Abcam) or pFLAG (1:1000) primary antibodies diluted in 2% BSA. Then, coverslips were washed three times in PBS, and then incubated with secondary antibody Alexa Fluor 594 and 488 diluted in 2% BSA in PBS (1:1000) for 1 hour at RT. Finally, they were washed, DAPI staining and mounting as described above. More than 100 cells from each experiment were scored (see Materials and Methods 10).

11. REPLICATION ANALYSIS

11.1. Analysis of FANCD2 foci

Cells were cultured on glass coverslips, pre-permeabilized with 0.25% Triton X-100 in PBS for 1 minute on ice and then fixed with 2% formaldehyde in PBS. After blocking with 3% BSA in PBS, cells were incubated with primary antibodies FANCD2 (1:100 dilution) and RNase H1 (1:400) diluted in 3% BSA in PBS. Afterwards, coverslips were washed three times in PBS and incubated with secondary antibodies conjugated with Alexa 488 and Alexa 546 (1:1000). Finally, coverslips were washed, DAPI staining and mounting as described above. More than 100 cells from each experiment were scored (see Materials and Methods 10). In pre-permeabilized cells the overexpressed RNase H1 stained only nucleus and nucleoli because the rest of the protein had been washed out.

11.2. Single DNA fiber analysis in human cells (DNA combing)

DNA combing was performed as previously described (Michalet et al., 1997). Cells were transfected with siRNA and with the empty pcDNA3 plasmid or the pcDNA3 RNase H1 plasmid for 48 h, as indicated in Matherial and Methods 5.2. Iodo-deoxyuridine (IdU) and Cloro-deoxyuridine (CldU) labels were added for 20 min each. Subsequently, cells were harvested using accutase, resuspended in cold PBS and embedded in 1% low melting agarose plugs in PBS. Plugs were

incubated in proteinase K buffer at 50 ºC overnight, 6 hours more with a new preparation of the same buffer and washed 5 times with TE buffer for 10 min at RT at 300 rpm. DNA was stained with YOYO-1 (Molecular Probes) to check the integrity of the DNA fibers. Afterwards, each plug was melted in 3 ml of 50 mM 2-(N-morpholino)ethanesulfonic acid (MES) pH 5.7 for 30-45 min at 67ºC. 3U of β-agarase (New England Biolabs) was added after the solution cooled down to 42ºC and it was incubated overnight. Next, DNA fibers were stretched on silanized coverslips by incubation for 15 min at RT and coverslips were removed from the reservoir at the speed of 300 µm/s. DNA was crosslinked to coverslips by baking at 60ºC for 2 hours.

For immunodetection, slides were dehydrated for 3 minutes in successive bath of 70%, 90% and 100% EtOH, incubated for 8 min in 0.5 M NaOH/ 1M NaCl, washed 5 times in PBS and blocked in PBS - 0.1% Triton X-100 - 1% BSA for 15 minutes. DNA molecules were counterstained with 18 µl of an anti-ssDNA antibody (DSHB, 1:500, 30 min) and an anti-mouse IgG coupled to Alexa 647 (Molecular Probes, 1:50, 30 min). CldU and IdU were detected with BU1/75 (AbCys, 1:20, 45 min) and BD44 (Becton Dickinson, 1:20, 45 min anti-BrdU antibodies, respectively. Antibodies were incubated in a humid chamber at 37 ºC and, between incubations, samples were washed 5 times for 2 minutes with PBS-0.1% Triton X-100. Secondary antibodies used were goat anti-mouse IgG Alexa 546 (1:50, 30 min) and chicken anti-rat Alexa 488 (1:50, 30 min). Finally, dried slides were mounted using 20 µl of Prolong Gold Antifade. Representative images of DNA fibers were assembled from different microscopic fields of view and were processed as described.

Proteinase K buffer: 10 mM Tris-HCl pH 7.5 - 50 mM EDTA - 1% Sarkosyl-0.5%.

TE buffer: 10 mM Tris-HCl pH 7.0 – 50 mM EDTA.

12. MICROSCOPY IMAGES ACQUISITION, DATA ANALYSIS AND STADISTICAL ANALYSIS

12.1. Fluorescence microscopy

DNA fibers were analyzed on a Leica DM4000 microscope equipped with a DFC365 FX camera (Leica). Data acquisition was performed with LAS AX (Leica). A 63x objective was used for immunofluorescence for immunofluorescence (γH2AX, FANCD2 and H3S10-P foci IF, PLA, S9.6 and nucleolin IF), a 40x objective was used for DNA combing experiments and a 10x objective was used for comet assays.

12.2. Data analysis

- γH2AX, FANCD2 and H3S10-P foci measurements were analyzed and processed with the MetaMorph v7.5.1.0. software using the granularity application.
- S9.6 signal intensity per nucleus were analyzed and processed with the MetaMorph v7.5.1.0. software using the multi wavelength cell scoring application. The S9.6 signal corresponding to the nucleolus area was previously removed using the nucleolin signal and granularity application.
- Comet assays tail moments were analyzed using Comet-score (version 1.5) or TriTek CometScore Professional (version 1.0.1.36) softwares. Tail moment (TM) reflects both the tail length (TL) and the fraction of DNA in the comet tail (TM=%DNA in tail x TL/100).
- Combing measurements were analyzed and processed with the MetaMorph v7.5.1.0 software using measurements applications with the following setup conditions: 50 μM = 310 pixels and 1 μM = 2.2 Kb. Data analysis was performed as previously described (Salas-Armenteros et al., 2017; Tuduri et al., 2009). For fork velocity only CldU tracks that follow an IdU track were considered. Fork asymmetry was expressed as the percentage of distance that is longer the longest track than the shortest, for each pair of sister replication forks during the CldU pulse ((longest-shortest)/longest) x 100). Only sister replication forks with present more than a 25% of difference were considered asymmetric.

Fork velocity (Kb/min) D / t

Fork asymmetry (%) ((L-S)/L) x 100)

Figure M1. DNA combing measurements.
D/t: Distance/time. S: shortest track. L: longest track.

For all experiments, at least three biological repeats (n) were performed. More than 100 cells were scored in each repeat, when possible. Otherwise, a minimum of 50 cells were counted in each repeat.

12.3. Statistical analysis

- γH2AX, FANCD2 and H3S10-P foci: Graphs shows the mean of the percentage of cells with foci from at least three biological repeats. Data were analyzed with EXCEL program. For statistical analysis, Student's t-test was performed and a P value < 0.05 was considered as statistically significant.
- S9.6 signal intensity per nucleus: Graphs shows the median of the measurements from at least three biological repeats. Data were analyzed wit GraphPad Prism software. For statistical analysis, Mann-Whitney U-test, two tailed was performed and P value < 0.05 was considered as statistically significant. (***, P < 0.001; **, P < 0.01; *, P < 0.05).
- Comet assay: Graphs shows the mean of the median of tail moment normalized with to the siC control from at least three biological repeats. Data were analyzed with EXCEL program and GraphPad Prism software. For statistical analysis, Mann-Whitney U-test was performed and P value < 0.05 was considered as statistically significant.
- DRIP: Graphs shows the signal values of RNA-DNA hybrids immunoprecipitated in each region as a function of input DNA normalized with respect to the siC control from at least three biological repeats. Data were analyzed with EXCEL program and GraphPad Prism software. For statistical

analysis, Mann-Whitney U-test was performed and P value < 0.05 was considered as statistically significant.

13. POLYMERASE CHAIN REACTION (PCR) ANALYSIS

13.1. Quantitative PCR analysis

Real-time quantitative PCRs (qPCRs) were performed on a 7500 Fast Real-Time PCR system (Applied Biosystems, Carlsbad, CA). For PCRs, 6 µl H2O, 2 µl primer mixture (each 10 µM), 2 µl DNA and 10 µl SYBR® green qPCR Mix (Bio-rad) were used. The program for PCR reaction used was the following: 1 cycle (10 minutes 95 °C), 40 cycles (15 s 95 °C and 1 minute 65 °C) and 1 dissociation cycle (15 s 95 °C, 1 minute 65 °C, 15 s 95 °C and 15 s 60 °C). DNA primers were designed using Primer express 3.0 Software (Applied Biosystems) and are listed in Table M7. qPCR primers were validated by qPCR by establishing that each pair of primers had the same amplification efficiency (the slope of the 10-fold serial dilutions of a calibration curve was between -3.3 and -3.4).

13.1.1. Reverse Transcription quantitative PCR (RT-PCR) analysis

Relative qPCRs were used to determine the relative mRNA levels in human cells. cDNA was obtain from total RNA extracted using RNeasy Mini Kit (Qiagen) (1 µg) by reverse transcription using QuantiTect Reverse transcription (Qiagen) and random primers. mRNA expression values were normalized to mRNA expression of the Hypozanthine PhosphoRibosylTransferase (HPRT) housekeeping gene.

13.1.2. qPCR analysis for DRIP quantification

Absolute qPCRs were used for DRIP quantification.

Table M7. DNA primers used in this study

Primer	Sequence 5' to 3'	Use
APOE Fwd	CCGGTGAGAAGCGCAGTCGG	DRIP
APOE Rvs	CCCAAGCCCGACCCCGAGTA	DRIP

Primer	Sequence 5' to 3'	Use
RPL13A Fwd	GCTTCCAGCACAGGACAGGTAT	DRIP
RPL13A Rvs	CACCCACTACCCGAGTTCAAG	DRIP
EGR1 Fwd	GCCAAGTCCTCCCTCTCTACTG	DRIP
EGR1 Rvs	GGAAGTGGGCAGAAAGGATTG	DRIP
DDX23 Fwd	AGCCATTATCCCTGGAGGAG	Relative mRNA expression
DDX23 Rvs	CTTCAGCCTCTCGTTCTGCT	Relative mRNA expression
AQR Fwd	TGGGAGAATCTGAACCTAATCC	Relative mRNA expression
AQR Rvs	GCAGGGTAACCAAGTAAACACA	Relative mRNA expression
SETX Fwd	CACACTATGGAGAGGGAAGCA	Relative mRNA expression
SETX Rvs	TTAGATCCAAGGCGATCCAG	Relative mRNA expression
UAP56 Fwd	GACAGCAGCTGGGGGAGATG	Relative mRNA expression
UAP56 Rvs	CTCATGCTGGACTTCTGACG	Relative mRNA expression
DDX5 Fwd	GCAACCATTGACGCCATG	Relative mRNA expression
DDX5 Rvs	CCAAGTCCAAGCCGCAAA	Relative mRNA expression
APOE Fwd	AAGCTGGAGGAGCAGGCC	Relative mRNA expression
APOE Rvs	ACTGGCGCTGCATGTCTTC	Relative mRNA expression
RPL13A Fwd	GGGAGCAAGGAAAGGGTCTTA	Relative mRNA expression
RPL13A Rvs	ACAATTCTCCGAGTGCTTTCAAG	Relative mRNA expression

14. PROTEIN ANALYSIS

14.1. Human cells protein extraction

Pellet of HeLa, HEK293T or K562 cells was collected using trypsin or accutase, washed twice in cold PBS and gently resuspended in 2X Laemmli loading buffer (100 µl/1x10^6 cells). The lysate was boiled at 95 ºC for 5 min and sonicated for another 5 min on the maximum intensity setting, with fifteen pulses of 30s on and

30s off in Bioruptor (Diagenode). Prior to gel loading, samples we boiled for 2 min.

2X Lammeli buffer: 200 Mm Tris-HCl, 40% glycerol, 8% SDS, 0.4% Bromophenol Blue, 400 mM β-mercaptoethanol.

14.2. SDS-PAGE

Proteins were separated in 29:1 acrylamide:bis-acrylamide SDS-PAGE with appropriate concentrations to the molecular size of the proteins of interest or in 4-20% gradient SDS-PAGE CriterionTM TGXTM Precast Gels (BioRad) following the method described in (Laemmli, 1970). Electrophoreses were performed in a Mini-PROTEAN 3 Cell (BioRad) using running buffer at 100 V. Page RulerTM (Fermentas, CA) was used as a protein marker.

Runnig buffer: 25 mM Tris base pH 8.3, 194 mM glycine, 0.1% SDS buffer.

14.3. Western Blot analysis

For Western blot, proteins were wet-transferred using Trans-Blot system (Biorad) for 2 h at 400 mA in 1X Transfer Buffer with 20% methanol or o/n at 30 V in 1X Tris-glycine Buffer at 4 °C. After transfer, the membranes were strained with Ponceau S (0.1% w/v Ponceau (Sigma) in 5% Acetic acid) to check protein loading and correct transfer.

5X Transfer buffer: 6 g/L Tris base, 28.8 g/L glycine and 0.5% SDS.

10X Tris-glycine buffer: 30 g/L Tris base, 143.2 g/L glycine pH 8.3.

14.4. Non-fluorescence WB

Proteins were transferred to a nitrocellulose membrane (Hybond-ECL, GE Healthcare). Membranes were blocked with 1X TBS - 0.1% Tween 20 - 5% milk or Blocking Buffer solution (ROCHE) for 1 h. Primary antibodies were incubated for 2h at RT or o/n at 4 °C in 1X TBS - 0.1% Tween 20 - 5% milk, blocking buffer solution or BSA. After 3 washes of 10 min each one with 1X TBS- 0.1% Tween 20, membranes were were incubated with the corresponding secondary

antibodies conjugated with the horseradish peroxidase for 1h hour and washed again. Finally, SuperSignalR West Pico (Pierce) was used for chemiluminescence detection.

Blocking Buffer solution: 1% Blocking reagent (Roche), 0.05% Tween 20, 0.05 M Tris-HCl pH 7.5. A stock of 10% Blocking reagent was previously prepared dissolving 10 g of blocking reagent in 100 ml maleic buffer (0.1 M Maleic acid, 0.15 M NaCl, pH 7.5 M adjusted with NaOH and autoclaved) with heat (50-60 °C) and shake.
Wash solution: 1X TBS – 0.1% Tween 20.

14.5. Fluorescent WB

A PVDF membrane with low fluorescence background (Inmobilon-FL, Millipore) was used. This membrane was first activated in methanol for 15 s and equilibrated in transfer buffer before continuing. Commercial Odyssey Blocking Buffer (LI-COR Biosciences) was used to block the membrane for 1 hat RT or o/n at 4 °C. Primary antibody was prepared (for appropriate dilution see Table M1) in blocking buffer -0.1% Tween 20 and incubated for 2 h. Three washes of 10 min were performed with 1X TBS - 0.1% Tween 20 followed by incubation of 1 h with IRDye secondary antibodies. Finally, membranes where washed again 3 times, rinsed in 1X TBS and immediately scanned or left drying. Image acquisition was performed in an Odyssey CLx Imager (LI-COR Biosciences).

15. GENOME WIDE EXPERIMENTS

15.1. RNA-seq

Total RNA was isolated from K562 cells transfected with siC or siUAP56 siRNA for 72 h with an RNeasy Mini kit (Qiagen). Then, total RNA-seq was performed after ribosomal RNA depletion applying the TruSeq Stranded Total RNA library and sequenced on the platform NextSEq500 (Illumina).

15.2. Chromatin immunoprecipitation (ChIP) assay (ChIP-seq)

K562 cells were crosslinked for 10 min with formaldehyde at a final concentration of 1%, resuspended in 2.5 ml of cell lysis buffer, then centrifuged and 1 ml of nuclei lysis buffer was added. Chromatin was sonicated on the maximum intensity setting, with fifteen pulses of 30s on and 30s off in Bioruptor (Diagenode), to obtain approx. 400 bp fragments. Samples were diluted up to 1300 µl with IP buffer. 100 µl and 1200 µl of diluted chromatin were used for input and immunoprecipitation, respectively. 30 µl of Dynabeads Protein A (Invitrogen) per sample was incubated overnight at 4 ºC with 4 µg of UAP56 antibody. A negative control the corresponding IgG was used to calculate the background signal. Then, Dynabeads-antibody complexes were added to the samples used for immunoprecipitation for 2h at 4 ºC and washed once with wash buffer 1, once with wash buffer 2, once with wash buffer 3 and twice with 1X TE. Input and immunoprecipitate were then un-crosslinked in TE -1% SDS and treated with proteinase K. DNA was isolated using NucleoSpin Gel and PCR Clean-up kit (Macherey-Nagel) and used to build the libraries using the ThruPLEX DNA-Seq 6S kit (Rubicon Genomics) according to manufacturer's instructions and then sequenced on the Illumina platform NextSEq500.

Cell lysis buffer: 5 mM PIPES pH 8, 85 mM KCl, 0.5% NP-40, 1 mM PMSF and protease inhibitor cocktail).

Nuclei lysis buffer: 1% SDS, 10 mM EDTA, 50 mM Tris-HCl pH 8, 1 mM PMSF and protease inhibitor cocktail.

IP buffer: 0.01% SDS, 1.1% Triton X-100, 1.2 mM EDTA, 16.7 mM Tris-HCl pH 8, 167 mM NaCl.

Wash buffer 1: 0.1% SDS, 1% Triton X-100, 2 mM EDTA, 20 mM Tris-HCl pH 8, 150 mM NaCl.

Wash buffer 2: 0.1% SDS, 1% Triton X-100, 2 mM EDTA, 20 mM Tris-HCl pH 8, 500 mM NaCl.

Wash buffer 3: 0.25 M LiCl, 1% NP-40, 1% sodium deoxycholate, 1 mM EDTA, 10 mM Tris-HCl pH 8.

15.3. DNA-RNA immunoprecipitation followed by high-throughput DNA sequencing (DRIP-seq)

DRIP-seq was performed as previously described (Sanz & Chedin, 2019) with minor modifications of the DRIP-qPCR (see Materials and Methods 8.3). Basically, genomic DNA was digested overnight with 30 U of HindIII, EcoRI, BsrGI, XbaI and SspI and 2mM spermidine. For the negative control, 10 μg of the digested DNA were treated with 4 μl RNase H (New England Biolabs) for 6 h at 37 ºC. Five immunoprecipitation were performed, in each one 8 μg of the digested DNA were bound to 20 μl of S9.6 antibody (1mg/ml) in 500 μl 1X binding buffer in TE, overnight at 4ºC. DNA-antibody complexes were immunoprecipitated using Dynabeads Protein A (Invitrogen) during 2h at 4ºC and washed 3 times with 1X binding buffer. DNA was eluted in 300 µl elution buffer, treated 45 min with 7 μl proteinase K at 55ºC and phenol-chloroform purified. Finally, DNA was resuspended in 10 μl of RNase-free water, with a total volume of 50 μl. Finally, the DNA was sonicated and checked on a 2100 Agilent Bioanalyzer. Afterwards, this DNA was used to build the libraries using the ThruPLEX DNA-Seq 6S kit (Rubicon Genomics) according to manufacturer's instruction and sequenced on an Illumina NextSeq500 platform.

15.4. RNA-DNA immunoprecipitation followed by cDNA conversion couple to high throughput sequencing (DRIPc-seq)

DRIPc-seq was performed essentially as described (Sanz & Chedin, 2019) and described in Materials and Methods 11.3. Briefly, after DRIP, the eluted DNA from five immunoprecipitations of each sample was treated with 6 U of DNase I (New England BioLabs) for 45 min at 37°C to degrade all DNA. The resulting RNA was subjected to libraries construction using the TruSeq Stranded Total RNA protocol (Illumina) from the fragmentation step. The quality of the libraries was checked on a 2100 Agilent Bioanalyzer prior to sequencing on an Illumina NextSeq500 platform.

16. GENOME WIDE DATA ANALYSIS

16.1. RNA-seq

Sequenced paired-ends reads were subjected to quality control pipeline using the FASTQ Toolkit v.1.0.0 software (Illumina) and then mapped to the human reference genome hg38 canonical using HISAT2 (Kim et al., 2019). Reads mapping to mitochondrial chromosome and duplicated reads were discarded using SAMtools (Li et al., 2009) for our purposes. After the obtainment of BAM files, counts per peak were established using FeatureCounts and RPKM normalized. For genes in which expression changes are detected (|linear fold change| > 1.5), siC Log_2expression and Log_2(siUAP56/siC) was compared and represented for genes longer than 5 Kb.

16.2. ChIP-seq

Sequenced paired-ends reads were subjected to quality control pipeline using the FASTQ Toolkit v.1.0.0 software (Illumina) and then mapped to the human reference genome hg38 canonical using using BWA-MEM (Li et al., 2009). Reads mapping to mitochondrial chromosome and duplicated reads were discarded using SAMtools (Li et al., 2009) for our purposes. BAM files were further analyzed with deepTools Bamcompare from deepTool2 package (Ramirez et al., 2016) for track generation. The results were visualized with the Integrative Genomics Viewer (IGV), developed and maintained by The Broad Institute and the Regents of the University of California and UC San Diego.

Peak calling was performed using MACS2 package (Zhang et al., 2008) selecting those whose enrichment signal over the input had a p-value < 0.01. As well, selected peaks were annotated to genes using ChIPseeker (Yu et al., 2015) and genes retrieved from Ensembl release 94 2018 (Zerbino et al., 2018). For our purposes, only genes with more than 5 Kb were analyzed, considering promoter as -2/+5 Kb from TSS and downstream as -2/+5 Kb from TES.

16.3. DRIP-seq and DRIPc-seq

Sequenced paired-ends reads were subjected to quality control pipeline using the FASTQ Toolkit v.1.0.0 software (Illumina) and then mapped to the human reference genome hg38 canonical using using BWA-MEM (Li et al., 2009). Reads mapping to mitochondrial chromosome and duplicated reads were discarded using SAMtools (Li et al., 2009) for our purposes. Additionally, For DRIPc-seq, reads were separated into minus and plus strand using the same tool. BAM files were further analyzed with deepTool2 package (Ramirez et al., 2016) for track generation setting a window bien size of 10 nt and a smooth value of 40. The results were visualized with the Integrative Genomics Viewer (IGV), developed and maintained by The Broad Institute and the Regents of the University of California and UC San Diego.

Peak calling on DRIP-seq and DRIPc-seq was performed using MACS2 package (Zhang et al., 2008). Then, number of counts per peak was calculated using FeatureCounts and RPKM normalized. For analysis, significant DRIPc peaks (q-value < 0.01) in siUAP56 depleted cells were established selecting those peaks whose DRIPc signal fold change was higher than 1.5X respect to the siC control cells. Afterwards, peaks were annotated to genes using ChIPseeker (Yu et al., 2015) and genes retrieved from Ensembl release 94 2018 (Zerbino et al., 2018). For our purposes, only genes with more than 5 Kb were analyzed, considering promoter as -2/+5 Kb from TSS and downstream as -2/+5 Kb from TES.

Gene metaplots were obtained using deepTools computematrix and plotheatmap. Venn diagrams were created using Biovenn (Hulsen et al., 2008).

- **Statistical tests**

  Statistical tests (Mann-Whitney U-test and Pearson's correlation were calculated using GraphPad Prism software. Hypergeometric tests were calculated using R scripts. In general, a P-value < 0.05 was considered as statistically significant.

REFERENCES

Aguilera, A. (2002). The connection between transcription and genomic instability. EMBO J *21*, 195-201.

Aguilera, A. (2005a). Cotranscriptional mRNP assembly: from the DNA to the nuclear pore. Curr Opin Cell Biol *17*, 242-250.

Aguilera, A. (2005b). mRNA processing and genomic instability. Nat Struct Mol Biol *12*, 737-738.

Aguilera, A., and Garcia-Muse, T. (2012). R loops: from transcription byproducts to threats to genome stability. Mol Cell *46*, 115-124.

Aguilera, A., and Garcia-Muse, T. (2013). Causes of genome instability. Annu Rev Genet *47*, 1-32.

Aguilera, A., and Gomez-Gonzalez, B. (2008). Genome instability: a mechanistic view of its causes and consequences. Nat Rev Genet *9*, 204-217.

Aguilera, A., and Gomez-Gonzalez, B. (2017). DNA-RNA hybrids: the risks of DNA breakage during transcription. Nat Struct Mol Biol *24*, 439-443.

Aguilera, A., and Klein, H.L. (1990). HPR1, a novel yeast gene that prevents intrachromosomal excision recombination, shows carboxy-terminal homology to the Saccharomyces cerevisiae TOP1 gene. Mol Cell Biol *10*, 1439-1451.

Alexander, R.D., Innocente, S.A., Barrass, J.D., and Beggs, J.D. (2010). Splicing-dependent RNA polymerase pausing in yeast. Mol Cell *40*, 582-593.

Arab, K., Karaulanov, E., Musheev, M., Trnka, P., Schafer, A., Grummt, I., and Niehrs, C. (2019). GADD45A binds R-loops and recruits TET1 to CpG island promoters. Nat Genet *51*, 217-223.

Aroeira, L.S., Aguilera, A., Sanchez-Tomero, J.A., Bajo, M.A., del Peso, G., Jimenez-Heffernan, J.A., Selgas, R., and Lopez-Cabrera, M. (2007). Epithelial to mesenchymal transition and peritoneal membrane failure in peritoneal dialysis patients: pathologic significance and potential therapeutic interventions. J Am Soc Nephrol *18*, 2004-2013.

Ayyanathan, K., Peng, H., Hou, Z., Fredericks, W.J., Goyal, R.K., Langer, E.M., Longmore, G.D., and Rauscher, F.J., 3rd (2007). The Ajuba LIM domain protein is a corepressor for SNAG domain mediated repression and participates in nucleocytoplasmic Shuttling. Cancer Res *67*, 9097-9106.

Barrallo-Gimeno, A., and Nieto, M.A. (2005). The Snail genes as inducers of cell movement and survival: implications in development and cancer. Development *132*, 3151-3161.

Bates, G.J., Nicol, S.M., Wilson, B.J., Jacobs, A.M., Bourdon, J.C., Wardrop, J., Gregory, D.J., Lane, D.P., Perkins, N.D., and Fuller-Pace, F.V. (2005).

The DEAD box protein p68: a novel transcriptional coactivator of the p53 tumour suppressor. EMBO J *24*, 543-553.

Batlle, E., Sancho, E., Franci, C., Dominguez, D., Monfar, M., Baulida, J., and Garcia De Herreros, A. (2000). The transcription factor snail is a repressor of E-cadherin gene expression in epithelial tumour cells. Nat Cell Biol *2*, 84-89.

Bentley, D.L. (2014). Coupling mRNA processing with transcription in time and space. Nat Rev Genet *15*, 163-175.

Bermejo, R., Capra, T., Gonzalez-Huici, V., Fachinetti, D., Cocito, A., Natoli, G., Katou, Y., Mori, H., Kurokawa, K., Shirahige, K.*, et al.* (2009). Genome-organizing factors Top2 and Hmo1 prevent chromosome fragility at sites of S phase transcription. Cell *138*, 870-884.

Bermejo, R., Lai, M.S., and Foiani, M. (2012). Preventing replication stress to maintain genome stability: resolving conflicts between replication and transcription. Mol Cell *45*, 710-718.

Bernstein, E., and Allis, C.D. (2005). RNA meets chromatin. Genes Dev *19*, 1635-1655.

Beyes, S., Andrieux, G., Schrempp, M., Aicher, D., Wenzel, J., Anton-Garcia, P., Boerries, M., and Hecht, A. (2019). Genome-wide mapping of DNA-binding sites identifies stemness-related genes as directly repressed targets of SNAIL1 in colorectal cancer cells. Oncogene.

Bhatia, V., Barroso, S.I., Garcia-Rubio, M.L., Tumini, E., Herrera-Moyano, E., and Aguilera, A. (2014). BRCA2 prevents R-loop accumulation and associates with TREX-2 mRNA export factor PCID2. Nature *511*, 362-365.

Bonnet, A., Grosso, A.R., Elkaoutari, A., Coleno, E., Presle, A., Sridhara, S.C., Janbon, G., Geli, V., de Almeida, S.F., and Palancade, B. (2017). Introns Protect Eukaryotic Genomes from Transcription-Associated Genetic Instability. Mol Cell *67*, 608-621 e606.

Boque-Sastre, R., Soler, M., Oliveira-Mateos, C., Portela, A., Moutinho, C., Sayols, S., Villanueva, A., Esteller, M., and Guil, S. (2015). Head-to-head antisense transcription and R-loop formation promotes transcriptional activation. Proc Natl Acad Sci U S A *112*, 5785-5790.

Brewer, B.J. (1988). When polymerases collide: replication and the transcriptional organization of the E. coli chromosome. Cell *53*, 679-686.

Burgess, R.C., and Misteli, T. (2015). Not All DDRs Are Created Equal: Non-Canonical DNA Damage Responses. Cell *162*, 944-947.

Cai, W., Xiong Chen, Z., Rane, G., Satendra Singh, S., Choo, Z., Wang, C., Yuan, Y., Zea Tan, T., Arfuso, F., Yap, C.T.*, et al.* (2017). Wanted DEAD/H or Alive: Helicases Winding Up in Cancers. J Natl Cancer Inst *109*.

Caretti, G., Schiltz, R.L., Dilworth, F.J., Di Padova, M., Zhao, P., Ogryzko, V., Fuller-Pace, F.V., Hoffman, E.P., Tapscott, S.J., and Sartorelli, V. (2006). The RNA helicases p68/p72 and the noncoding RNA SRA are coregulators of MyoD and skeletal muscle differentiation. Dev Cell *11*, 547-560.

Carter, C.L., Lin, C., Liu, C.Y., Yang, L., and Liu, Z.R. (2010). Phosphorylated p68 RNA helicase activates Snail1 transcription by promoting HDAC1 dissociation from the Snail1 promoter. Oncogene *29*, 5427-5436.

Castellano-Pozo, M., Garcia-Muse, T., and Aguilera, A. (2012a). The Caenorhabditis elegans THO complex is required for the mitotic cell cycle and development. PLoS One *7*, e52447.

Castellano-Pozo, M., Garcia-Muse, T., and Aguilera, A. (2012b). R-loops cause replication impairment and genome instability during meiosis. EMBO Rep *13*, 923-929.

Castellano-Pozo, M., Santos-Pereira, J.M., Rondon, A.G., Barroso, S., Andujar, E., Perez-Alegre, M., Garcia-Muse, T., and Aguilera, A. (2013). R loops are linked to histone H3 S10 phosphorylation and chromatin condensation. Mol Cell *52*, 583-590.

Cebria-Costa, J.P., Pascual-Reguant, L., Gonzalez-Perez, A., Serra-Bardenys, G., Querol, J., Cosin, M., Verde, G., Cigliano, R.A., Sanseverino, W., Segura-Bayona, S.*, et al.* (2019). LOXL2-mediated H3K4 oxidation reduces chromatin accessibility in triple-negative breast cancer cells. Oncogene.

Cerritelli, S.M., and Crouch, R.J. (2009). Ribonuclease H: the enzymes in eukaryotes. FEBS J *276*, 1494-1505.

Chakraborty, P., Huang, J.T.J., and Hiom, K. (2018). DHX9 helicase promotes R-loop formation in cells with impaired RNA splicing. Nat Commun *9*, 4346.

Chan, Y.A., Aristizabal, M.J., Lu, P.Y., Luo, Z., Hamza, A., Kobor, M.S., Stirling, P.C., and Hieter, P. (2014). Genome-wide profiling of yeast DNA:RNA hybrid prone sites with DRIP-chip. PLoS Genet *10*, e1004288.

Chanarat, S., Seizl, M., and Strasser, K. (2011). The Prp19 complex is a novel transcription elongation factor required for TREX occupancy at transcribed genes. Genes Dev *25*, 1147-1158.

Chang, C.T., Hautbergue, G.M., Walsh, M.J., Viphakone, N., van Dijk, T.B., Philipsen, S., and Wilson, S.A. (2013). Chtop is a component of the dynamic TREX mRNA export complex. EMBO J *32*, 473-486.

Chaudhuri, J., and Alt, F.W. (2004). Class-switch recombination: interplay of transcription, DNA deamination and DNA repair. Nat Rev Immunol *4*, 541-552.

Chavez, S., and Aguilera, A. (1997). The yeast HPR1 gene has a functional role in transcriptional elongation that uncovers a novel source of genome instability. Genes Dev *11*, 3459-3470.

Chavez, S., Beilharz, T., Rondon, A.G., Erdjument-Bromage, H., Tempst, P., Svejstrup, J.Q., Lithgow, T., and Aguilera, A. (2000). A protein complex containing Tho2, Hpr1, Mft1 and a novel protein, Thp2, connects transcription elongation with mitotic recombination in Saccharomyces cerevisiae. EMBO J *19*, 5824-5834.

Chedin, F. (2016). Nascent Connections: R-Loops and Chromatin Patterning. Trends Genet *32*, 828-838.

Chen, L., Chen, J.Y., Zhang, X., Gu, Y., Xiao, R., Shao, C., Tang, P., Qian, H., Luo, D., Li, H.*, et al.* (2017). R-ChIP Using Inactive RNase H Reveals Dynamic Coupling of R-loops with Transcriptional Pausing at Gene Promoters. Mol Cell *68*, 745-757 e745.

Chen, P.B., Chen, H.V., Acharya, D., Rando, O.J., and Fazzio, T.G. (2015). R loops regulate promoter-proximal chromatin architecture and cellular differentiation. Nat Struct Mol Biol *22*, 999-1007.

Cheng, H., Dufu, K., Lee, C.S., Hsu, J.L., Dias, A., and Reed, R. (2006). Human mRNA export machinery recruited to the 5' end of mRNA. Cell *127*, 1389-1400.

Chon, H., Sparks, J.L., Rychlik, M., Nowotny, M., Burgers, P.M., Crouch, R.J., and Cerritelli, S.M. (2013). RNase H2 roles in genome integrity revealed by unlinking its activities. Nucleic Acids Res *41*, 3130-3143.

Cordin, O., Banroques, J., Tanner, N.K., and Linder, P. (2006). The DEAD-box protein family of RNA helicases. Gene *367*, 17-37.

Cristini, A., Groh, M., Kristiansen, M.S., and Gromak, N. (2018). RNA/DNA Hybrid Interactome Identifies DXH9 as a Molecular Player in Transcriptional Termination and R-Loop-Associated DNA Damage. Cell Rep *23*, 1891-1905.

Crossley, M.P., Bocek, M., and Cimprich, K.A. (2019). R-Loops as Cellular Regulators and Genomic Threats. Mol Cell *73*, 398-411.

Dai, T.Y., Cao, L., Yang, Z.C., Li, Y.S., Tan, L., Ran, X.Z., and Shi, C.M. (2014). P68 RNA helicase as a molecular target for cancer therapy. J Exp Clin Cancer Res *33*, 64.

Dardenne, E., Polay Espinoza, M., Fattet, L., Germann, S., Lambert, M.P., Neil, H., Zonta, E., Mortada, H., Gratadou, L., Deygas, M.*, et al.* (2014). RNA helicases DDX5 and DDX17 dynamically orchestrate transcription, miRNA, and splicing programs in cell differentiation. Cell Rep *7*, 1900-1913.

Deshpande, A.M., and Newlon, C.S. (1996). DNA replication fork pause sites dependent on transcription. Science *272*, 1030-1033.

Dominguez-Sanchez, M.S., Barroso, S., Gomez-Gonzalez, B., Luna, R., and Aguilera, A. (2011). Genome instability and transcription elongation impairment in human cells depleted of THO/TREX. PLoS Genet *7*, e1002386.

Drolet, M., Phoenix, P., Menzel, R., Masse, E., Liu, L.F., and Crouch, R.J. (1995). Overexpression of RNase H partially complements the growth defect of an Escherichia coli delta topA mutant: R-loop formation is a major problem in the absence of DNA topoisomerase I. Proc Natl Acad Sci U S A *92*, 3526-3530.

Dufu, K., Livingstone, M.J., Seebacher, J., Gygi, S.P., Wilson, S.A., and Reed, R. (2010). ATP is required for interactions between UAP56 and two conserved mRNA export proteins, Aly and CIP29, to assemble the TREX complex. Genes Dev *24*, 2043-2053.

Dumelie, J.G., and Jaffrey, S.R. (2017). Defining the location of promoter-associated R-loops at near-nucleotide resolution using bisDRIP-seq. Elife *6*.

Eder, P.S., Walder, R.Y., and Walder, J.A. (1993). Substrate specificity of human RNase H1 and its role in excision repair of ribose residues misincorporated in DNA. Biochimie *75*, 123-126.

El Achkar, E., Gerbault-Seureau, M., Muleris, M., Dutrillaux, B., and Debatisse, M. (2005). Premature condensation induces breaks at the interface of early and late replicating chromosome bands bearing common fragile sites. Proc Natl Acad Sci U S A *102*, 18069-18074.

El Hage, A., French, S.L., Beyer, A.L., and Tollervey, D. (2010). Loss of Topoisomerase I leads to R-loop-mediated transcriptional blocks during ribosomal RNA synthesis. Genes Dev *24*, 1546-1558.

Fleckner, J., Zhang, M., Valcarcel, J., and Green, M.R. (1997). U2AF65 recruits a novel human DEAD box protein required for the U2 snRNP-branchpoint interaction. Genes Dev *11*, 1864-1872.

Folco, E.G., Lee, C.S., Dufu, K., Yamazaki, T., and Reed, R. (2012). The proteins PDIP3 and ZC11A associate with the human TREX complex in an ATP-dependent manner and function in mRNA export. PLoS One *7*, e43804.

Ford, M.J., Anton, I.A., and Lane, D.P. (1988). Nuclear protein with sequence homology to translation initiation factor eIF-4A. Nature *332*, 736-738.

Fuller-Pace, F.V. (2013). DEAD box RNA helicase functions in cancer. RNA Biol *10*, 121-132.

Gaillard, H., and Aguilera, A. (2013). Transcription coupled repair at the interface between transcription elongation and mRNP biogenesis. Biochim Biophys Acta *1829*, 141-150.

Gaillard, H., and Aguilera, A. (2016). Transcription as a Threat to Genome Integrity. Annu Rev Biochem *85*, 291-317.

Gaillard, H., Garcia-Muse, T., and Aguilera, A. (2015). Replication stress and cancer. Nat Rev Cancer *15*, 276-289.

Gaillard, H., Herrera-Moyano, E., and Aguilera, A. (2013). Transcription-associated genome instability. Chem Rev *113*, 8638-8661.

Gan, W., Guan, Z., Liu, J., Gui, T., Shen, K., Manley, J.L., and Li, X. (2011). R-loop-mediated genomic instability is caused by impairment of replication fork progression. Genes Dev *25*, 2041-2056.

Garcia-Muse, T., and Aguilera, A. (2016). Transcription-replication conflicts: how they occur and how they are resolved. Nat Rev Mol Cell Biol *17*, 553-563.

Garcia-Pichardo, D., Canas, J.C., Garcia-Rubio, M.L., Gomez-Gonzalez, B., Rondon, A.G., and Aguilera, A. (2017). Histone Mutants Separate R Loop Formation from Genome Instability Induction. Mol Cell *66*, 597-609 e595.

Garcia-Rubio, M., Aguilera, P., Lafuente-Barquero, J., Ruiz, J.F., Simon, M.N., Geli, V., Rondon, A.G., and Aguilera, A. (2018). Yra1-bound RNA-DNA hybrids cause orientation-independent transcription-replication collisions and telomere instability. Genes Dev *32*, 965-977.

Garcia-Rubio, M., Chavez, S., Huertas, P., Tous, C., Jimeno, S., Luna, R., and Aguilera, A. (2008). Different physiological relevance of yeast THO/TREX subunits in gene expression and genome integrity. Mol Genet Genomics *279*, 123-132.

Garcia-Rubio, M., Huertas, P., Gonzalez-Barrera, S., and Aguilera, A. (2003). Recombinogenic effects of DNA-damaging agents are synergistically increased by transcription in Saccharomyces cerevisiae. New insights into transcription-associated recombination. Genetics *165*, 457-466.

Garcia-Rubio, M.L., Perez-Calero, C., Barroso, S.I., Tumini, E., Herrera-Moyano, E., Rosado, I.V., and Aguilera, A. (2015). The Fanconi Anemia Pathway Protects Genome Integrity from R-loops. PLoS Genet *11*, e1005674.

Gatfield, D., Le Hir, H., Schmitt, C., Braun, I.C., Kocher, T., Wilm, M., and Izaurralde, E. (2001). The DExH/D box protein HEL/UAP56 is essential for mRNA nuclear export in Drosophila. Curr Biol *11*, 1716-1721.

Gavalda, S., Gallardo, M., Luna, R., and Aguilera, A. (2013). R-loop mediated transcription-associated recombination in trf4Delta mutants reveals new links between RNA surveillance and genome integrity. PLoS One *8*, e65541.

Geissler, V., Altmeyer, S., Stein, B., Uhlmann-Schiffler, H., and Stahl, H. (2013). The RNA helicase Ddx5/p68 binds to hUpf3 and enhances NMD of Ddx17/p72 and Smg5 mRNA. Nucleic Acids Res *41*, 7875-7888.

Gersappe, A., Burger, L., and Pintel, D.J. (1999). A premature termination codon in either exon of minute virus of mice P4 promoter-generated pre-mRNA can inhibit nuclear splicing of the intervening intron in an open reading frame-dependent manner. J Biol Chem *274*, 22452-22458.

Ginno, P.A., Lott, P.L., Christensen, H.C., Korf, I., and Chedin, F. (2012). R-loop formation is a distinctive characteristic of unmethylated human CpG island promoters. Mol Cell *45*, 814-825.

Gomez-Gonzalez, B., and Aguilera, A. (2007). Activation-induced cytidine deaminase action is strongly stimulated by mutations of the THO complex. Proc Natl Acad Sci U S A *104*, 8409-8414.

Gomez-Gonzalez, B., and Aguilera, A. (2019). Transcription-mediated replication hindrance: a major driver of genome instability. Genes Dev *33*, 1008-1026.

Gomez-Gonzalez, B., Felipe-Abrio, I., and Aguilera, A. (2009). The S-phase checkpoint is required to respond to R-loops accumulated in THO mutants. Mol Cell Biol *29*, 5203-5213.

Gomez-Gonzalez, B., Garcia-Rubio, M., Bermejo, R., Gaillard, H., Shirahige, K., Marin, A., Foiani, M., and Aguilera, A. (2011). Genome-wide function of THO/TREX in active genes prevents R-loop-dependent replication obstacles. EMBO J *30*, 3106-3119.

Gonatopoulos-Pournatzis, T., and Cowling, V.H. (2014). Cap-binding complex (CBC). Biochem J *457*, 231-242.

Goodarzi, A.A., Noon, A.T., Deckbar, D., Ziv, Y., Shiloh, Y., Lobrich, M., and Jeggo, P.A. (2008). ATM signaling facilitates repair of DNA double-strand breaks associated with heterochromatin. Mol Cell *31*, 167-177.

Gottipati, P., Cassel, T.N., Savolainen, L., and Helleday, T. (2008). Transcription-associated recombination is dependent on replication in Mammalian cells. Mol Cell Biol *28*, 154-164.

Gregory, R.I., Yan, K.P., Amuthan, G., Chendrimada, T., Doratotaj, B., Cooch, N., and Shiekhattar, R. (2004). The Microprocessor complex mediates the genesis of microRNAs. Nature *432*, 235-240.

Grunseich, C., Wang, I.X., Watts, J.A., Burdick, J.T., Guber, R.D., Zhu, Z., Bruzel, A., Lanman, T., Chen, K., Schindler, A.B.*, et al.* (2018). Senataxin Mutation Reveals How R-Loops Promote Transcription by Blocking DNA Methylation at Gene Promoters. Mol Cell *69*, 426-437 e427.

Guarino, M., Rubino, B., and Ballabio, G. (2007). The role of epithelial-mesenchymal transition in cancer pathology. Pathology *39*, 305-318.

Ha, M., and Kim, V.N. (2014). Regulation of microRNA biogenesis. Nat Rev Mol Cell Biol *15*, 509-524.

Hamperl, S., Bocek, M.J., Saldivar, J.C., Swigut, T., and Cimprich, K.A. (2017). Transcription-Replication Conflict Orientation Modulates R-Loop Levels and Activates Distinct DNA Damage Responses. Cell *170*, 774-786 e719.

Hamperl, S., and Cimprich, K.A. (2016). Conflict Resolution in the Genome: How Transcription and Replication Make It Work. Cell *167*, 1455-1467.

Hartono, S.R., Malapert, A., Legros, P., Bernard, P., Chedin, F., and Vanoosthuyse, V. (2018). The Affinity of the S9.6 Antibody for Double-Stranded RNAs Impacts the Accurate Mapping of R-Loops in Fission Yeast. J Mol Biol *430*, 272-284.

Hatchi, E., Skourti-Stathaki, K., Ventz, S., Pinello, L., Yen, A., Kamieniarz-Gdula, K., Dimitrov, S., Pathania, S., McKinney, K.M., Eaton, M.L.*, et al.* (2015). BRCA1 recruitment to transcriptional pause sites is required for R-loop-driven DNA damage repair. Mol Cell *57*, 636-647.

Heath, C.G., Viphakone, N., and Wilson, S.A. (2016). The role of TREX in gene expression and disease. Biochem J *473*, 2911-2935.

Helmrich, A., Ballarino, M., Nudler, E., and Tora, L. (2013). Transcription-replication encounters, consequences and genomic instability. Nat Struct Mol Biol *20*, 412-418.

Helmrich, A., Ballarino, M., and Tora, L. (2011). Collisions between replication and transcription complexes cause common fragile site instability at the longest human genes. Mol Cell *44*, 966-977.

Herold, A., Teixeira, L., and Izaurralde, E. (2003). Genome-wide analysis of nuclear mRNA export pathways in Drosophila. EMBO J *22*, 2472-2483.

Herranz, N., Pasini, D., Diaz, V.M., Franci, C., Gutierrez, A., Dave, N., Escriva, M., Hernandez-Munoz, I., Di Croce, L., Helin, K.*, et al.* (2008). Polycomb complex 2 is required for E-cadherin repression by the Snail1 transcription factor. Mol Cell Biol *28*, 4772-4781.

Herrera-Moyano, E., Mergui, X., Garcia-Rubio, M.L., Barroso, S., and Aguilera, A. (2014). The yeast and human FACT chromatin-reorganizing complexes solve R-loop-mediated transcription-replication conflicts. Genes Dev *28*, 735-748.

Hodroj, D., Recolin, B., Serhal, K., Martinez, S., Tsanov, N., Abou Merhi, R., and Maiorano, D. (2017a). An ATR-dependent function for the Ddx19 RNA helicase in nuclear R-loop metabolism. EMBO J *36*, 1182-1198.

Hodroj, D., Serhal, K., and Maiorano, D. (2017b). Ddx19 links mRNA nuclear export with progression of transcription and replication and suppresses genomic instability upon DNA damage in proliferating cells. Nucleus *8*, 489-495.

Huertas, P., and Aguilera, A. (2003). Cotranscriptionally formed DNA:RNA hybrids mediate transcription elongation impairment and transcription-associated recombination. Mol Cell *12*, 711-721.

Huertas, P., Garcia-Rubio, M.L., Wellinger, R.E., Luna, R., and Aguilera, A. (2006). An hpr1 point mutation that impairs transcription and mRNP biogenesis without increasing recombination. Mol Cell Biol *26*, 7451-7465.

Hulsen, T., de Vlieg, J., and Alkema, W. (2008). BioVenn - a web application for the comparison and visualization of biological lists using area-proportional Venn diagrams. BMC Genomics *9*, 488.

Iggo, R.D., Jamieson, D.J., MacNeill, S.A., Southgate, J., McPheat, J., and Lane, D.P. (1991). p68 RNA helicase: identification of a nucleolar form and cloning of related genes containing a conserved intron in yeasts. Mol Cell Biol *11*, 1326-1333.

Izquierdo, J.M., and Valcarcel, J. (2006). A simple principle to explain the evolution of pre-mRNA splicing. Genes Dev *20*, 1679-1684.

Jarmoskaite, I., and Russell, R. (2014). RNA helicase proteins as chaperones and remodelers. Annu Rev Biochem *83*, 697-725.

Jensen, T.H., Boulay, J., Rosbash, M., and Libri, D. (2001). The DECD box putative ATPase Sub2p is an early mRNA export factor. Curr Biol *11*, 1711-1715.

Jiang, F., Taylor, D.W., Chen, J.S., Kornfeld, J.E., Zhou, K., Thompson, A.J., Nogales, E., and Doudna, J.A. (2016). Structures of a CRISPR-Cas9 R-loop complex primed for DNA cleavage. Science *351*, 867-871.

Jimeno, S., Rondon, A.G., Luna, R., and Aguilera, A. (2002). The yeast THO complex and mRNA export factors link RNA metabolism with transcription and genome instability. EMBO J *21*, 3526-3535.

Kabeche, L., Nguyen, H.D., Buisson, R., and Zou, L. (2018). A mitosis-specific and R loop-driven ATR pathway promotes faithful chromosome segregation. Science *359*, 108-114.

Kapadia, F., Pryor, A., Chang, T.H., and Johnson, L.F. (2006). Nuclear localization of poly(A)+ mRNA following siRNA reduction of expression of the mammalian RNA helicases UAP56 and URH49. Gene *384*, 37-44.

Katahira, J., Ishikawa, H., Tsujimura, K., Kurono, S., and Hieda, M. (2019). Human THO coordinates transcription termination and subsequent transcript release from the HSP70 locus. Genes Cells *24*, 272-283.

Kim, D., Paggi, J.M., Park, C., Bennett, C., and Salzberg, S.L. (2019). Graph-based genome alignment and genotyping with HISAT2 and HISAT-genotype. Nat Biotechnol *37*, 907-915.

Kim, J., Sturgill, D., Sebastian, R., Khurana, S., Tran, A.D., Edwards, G.B., Kruswick, A., Burkett, S., Hosogane, E.K., Hannon, W.W*., et al.* (2018). Replication Stress Shapes a Protective Chromatin Environment across Fragile Genomic Regions. Mol Cell *69*, 36-47 e37.

Kim, N., and Jinks-Robertson, S. (2012). Transcription as a source of genome instability. Nat Rev Genet *13*, 204-214.

Kistler, A.L., and Guthrie, C. (2001). Deletion of MUD2, the yeast homolog of U2AF65, can bypass the requirement for sub2, an essential spliceosomal ATPase. Genes Dev *15*, 42-49.

Kogoma, T. (1997). Stable DNA replication: interplay between DNA replication, homologous recombination, and transcription. Microbiol Mol Biol Rev *61*, 212-238.

Kohler, A., and Hurt, E. (2007). Exporting RNA from the nucleus to the cytoplasm. Nat Rev Mol Cell Biol *8*, 761-773.

Kornblihtt, A.R., de la Mata, M., Fededa, J.P., Munoz, M.J., and Nogues, G. (2004). Multiple links between transcription and splicing. RNA *10*, 1489-1498.

Kornblihtt, A.R., Schor, I.E., Allo, M., Dujardin, G., Petrillo, E., and Munoz, M.J. (2013). Alternative splicing: a pivotal step between eukaryotic transcription and translation. Nat Rev Mol Cell Biol *14*, 153-165.

Kothari, A.N., Mi, Z., Zapf, M., and Kuo, P.C. (2014). Novel clinical therapeutics targeting the epithelial to mesenchymal transition. Clin Transl Med *3*, 35.

Laemmli, U.K. (1970). Cleavage of structural proteins during the assembly of the head of bacteriophage T4. Nature *227*, 680-685.

Lamm, G.M., Nicol, S.M., Fuller-Pace, F.V., and Lamond, A.I. (1996). p72: a human nuclear DEAD box protein highly related to p68. Nucleic Acids Res *24*, 3739-3747.

Lane, D.P., and Hoeffler, W.K. (1980). SV40 large T shares an antigenic determinant with a cellular protein of molecular weight 68,000. Nature *288*, 167-170.

Lang, K.S., Hall, A.N., Merrikh, C.N., Ragheb, M., Tabakh, H., Pollock, A.J., Woodward, J.J., Dreifus, J.E., and Merrikh, H. (2017). Replication-Transcription Conflicts Generate R-Loops that Orchestrate Bacterial Stress Survival and Pathogenesis. Cell *170*, 787-799 e718.

Li, H., Handsaker, B., Wysoker, A., Fennell, T., Ruan, J., Homer, N., Marth, G., Abecasis, G., Durbin, R., and Genome Project Data Processing, S. (2009). The Sequence Alignment/Map format and SAMtools. Bioinformatics *25*, 2078-2079.

Li, L., Germain, D.R., Poon, H.Y., Hildebrandt, M.R., Monckton, E.A., McDonald, D., Hendzel, M.J., and Godbout, R. (2016). DEAD Box 1 Facilitates Removal of RNA and Homologous Recombination at DNA Double-Strand Breaks. Mol Cell Biol *36*, 2794-2810.

Li, X., and Manley, J.L. (2005). Inactivation of the SR protein splicing factor ASF/SF2 results in genomic instability. Cell *122*, 365-378.

Libri, D., Dower, K., Boulay, J., Thomsen, R., Rosbash, M., and Jensen, T.H. (2002). Interactions between mRNA export commitment, 3'-end quality control, and nuclear degradation. Mol Cell Biol *22*, 8254-8266.

Libri, D., Graziani, N., Saguez, C., and Boulay, J. (2001). Multiple roles for the yeast SUB2/yUAP56 gene in splicing. Genes Dev *15*, 36-41.

Linder, P., and Jankowsky, E. (2011). From unwinding to clamping - the DEAD box RNA helicase family. Nat Rev Mol Cell Biol *12*, 505-516.

Linskens, M.H., and Huberman, J.A. (1988). Organization of replication of ribosomal DNA in Saccharomyces cerevisiae. Mol Cell Biol *8*, 4927-4935.

Liu, B., and Alberts, B.M. (1995). Head-on collision between a DNA replication apparatus and RNA polymerase transcription complex. Science *267*, 1131-1137.

Luna, R., Jimeno, S., Marin, M., Huertas, P., Garcia-Rubio, M., and Aguilera, A. (2005). Interdependence between transcription and mRNP processing and export, and its impact on genetic stability. Mol Cell *18*, 711-722.

Luna, R., Rondon, A.G., and Aguilera, A. (2012). New clues to understand the role of THO and other functionally related factors in mRNP biogenesis. Biochim Biophys Acta *1819*, 514-520.

Luo, M.L., Zhou, Z., Magni, K., Christoforides, C., Rappsilber, J., Mann, M., and Reed, R. (2001). Pre-mRNA splicing and mRNA export linked by direct interactions between UAP56 and Aly. Nature *413*, 644-647.

Lykke-Andersen, S., and Jensen, T.H. (2015). Nonsense-mediated mRNA decay: an intricate machinery that shapes transcriptomes. Nat Rev Mol Cell Biol *16*, 665-677.

Ma, W.K., Cloutier, S.C., and Tran, E.J. (2013). The DEAD-box protein Dbp2 functions with the RNA-binding protein Yra1 to promote mRNP assembly. J Mol Biol *425*, 3824-3838.

Ma, W.K., Paudel, B.P., Xing, Z., Sabath, I.G., Rueda, D., and Tran, E.J. (2016). Recruitment, Duplex Unwinding and Protein-Mediated Inhibition of the Dead-Box RNA Helicase Dbp2 at Actively Transcribed Chromatin. J Mol Biol *428*, 1091-1106.

MacMorris, M., Brocker, C., and Blumenthal, T. (2003). UAP56 levels affect viability and mRNA export in Caenorhabditis elegans. RNA *9*, 847-857.

Mani, S.A., Guo, W., Liao, M.J., Eaton, E.N., Ayyanan, A., Zhou, A.Y., Brooks, M., Reinhard, F., Zhang, C.C., Shipitsin, M.*, et al.* (2008). The epithelial-mesenchymal transition generates cells with properties of stem cells. Cell *133*, 704-715.

Maniatis, T., and Reed, R. (2002). An extensive network of coupling among gene expression machines. Nature *416*, 499-506.

Manzo, S.G., Hartono, S.R., Sanz, L.A., Marinello, J., De Biasi, S., Cossarizza, A., Capranico, G., and Chedin, F. (2018). DNA Topoisomerase I differentially modulates R-loops across the human genome. Genome Biol *19*, 100.

Masuda, S., Das, R., Cheng, H., Hurt, E., Dorman, N., and Reed, R. (2005). Recruitment of the human TREX complex to mRNA during splicing. Genes Dev *19*, 1512-1517.

Maturi, V., Moren, A., Enroth, S., Heldin, C.H., and Moustakas, A. (2018). Genomewide binding of transcription factor Snail1 in triple-negative breast cancer cells. Mol Oncol *12*, 1153-1174.

Mazurek, A., Park, Y., Miething, C., Wilkinson, J.E., Gillis, J., Lowe, S.W., Vakoc, C.R., and Stillman, B. (2014). Acquired dependence of acute myeloid leukemia on the DEAD-box RNA helicase DDX5. Cell Rep *7*, 1887-1899.

McDonald, O.G., Wu, H., Timp, W., Doi, A., and Feinberg, A.P. (2011). Genome-scale epigenetic reprogramming during epithelial-to-mesenchymal transition. Nat Struct Mol Biol *18*, 867-874.

Meinel, D.M., Burkert-Kautzsch, C., Kieser, A., O'Duibhir, E., Siebert, M., Mayer, A., Cramer, P., Soding, J., Holstege, F.C., and Strasser, K. (2013). Recruitment of TREX to the transcription machinery by its direct binding to the phospho-CTD of RNA polymerase II. PLoS Genet *9*, e1003914.

Merrikh, H., Zhang, Y., Grossman, A.D., and Wang, J.D. (2012). Replication-transcription conflicts in bacteria. Nat Rev Microbiol *10*, 449-458.

Mersaoui, S.Y., Yu, Z., Coulombe, Y., Karam, M., Busatto, F.F., Masson, J.Y., and Richard, S. (2019). Arginine methylation of the DDX5 helicase RGG/RG motif by PRMT5 regulates resolution of RNA:DNA hybrids. EMBO J *38*, e100986.

Michalet, X., Ekong, R., Fougerousse, F., Rousseaux, S., Schurra, C., Hornigold, N., van Slegtenhorst, M., Wolfe, J., Povey, S., Beckmann, J.S.*, et al.* (1997). Dynamic molecular combing: stretching the whole human genome for high-resolution studies. Science *277*, 1518-1523.

Millanes-Romero, A., Herranz, N., Perrera, V., Iturbide, A., Loubat-Casanovas, J., Gil, J., Jenuwein, T., Garcia de Herreros, A., and Peiro, S. (2013). Regulation of heterochromatin transcription by Snail1/LOXL2 during epithelial-to-mesenchymal transition. Mol Cell *52*, 746-757.

Millevoi, S., and Vagner, S. (2010). Molecular mechanisms of eukaryotic pre-mRNA 3' end processing regulation. Nucleic Acids Res *38*, 2757-2774.

Mischo, H.E., Chun, Y., Harlen, K.M., Smalec, B.M., Dhir, S., Churchman, L.S., and Buratowski, S. (2018). Cell-Cycle Modulation of Transcription Termination Factor Sen1. Mol Cell *70*, 312-326 e317.

Mischo, H.E., Gomez-Gonzalez, B., Grzechnik, P., Rondon, A.G., Wei, W., Steinmetz, L., Aguilera, A., and Proudfoot, N.J. (2011). Yeast Sen1 helicase protects the genome from transcription-associated instability. Mol Cell *41*, 21-32.

Muller-McNicoll, M., and Neugebauer, K.M. (2013). How cells get the message: dynamic assembly and function of mRNA-protein complexes. Nat Rev Genet *14*, 275-287.

Nadel, J., Athanasiadou, R., Lemetre, C., Wijetunga, N.A., P, O.B., Sato, H., Zhang, Z., Jeddeloh, J., Montagna, C., Golden, A.*, et al.* (2015). RNA:DNA hybrids in the human genome have distinctive nucleotide characteristics, chromatin composition, and transcriptional relationships. Epigenetics Chromatin *8*, 46.

Nakama, M., Kawakami, K., Kajitani, T., Urano, T., and Murakami, Y. (2012). DNA-RNA hybrid formation mediates RNAi-directed heterochromatin formation. Genes Cells *17*, 218-233.

Negrini, S., Gorgoulis, V.G., and Halazonetis, T.D. (2010). Genomic instability--an evolving hallmark of cancer. Nat Rev Mol Cell Biol *11*, 220-228.

Nieto, M.A., Huang, R.Y., Jackson, R.A., and Thiery, J.P. (2016). Emt: 2016. Cell *166*, 21-45.

Nowotny, M., Cerritelli, S.M., Ghirlando, R., Gaidamakov, S.A., Crouch, R.J., and Yang, W. (2008). Specific recognition of RNA/DNA hybrid and enhancement of human RNase H1 activity by HBD. EMBO J *27*, 1172-1181.

Paulsen, R.D., Soni, D.V., Wollman, R., Hahn, A.T., Yee, M.C., Guan, A., Hesley, J.A., Miller, S.C., Cromwell, E.F., Solow-Cordero, D.E.*, et al.* (2009). A genome-wide siRNA screen reveals diverse cellular processes and pathways that mediate genome stability. Mol Cell *35*, 228-239.

Pause, A., Methot, N., Svitkin, Y., Merrick, W.C., and Sonenberg, N. (1994). Dominant negative mutants of mammalian translation initiation factor eIF-4A define a critical role for eIF-4F in cap-dependent and cap-independent initiation of translation. EMBO J *13*, 1205-1215.

Pefanis, E., Wang, J., Rothschild, G., Lim, J., Kazadi, D., Sun, J., Federation, A., Chao, J., Elliott, O., Liu, Z.P.*, et al.* (2015). RNA exosome-regulated long non-coding RNA transcription controls super-enhancer activity. Cell *161*, 774-789.

Peinado, H., Ballestar, E., Esteller, M., and Cano, A. (2004). Snail mediates E-cadherin repression by the recruitment of the Sin3A/histone deacetylase 1 (HDAC1)/HDAC2 complex. Mol Cell Biol *24*, 306-319.

Peinado, H., Del Carmen Iglesias-de la Cruz, M., Olmeda, D., Csiszar, K., Fong, K.S., Vega, S., Nieto, M.A., Cano, A., and Portillo, F. (2005). A molecular role for lysyl oxidase-like 2 enzyme in snail regulation and tumor progression. EMBO J *24*, 3446-3458.

Peinado, H., Olmeda, D., and Cano, A. (2007). Snail, Zeb and bHLH factors in tumour progression: an alliance against the epithelial phenotype? Nat Rev Cancer *7*, 415-428.

Pena, A., Gewartowski, K., Mroczek, S., Cuellar, J., Szykowska, A., Prokop, A., Czarnocki-Cieciura, M., Piwowarski, J., Tous, C., Aguilera, A.*, et al.* (2012). Architecture and nucleic acids recognition mechanism of the THO complex, an mRNP assembly factor. EMBO J *31*, 1605-1616.

Petryk, N., Kahli, M., d'Aubenton-Carafa, Y., Jaszczyszyn, Y., Shen, Y., Silvain, M., Thermes, C., Chen, C.L., and Hyrien, O. (2016). Replication landscape of the human genome. Nat Commun *7*, 10208.

Phillips, D.D., Garboczi, D.N., Singh, K., Hu, Z., Leppla, S.H., and Leysath, C.E. (2013). The sub-nanomolar binding of DNA-RNA hybrids by the single-chain Fv fragment of antibody S9.6. J Mol Recognit *26*, 376-381.

Piruat, J.I., and Aguilera, A. (1998). A novel yeast gene, THO2, is involved in RNA pol II transcription and provides new evidence for transcriptional elongation-associated recombination. EMBO J *17*, 4859-4872.

Prado, F., and Aguilera, A. (2005). Impairment of replication fork progression mediates RNA polII transcription-associated recombination. EMBO J *24*, 1267-1276.

Proudfoot, N.J. (2016). Transcriptional termination in mammals: Stopping the RNA polymerase II juggernaut. Science *352*, aad9926.

Proudfoot, N.J., Furger, A., and Dye, M.J. (2002). Integrating mRNA processing with transcription. Cell *108*, 501-512.

Pryor, A., Tung, L., Yang, Z., Kapadia, F., Chang, T.H., and Johnson, L.F. (2004). Growth-regulated expression and G0-specific turnover of the mRNA that encodes URH49, a mammalian DExH/D box protein that is highly related to the mRNA export protein UAP56. Nucleic Acids Res *32*, 1857-1865.

Putnam, A.A., and Jankowsky, E. (2013). DEAD-box helicases as integrators of RNA, nucleotide and protein binding. Biochim Biophys Acta *1829*, 884-893.

Ramirez, F., Ryan, D.P., Gruning, B., Bhardwaj, V., Kilpert, F., Richter, A.S., Heyne, S., Dundar, F., and Manke, T. (2016). deepTools2: a next generation web server for deep-sequencing data analysis. Nucleic Acids Res *44*, W160-165.

Reed, R., and Cheng, H. (2005). TREX, SR proteins and export of mRNA. Curr Opin Cell Biol *17*, 269-273.

Reed, R., and Hurt, E. (2002). A conserved mRNA export machinery coupled to pre-mRNA splicing. Cell *108*, 523-531.

Ren, Y., Schmiege, P., and Blobel, G. (2017). Structural and biochemical analyses of the DEAD-box ATPase Sub2 in association with THO or Yra1. Elife *6*.

Ribeiro de Almeida, C., Dhir, S., Dhir, A., Moghaddam, A.E., Sattentau, Q., Meinhart, A., and Proudfoot, N.J. (2018). RNA Helicase DDX1 Converts RNA G-Quadruplex Structures into R-Loops to Promote IgH Class Switch Recombination. Mol Cell *70*, 650-662 e658.

Rondon, A.G., and Aguilera, A. (2019). What causes an RNA-DNA hybrid to compromise genome integrity? DNA Repair (Amst) *81*, 102660.

Rondon, A.G., Jimeno, S., and Aguilera, A. (2010). The interface between transcription and mRNP export: from THO to THSC/TREX-2. Biochim Biophys Acta *1799*, 533-538.

Rougemaille, M., Dieppois, G., Kisseleva-Romanova, E., Gudipati, R.K., Lemoine, S., Blugeon, C., Boulay, J., Jensen, T.H., Stutz, F., Devaux, F.*, et al.* (2008). THO/Sub2p functions to coordinate 3'-end processing with gene-nuclear pore association. Cell *135*, 308-321.

Saguez, C., Gonzales, F.A., Schmid, M., Boggild, A., Latrick, C.M., Malagon, F., Putnam, A., Sanderson, L., Jankowsky, E., Brodersen, D.E.*, et al.* (2013). Mutational analysis of the yeast RNA helicase Sub2p reveals conserved domains required for growth, mRNA export, and genomic stability. RNA *19*, 1363-1371.

Saguez, C., Schmid, M., Olesen, J.R., Ghazy, M.A., Qu, X., Poulsen, M.B., Nasser, T., Moore, C., and Jensen, T.H. (2008). Nuclear mRNA surveillance in THO/sub2 mutants is triggered by inefficient polyadenylation. Mol Cell *31*, 91-103.

Salas-Armenteros, I., Perez-Calero, C., Bayona-Feliu, A., Tumini, E., Luna, R., and Aguilera, A. (2017). Human THO-Sin3A interaction reveals new mechanisms to prevent R-loops that cause genome instability. EMBO J *36*, 3532-3547.

Sambrook, J., Fritsch, E.F., and Maniatis, T. (1989). Molecular cloning : a laboratory manual, 2nd edn (New York: Cold Spring Harbor Laboratory).

Santos-Pereira, J.M., and Aguilera, A. (2015). R loops: new modulators of genome dynamics and function. Nat Rev Genet *16*, 583-597.

Sanz, L.A., and Chedin, F. (2019). High-resolution, strand-specific R-loop mapping via S9.6-based DNA-RNA immunoprecipitation and high-throughput sequencing. Nat Protoc *14*, 1734-1755.

Sanz, L.A., Hartono, S.R., Lim, Y.W., Steyaert, S., Rajpurkar, A., Ginno, P.A., Xu, X., and Chedin, F. (2016). Prevalent, Dynamic, and Conserved R-Loop Structures Associate with Specific Epigenomic Signatures in Mammals. Mol Cell *63*, 167-178.

Saponaro, M., Kantidakis, T., Mitter, R., Kelly, G.P., Heron, M., Williams, H., Soding, J., Stewart, A., and Svejstrup, J.Q. (2014). RECQL5 controls transcript elongation and suppresses genome instability associated with transcription stress. Cell *157*, 1037-1049.

Saporita, A.J., Chang, H.C., Winkeler, C.L., Apicelli, A.J., Kladney, R.D., Wang, J., Townsend, R.R., Michel, L.S., and Weber, J.D. (2011). RNA helicase

DDX5 is a p53-independent target of ARF that participates in ribosome biogenesis. Cancer Res *71*, 6708-6717.

Sarkar, M., and Ghosh, M.K. (2016). DEAD box RNA helicases: crucial regulators of gene expression and oncogenesis. Front Biosci (Landmark Ed) *21*, 225-250.

Schwab, R.A., Nieminuszczy, J., Shah, F., Langton, J., Lopez Martinez, D., Liang, C.C., Cohn, M.A., Gibbons, R.J., Deans, A.J., and Niedzwiedz, W. (2015). The Fanconi Anemia Pathway Maintains Genome Stability by Coordinating Replication and Transcription. Mol Cell *60*, 351-361.

Selth, L.A., Sigurdsson, S., and Svejstrup, J.Q. (2010). Transcript Elongation by RNA Polymerase II. Annu Rev Biochem *79*, 271-293.

Sengoku, T., Nureki, O., Nakamura, A., Kobayashi, S., and Yokoyama, S. (2006). Structural basis for RNA unwinding by the DEAD-box protein Drosophila Vasa. Cell *125*, 287-300.

Shen, H., Zheng, X., Shen, J., Zhang, L., Zhao, R., and Green, M.R. (2008). Distinct activities of the DExD/H-box splicing factor hUAP56 facilitate stepwise assembly of the spliceosome. Genes Dev *22*, 1796-1803.

Shen, J., Zhang, L., and Zhao, R. (2007). Biochemical characterization of the ATPase and helicase activity of UAP56, an essential pre-mRNA splicing and mRNA export factor. J Biol Chem *282*, 22544-22550.

Shi, H., Cordin, O., Minder, C.M., Linder, P., and Xu, R.M. (2004). Crystal structure of the human ATP-dependent splicing and export factor UAP56. Proc Natl Acad Sci U S A *101*, 17628-17633.

Shivji, M.K.K., Renaudin, X., Williams, C.H., and Venkitaraman, A.R. (2018). BRCA2 Regulates Transcription Elongation by RNA Polymerase II to Prevent R-Loop Accumulation. Cell Rep *22*, 1031-1039.

Shkreta, L., and Chabot, B. (2015). The RNA Splicing Response to DNA Damage. Biomolecules *5*, 2935-2977.

Silva, S., Camino, L.P., and Aguilera, A. (2018). Human mitochondrial degradosome prevents harmful mitochondrial R loops and mitochondrial genome instability. Proc Natl Acad Sci U S A *115*, 11024-11029.

Singh, D.K., Pandita, R.K., Singh, M., Chakraborty, S., Hambarde, S., Ramnarain, D., Charaka, V., Ahmed, K.M., Hunt, C.R., and Pandita, T.K. (2018). MOF Suppresses Replication Stress and Contributes to Resolution of Stalled Replication Forks. Mol Cell Biol *38*.

Singleton, M.R., Dillingham, M.S., and Wigley, D.B. (2007). Structure and mechanism of helicases and nucleic acid translocases. Annu Rev Biochem *76*, 23-50.

Skourti-Stathaki, K., and Proudfoot, N.J. (2014). A double-edged sword: R loops as threats to genome integrity and powerful regulators of gene expression. Genes Dev *28*, 1384-1396.

Skourti-Stathaki, K., Proudfoot, N.J., and Gromak, N. (2011). Human senataxin resolves RNA/DNA hybrids formed at transcriptional pause sites to promote Xrn2-dependent termination. Mol Cell *42*, 794-805.

Sloan, C.A., Chan, E.T., Davidson, J.M., Malladi, V.S., Strattan, J.S., Hitz, B.C., Gabdank, I., Narayanan, A.K., Ho, M., Lee, B.T.*, et al.* (2016). ENCODE data at the ENCODE portal. Nucleic Acids Res *44*, D726-732.

Soderberg, O., Gullberg, M., Jarvius, M., Ridderstrale, K., Leuchowius, K.J., Jarvius, J., Wester, K., Hydbring, P., Bahram, F., Larsson, L.G.*, et al.* (2006). Direct observation of individual endogenous protein complexes in situ by proximity ligation. Nat Methods *3*, 995-1000.

Sollier, J., Stork, C.T., Garcia-Rubio, M.L., Paulsen, R.D., Aguilera, A., and Cimprich, K.A. (2014). Transcription-coupled nucleotide excision repair factors promote R-loop-induced genome instability. Mol Cell *56*, 777-785.

Song, C., Hotz-Wagenblatt, A., Voit, R., and Grummt, I. (2017). SIRT7 and the DEAD-box helicase DDX21 cooperate to resolve genomic R loops and safeguard genome stability. Genes Dev *31*, 1370-1381.

Sridhara, S.C., Carvalho, S., Grosso, A.R., Gallego-Paez, L.M., Carmo-Fonseca, M., and de Almeida, S.F. (2017). Transcription Dynamics Prevent RNA-Mediated Genomic Instability through SRPK2-Dependent DDX23 Phosphorylation. Cell Rep *18*, 334-343.

Stemmler, M.P., Eccles, R.L., Brabletz, S., and Brabletz, T. (2019). Non-redundant functions of EMT transcription factors. Nat Cell Biol *21*, 102-112.

Stirling, P.C., Chan, Y.A., Minaker, S.W., Aristizabal, M.J., Barrett, I., Sipahimalani, P., Kobor, M.S., and Hieter, P. (2012). R-loop-mediated genome instability in mRNA cleavage and polyadenylation mutants. Genes Dev *26*, 163-175.

Strasser, K., Masuda, S., Mason, P., Pfannstiel, J., Oppizzi, M., Rodriguez-Navarro, S., Rondon, A.G., Aguilera, A., Struhl, K., Reed, R.*, et al.* (2002). TREX is a conserved complex coupling transcription with messenger RNA export. Nature *417*, 304-308.

Stuckey, R., Garcia-Rodriguez, N., Aguilera, A., and Wellinger, R.E. (2015). Role for RNA:DNA hybrids in origin-independent replication priming in a eukaryotic system. Proc Natl Acad Sci U S A *112*, 5779-5784.

Sugiura, T., Sakurai, K., and Nagano, Y. (2007). Intracellular characterization of DDX39, a novel growth-associated RNA helicase. Exp Cell Res *313*, 782-790.

Sulli, G., Di Micco, R., and d'Adda di Fagagna, F. (2012). Crosstalk between chromatin state and DNA damage response in cellular senescence and cancer. Nat Rev Cancer *12*, 709-720.

Sun, X., Perlick, H.A., Dietz, H.C., and Maquat, L.E. (1998). A mutated human homologue to yeast Upf1 protein has a dominant-negative effect on the decay of nonsense-containing mRNAs in mammalian cells. Proc Natl Acad Sci U S A *95*, 10009-10014.

Tedeschi, F.A., Cloutier, S.C., Tran, E.J., and Jankowsky, E. (2018). The DEAD-box protein Dbp2p is linked to noncoding RNAs, the helicase Sen1p, and R-loops. RNA *24*, 1693-1705.

Thiery, J.P. (2003). Epithelial-mesenchymal transitions in development and pathologies. Curr Opin Cell Biol *15*, 740-746.

Thiery, J.P., Acloque, H., Huang, R.Y., and Nieto, M.A. (2009). Epithelial-mesenchymal transitions in development and disease. Cell *139*, 871-890.

Thiery, J.P., and Sleeman, J.P. (2006). Complex networks orchestrate epithelial-mesenchymal transitions. Nat Rev Mol Cell Biol *7*, 131-142.

Tous, C., and Aguilera, A. (2007). Impairment of transcription elongation by R-loops in vitro. Biochem Biophys Res Commun *360*, 428-432.

Tran, P.L.T., Pohl, T.J., Chen, C.F., Chan, A., Pott, S., and Zakian, V.A. (2017). PIF1 family DNA helicases suppress R-loop mediated genome instability at tRNA genes. Nat Commun *8*, 15025.

Tuduri, S., Crabbe, L., Conti, C., Tourriere, H., Holtgreve-Grez, H., Jauch, A., Pantesco, V., De Vos, J., Thomas, A., Theillet, C.*, et al.* (2009). Topoisomerase I suppresses genomic instability by preventing interference between replication and transcription. Nat Cell Biol *11*, 1315-1324.

Vinciguerra, P., and Stutz, F. (2004). mRNA export: an assembly line from genes to nuclear pores. Curr Opin Cell Biol *16*, 285-292.

Wahba, L., Amon, J.D., Koshland, D., and Vuica-Ross, M. (2011). RNase H and multiple RNA biogenesis factors cooperate to prevent RNA:DNA hybrids from generating genome instability. Mol Cell *44*, 978-988.

Wahba, L., Costantino, L., Tan, F.J., Zimmer, A., and Koshland, D. (2016). S1-DRIP-seq identifies high expression and polyA tracts as major contributors to R-loop formation. Genes Dev *30*, 1327-1338.

Wang, H., Gao, X., Huang, Y., Yang, J., and Liu, Z.R. (2009). P68 RNA helicase is a nucleocytoplasmic shuttling protein. Cell Res *19*, 1388-1400.

Wang, X., Liu, H., Zhao, C., Li, W., Xu, H., and Chen, Y. (2016). The DEAD-box RNA helicase 51 controls non-small cell lung cancer proliferation by regulating cell cycle progression via multiple pathways. Sci Rep *6*, 26108.

Wang, Y., Shi, J., Chai, K., Ying, X., and Zhou, B.P. (2013). The Role of Snail in EMT and Tumorigenesis. Curr Cancer Drug Targets *13*, 963-972.

Wei, X., Samarabandu, J., Devdhar, R.S., Siegel, A.J., Acharya, R., and Berezney, R. (1998). Segregation of transcription and replication sites into higher order domains. Science *281*, 1502-1506.

Wellinger, R.E., Prado, F., and Aguilera, A. (2006). Replication fork progression is impaired by transcription in hyperrecombinant yeast cells lacking a functional THO complex. Mol Cell Biol *26*, 3327-3334.

Will, C.L., and Luhrmann, R. (2011). Spliceosome structure and function. Cold Spring Harb Perspect Biol *3*.

Wongtrakoongate, P., Riddick, G., Fucharoen, S., and Felsenfeld, G. (2015). Association of the Long Non-coding RNA Steroid Receptor RNA Activator (SRA) with TrxG and PRC2 Complexes. PLoS Genet *11*, e1005615.

Wortham, N.C., Ahamed, E., Nicol, S.M., Thomas, R.S., Periyasamy, M., Jiang, J., Ochocka, A.M., Shousha, S., Huson, L., Bray, S.E*., et al.* (2009). The DEAD-box protein p72 regulates ERalpha-/oestrogen-dependent transcription and cell growth, and is associated with improved survival in ERalpha-positive breast cancer. Oncogene *28*, 4053-4064.

Wu, Y., Evers, B.M., and Zhou, B.P. (2009). Small C-terminal domain phosphatase enhances snail activity through dephosphorylation. J Biol Chem *284*, 640-648.

Xing, Z., Ma, W.K., and Tran, E.J. (2019). The DDX5/Dbp2 subfamily of DEAD-box RNA helicases. Wiley Interdiscip Rev RNA *10*, e1519.

Xing, Z., Wang, S., and Tran, E.J. (2017). Characterization of the mammalian DEAD-box protein DDX5 reveals functional conservation with S. cerevisiae ortholog Dbp2 in transcriptional control and glucose metabolism. RNA *23*, 1125-1138.

Xu, B., and Clayton, D.A. (1996). RNA-DNA hybrid formation at the human mitochondrial heavy-strand origin ceases at replication start sites: an implication for RNA-DNA hybrids serving as primers. EMBO J *15*, 3135-3143.

Yamazaki, T., Fujiwara, N., Yukinaga, H., Ebisuya, M., Shiki, T., Kurihara, T., Kioka, N., Kambe, T., Nagao, M., Nishida, E*., et al.* (2010). The closely

related RNA helicases, UAP56 and URH49, preferentially form distinct mRNA export machineries and coordinately regulate mitotic progression. Mol Biol Cell *21*, 2953-2965.

Yang, Q., Del Campo, M., Lambowitz, A.M., and Jankowsky, E. (2007). DEAD-box proteins unwind duplexes by local strand separation. Mol Cell *28*, 253-263.

Yasuhara, T., Kato, R., Hagiwara, Y., Shiotani, B., Yamauchi, M., Nakada, S., Shibata, A., and Miyagawa, K. (2018). Human Rad52 Promotes XPG-Mediated R-loop Processing to Initiate Transcription-Associated Homologous Recombination Repair. Cell *175*, 558-570 e511.

Yu, G., Wang, L.G., and He, Q.Y. (2015). ChIPseeker: an R/Bioconductor package for ChIP peak annotation, comparison and visualization. Bioinformatics *31*, 2382-2383.

Yu, K., Chedin, F., Hsieh, C.L., Wilson, T.E., and Lieber, M.R. (2003). R-loops at immunoglobulin class switch regions in the chromosomes of stimulated B cells. Nat Immunol *4*, 442-451.

Zeman, M.K., and Cimprich, K.A. (2014). Causes and consequences of replication stress. Nat Cell Biol *16*, 2-9.

Zenklusen, D., Vinciguerra, P., Wyss, J.C., and Stutz, F. (2002). Stable mRNP formation and export require cotranscriptional recruitment of the mRNA export factors Yra1p and Sub2p by Hpr1p. Mol Cell Biol *22*, 8241-8253.

Zerbino, D.R., Achuthan, P., Akanni, W., Amode, M.R., Barrell, D., Bhai, J., Billis, K., Cummins, C., Gall, A., Giron, C.G.*, et al.* (2018). Ensembl 2018. Nucleic Acids Res *46*, D754-D761.

Zhang, H., Xing, Z., Mani, S.K., Bancel, B., Durantel, D., Zoulim, F., Tran, E.J., Merle, P., and Andrisani, O. (2016). RNA helicase DEAD box protein 5 regulates Polycomb repressive complex 2/Hox transcript antisense intergenic RNA function in hepatitis B virus infection and hepatocarcinogenesis. Hepatology *64*, 1033-1048.

Zhang, X., Chiang, H.C., Wang, Y., Zhang, C., Smith, S., Zhao, X., Nair, S.J., Michalek, J., Jatoi, I., Lautner, M.*, et al.* (2017). Attenuation of RNA polymerase II pausing mitigates BRCA1-associated R-loop accumulation and tumorigenesis. Nat Commun *8*, 15908.

Zhang, Y., Liu, T., Meyer, C.A., Eeckhoute, J., Johnson, D.S., Bernstein, B.E., Nusbaum, C., Myers, R.M., Brown, M., Li, W.*, et al.* (2008). Model-based analysis of ChIP-Seq (MACS). Genome Biol *9*, R137.

Zhao, D.Y., Gish, G., Braunschweig, U., Li, Y., Ni, Z., Schmitges, F.W., Zhong, G., Liu, K., Li, W., Moffat, J.*, et al.* (2016). SMN and symmetric arginine

dimethylation of RNA polymerase II C-terminal domain control termination. Nature *529*, 48-53.

Zhao, R., Shen, J., Green, M.R., MacMorris, M., and Blumenthal, T. (2004). Crystal structure of UAP56, a DExD/H-box protein involved in pre-mRNA splicing and mRNA export. Structure *12*, 1373-1381.

Zhu, X., Li, K., and Salah, A. (2013). A data parallel strategy for aligning multiple biological sequences on multi-core computers. Comput Biol Med *43*, 350-361.

Zonta, E., Bittencourt, D., Samaan, S., Germann, S., Dutertre, M., and Auboeuf, D. (2013). The RNA helicase DDX5/p68 is a key factor promoting c-fos expression at different levels from transcription to mRNA export. Nucleic Acids Res *41*, 554-564.